

Final Report, June 22, 2018
Satisfying Task 5
WORK ORDER UNDER THE CONTRACT BETWEEN TCEQ AND CONTRACTOR:
The University of Texas at Austin

GAD Number 582-18-81721-01 (FY-2018 PGA)
Analysis of Foreign and Transport Contributions to PM_{2.5}
Concentrations at the Houston Clinton Drive, Galveston 99th Street,
and El Paso Chamizal Monitors

Prepared by

Dave Sullivan, Ph.D.

The University of Texas at Austin (UT)

Center for Energy and Environmental Resources

Building 133, MC R7100, 10100 Burnet Rd. Austin, TX 78758-4445

Phone: 512-471-7805, Email: sullivan231@mail.utexas.edu

Contents

1. Background.....	3
2. Sampling Operations.....	5
3. Data Analysis Findings.....	7
3.1 Clinton Dr. Sampling Results	7
3.1.1 Clinton Dr. source apportionment.....	7
3.1.2 Characterization of factors by wind direction and day of week	15
3.1.3 Trends in Houston Using TEOM Data	28
3.1.4 Sulfate at Clinton Dr.	29
3.1.5 HYSPLIT Back-Trajectory Cluster Analysis for Clinton Dr. Sulfate Source Apportionment	31
3.1.6 North African Dust Affecting Clinton Dr.	36
3.1.7 Joint Research with Texas A&M & Univ. of Houston into Crustal & Fire Factor Transport.....	43
3.1.8 Fire back trajectory analysis	52
3.1.9 Sulfate in Fire Samples at Clinton Dr.	54
3.1.10 2017 Houston Area TEOM and Beta-attenuation Monitor PM _{2.5} Data.....	55
3.1.11 Effect of Hurricane Harvey on PM _{2.5}	57
3.2 Galveston Sampling Results	62
3.2.1 PMF Analysis for Galveston.....	62
3.3 Chamizal Sampling Results	65
3.3.1 PMF Analysis for Chamizal.....	65

3.3.2 PM _{2.5} Case Study May 16, 2017	67
3.4 West Texas PM _{2.5}	75
3.4.1 Guadalupe Mountains National Park PM _{2.5} Data	75
3.4.2 Wind Speed and Direction at Guadalupe Mountains National Park.....	77
3.4.3 PMF Analysis for Guadalupe National Park	85
4. Conclusion and Recommendations.....	96

1. Background

PM_{2.5} is particulate matter with an aerodynamic diameter less than or equal to 2.5 microns. This report is the ***final report*** on PM_{2.5} sampling at Galveston continuous ambient monitoring station (CAMS) 1034, data analysis of speciated and total mass PM_{2.5} concentrations from Galveston CAMS 1034 and from the Clinton Drive CAMS 403 monitor in Houston, and data analysis of speciated and total mass from the Chamizal CAMS 41 monitor in El Paso. One important goal of this work is to assess foreign and domestic transport contributions to PM_{2.5} concentrations in Houston and El Paso. This work has been conducted by The University of Texas at Austin (UT) Center for Energy and Environmental Resources for the Texas Commission on Environmental Quality (TCEQ).

The annual average PM_{2.5} concentrations at the Clinton Dr. monitor in Houston are generally the highest annual average PM_{2.5} concentrations in Southeast Texas. African dust and smoke from burning vegetation in southern Mexico and Central America contribute on some days to high PM_{2.5} concentrations measured at Clinton Dr. and other Texas sites. Within the past decade, cooperative efforts (based on prior UT research) led by the Texas Commission on Environmental Quality (TCEQ) have led to reduced annual average PM_{2.5} concentrations at Clinton Dr. to levels that comply with the annual National Ambient Air Quality Standards (NAAQS). When work on speciated sampling began, the level of the annual mean primary NAAQS was 15 micrograms per cubic meter ($\mu\text{g}/\text{m}^3$). The U.S. Environmental Protection Agency (EPA) changed the level of the primary PM_{2.5} annual average NAAQS from 15.0 $\mu\text{g}/\text{m}^3$ to 12.0 $\mu\text{g}/\text{m}^3$ in 2012. The 2009 through 2011 PM_{2.5} annual average design value, i.e., the three-year average value for comparison to the level of the annual PM_{2.5} NAAQS, was 12.3 $\mu\text{g}/\text{m}^3$ for Clinton Dr.. Before exceptional event days are removed, the design value for 2010 through 2012 was 12.1 $\mu\text{g}/\text{m}^3$, and after removal of selected exceptional event days the three-year average PM_{2.5} concentration at Clinton Dr. reduced to 12.0 $\mu\text{g}/\text{m}^3$.

Figure 1 shows the annual average concentrations¹ of PM_{2.5} at Houston area Federal Reference Method (FRM) samplers from 2005 through 2017. The Houston North Loop site did not meet data completeness requirements in 2015 and 2016, years for which the North Loop average exceeded the Clinton Dr. average. Figure 2 shows the PM_{2.5} annual average NAAQS design values for Houston area sites meeting data completeness requirements.

Similar and possibly related pollutant transport issues affect other parts of the State. In El Paso, TX, before removal of exceptional event impacts on the PM_{2.5} values at the Chamizal monitor, the measured PM_{2.5} concentrations there have caused concern about maintaining attainment of the PM_{2.5} NAAQS. Recently, exceedances of the 24-hr level of the NAAQS at El Paso sites have been an issue.

There are five purposes of this project:

- 1) One purpose is to produce PM_{2.5} chemical speciation data from the TCEQ Galveston monitoring site.

¹ Annual averages are calculated taking the mean within each quarter of the year and then averaging the four quarterly means. Tests are applied for data completeness within each quarter and four complete quarters are required for an annual average.

- 2) A second purpose is to carry out advanced analysis of the data from all PM_{2.5} monitoring sites in the Houston region to determine quantitatively the contribution of African dust and smoke from southern Mexico and Central America to PM_{2.5} concentrations measured on individual days impacted by either or both of these sources at Clinton Dr.
- 3) A third purpose is to help determine the contribution of incoming regional PM_{2.5} concentrations from the continental U.S. to PM_{2.5} concentrations measured at Clinton Dr.
- 4) A fourth purpose is to determine the source types and directions contributing to local and regional contributions to the PM_{2.5} concentrations measured at Clinton Dr.
- 5) A fifth purpose is to identify the impacts of regional dust storms on PM_{2.5} concentrations at the Chamizal monitoring site in El Paso.

Figure 1. Annual average PM_{2.5} concentrations at TCEQ FRM sampling sites, 2005 – 2017; note North Loop did not meet data completeness requirements in 2015, 2016

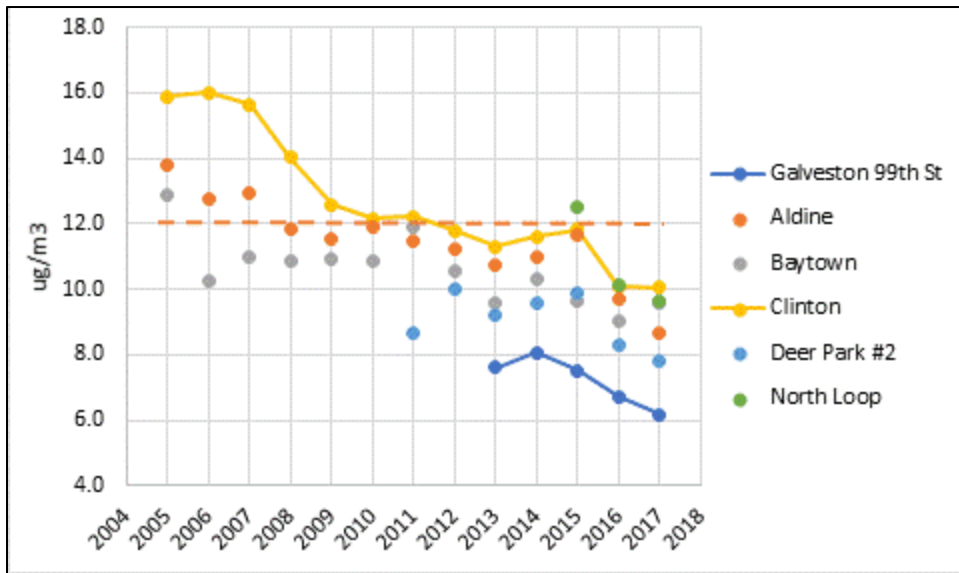
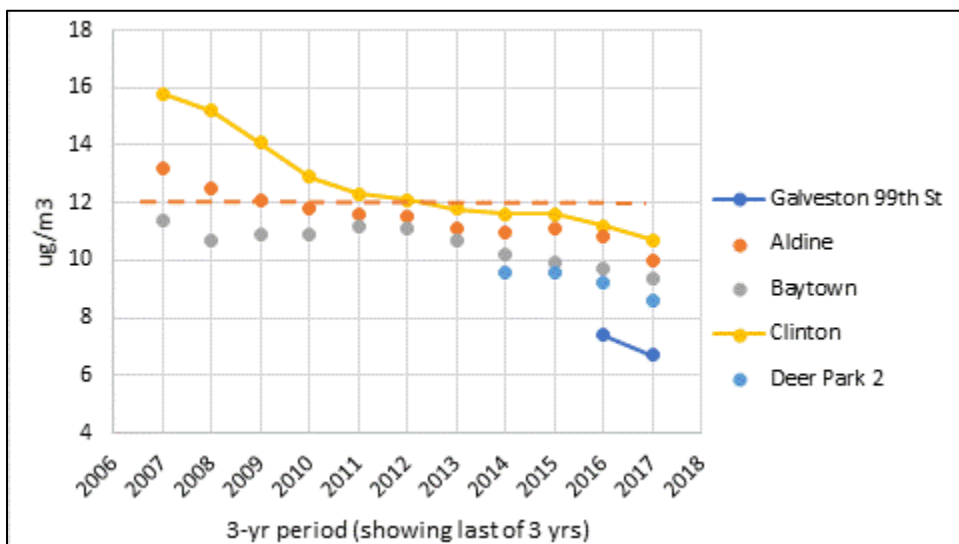


Figure 2. Annual average NAAQS design values for PM_{2.5} at TCEQ FRM sites, 2007 – 2017



2. Sampling Operations

No sampling problems have been observed under the current project extension. Sampling under this project ended on March 31, 2018. On April 26, 2018, the Galveston PM_{2.5} sampler was returned to the TCEQ Building B in Austin.

The EPA sampling schedules for 2017 and 2018 appear in Figure 3 and Figure 4, and were downloaded from <http://www.epa.gov/ttnamti1/calendar.html>, accessed May 2018. Calendars from earlier years are also available at this Website. UT had been responsible for the Galveston sampling, which had occurred as follows:

- Every sixth-day samples were taken at the Clinton Dr. and Galveston 99th Street sampling sites from October 2, 2014 through March 31, 2015.
- Every day sampling at Clinton Dr. and Galveston began on Wed. April 1, 2015 and ended September 30, 2015.
- Every sixth-day samples are being taken at the Clinton Dr. and Galveston 99th Street sampling sites from October 1, 2015 to March 31, 2016.
- Every day sampling began again at Clinton Dr. and Galveston on Friday April 1, 2016 and ended September 30, 2016.
- Every sixth-day samples were taken at the Clinton Dr. and Galveston 99th Street sampling sites from October 1, 2016 to May 31, 2017.
- The current extension funded daily sampling to July 1, 2017 – September 30, 2017.
- Every 6th day sampling was conducted October 1, 2017 – March 31, 2018:

Figure 3. EPA 2017 sampling scheduling for filter and canister sampling. Dates coded in green and purple are every 6th day dates

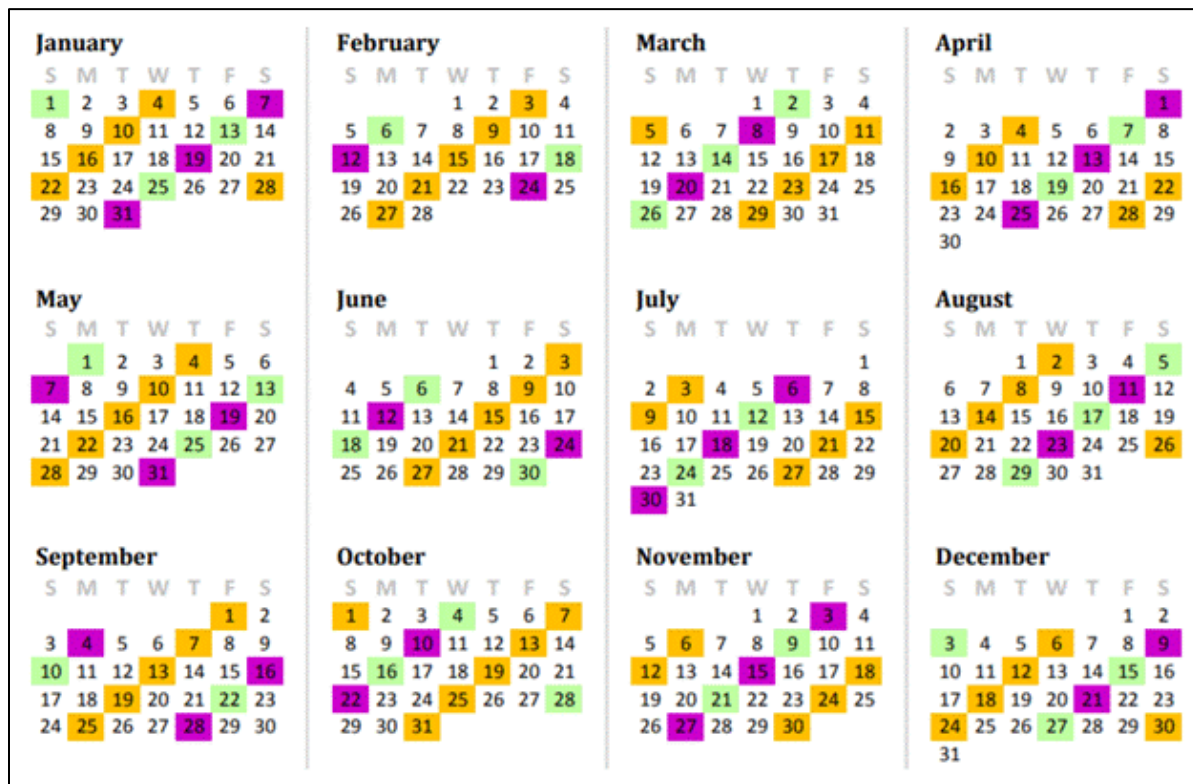
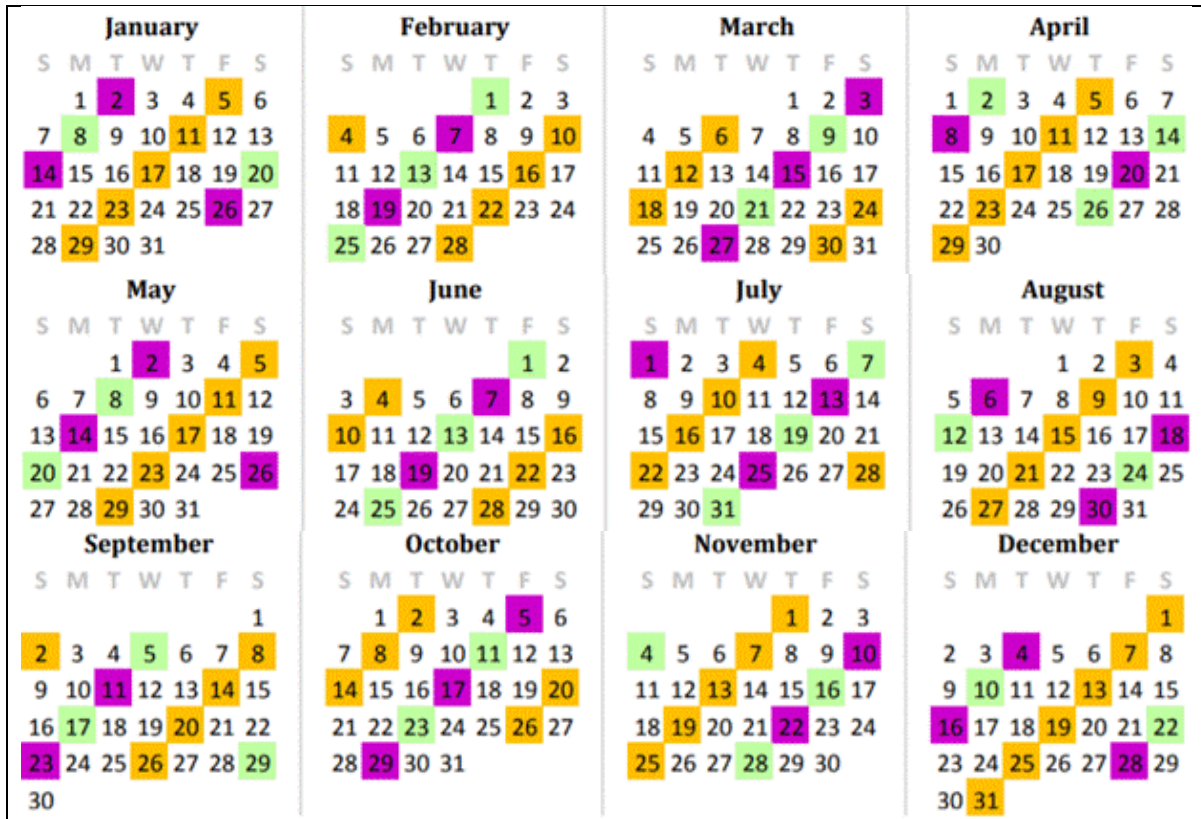


Figure 4. EPA 2018 sampling scheduling for filter and canister sampling. Dates coded in green and purple are every 6th day dates



3. Data Analysis Findings

3.1 Clinton Dr. Sampling Results

From January 2005 through June 2016, some 1,469 valid samples were collected and speciated for ions, carbon fractions, and elements. Of these, 1,251 samples contained a complete set of valid species useful for multivariate data analysis. From 2010 and later, 788 samples had complete data, and were of use in this project to represent present local conditions. Several outliers have been excluded from analysis.

3.1.1 Clinton Dr. source apportionment

Statistical methods including principal component analysis (PCA), chemical mass balance (CMB), and positive matrix factorization² (PMF) have proven powerful in qualifying the contributions more precisely and from more source types.

CMB requires information on source composition as well as speciated ambient concentration data. PCA only requires speciated ambient concentration data, but source solutions are limited. PMF uses both the speciated ambient concentration measurements and estimated uncertainties in the measurements in an interactive process in which a user guesses at the number of source factors, as in classical factor analysis (FA), and continually refines the model until diagnostics point to an optimal solution. PMF decomposes a matrix of speciated sample data into two matrices: a factor contributions matrix and a factor profiles matrix. The speciated data set comprises a matrix X with rows for dates and columns for species, with n rows for the number of data points and m columns for the number of species. The user selects a number of factors p that contribute to the mix of measured concentrations, and PMF identifies the optimal signature or profile f of each source, and the amount of mass g contributed by each factor to each sample:

$$x_{ij} = \sum_{k=1,p} g_{ik} f_{kj} + e_{ij}, \quad i = 1, \dots, n, \quad j = 1, \dots, m$$

where e_{ij} is the residual for each sample/species. Other constraints exist in the model to limit the extent of negative values for estimated source contributions. Subject to the constraints, PMF minimizes the objective function Q given by:

$$Q = \sum_{i=1,n} \sum_{j=1,m} [e_{ij} / u_{ij}]^2$$

where u_{ij} are the values for the uncertainty matrix.

The interpretation of the factors is left to the user. Experience and past research findings help assign the factors to known real-world sources. For example, elemental potassium (K) is often related to burning; elemental silicon (Si) and aluminum (Al) are related to crustal material (soil); sulfate (SO_4^{2-}) and ammonium (NH_4^+) are ion pairs from ammonium sulfate ($(\text{NH}_4)_2\text{SO}_4$) that forms in the air downwind of sulfur dioxide and ammonia emission sources.

As noted above, PMF uses both the concentrations matrix X and the estimates of uncertainty in each concentration. These uncertainties may be calculated at the laboratory where the chemical analysis on filter samples was conducted or estimated by a data user who has access to the published method detection levels and an estimated percentage error per sample. The data collected in this project has an uncertainty assigned to each species in each sample by the

² Paatero, P.; Tapper, U. (1994). Positive matrix factorization: A non-negative factor model with optimal utilization of error estimates of data values. *Environmetrics*, 5: 111-126.

Reff, A.; Eberly, S.I.; Bhawe, P.V. (2007). Receptor modeling of ambient particulate matter data using positive matrix factorization: Review of existing methods. *J. Air Waste Manage. Assoc.*, 57(2): 146-154.

laboratory that derived the concentrations. The PMF application assesses the statistical behavior of data variability relative to the estimated uncertainty in each datum, and suggests which species have adequate information content in the form of a signal-to-noise ratio (SNR). Omitted species have SNRs close to 0.0 (e.g., magnesium, europium, terbium elements), were judged to be redundant (sulfur element), or had median values of 0, suggesting low information content. There is some double counting or redundancy in using both the potassium element and potassium ion, but they appear to contain different information.

The key indicator for PMF performance is a goodness of fit parameter denoted “Q” that is total sum of uncertainty-scaled residuals. Two Q values are calculated in a model run: one using all data labeled Q(true) and one run excluding some model-identified outlier points labeled Q(robust). A good model should have the Q value derived from the input parameters (number of factors and number of parameters to be estimated in the model) close to Q(true) and to Q(robust). The derived value of Q is given by

$$Q = n*m - p*(n + m)$$

For this study, UT conducted a wide range of PMF runs varying the number of factors, the species included in the model, and the level of uncertainty assigned to species. Small rotations of the PMF solution can be tried to get more robust separation between factors (FPEAK). With a small FPEAK, trial solutions were rerun in the PMF 5.0 FPEAK Bootstrap mode to assess solution stability and robustness.

For this project, UT performed many PMF runs varying the number of factors, the species included in the model, and the levels of uncertainty assigned to species. In the last set of PMF runs in May 2018, trial solutions were rerun in the PMF 5.0 FPEAK and Bootstrap modes. In some earlier runs, only every-sixth day samples from January 2010 to June 2016 were used. There are 395 every-sixth day dates between January 1, 2010 and July 1, 2016. These results are presented below. For the most recent runs, all available data excepting some outlier observations were used. The final PMF runs used 774 of the 788 observations. These results are also presented below. Dates deliberately excluded from PMF were days near July 4 (Independence Day) and December 31 (New Year’s Eve) owing to the presence of elevated potassium indicating celebratory fireworks and few additional days with very unusually high concentrations of one or two species. Table 1 lists the species used in the PMF runs. Total mass (MSG) was also used to facilitate estimating the gravimetric mass of derived PMF factors.

It should be noted that the current Clinton Dr. data set has no ion data from December 23, 2015 through March 13, 2016, losing a significant portion of the most recent data.

Table 1. Twenty-one species used in Clinton Dr. PMF runs (Total mass also used)

Species	Variable name
Nitrate ion	N3I
Sulfate ion	S4I
Ammonium ion	N4I
Sodium ion	NAI
Potassium ion	KPI
Organic carbon (OC)	OCT
Elemental carbon (EC)	ECT
Aluminum element	AL
Silicon element	SI
Chlorine element	CL
Potassium element	KP
Calcium element	CA
Titanium element	TI
Vanadium element	VA
Manganese element	MN
Iron element	FE
Nickel element	NI
Copper element	CU
Zinc element	ZN
Bromine element	BR
Strontium element	SR

A set of the 10 factors profiles from having run the PMF program on 774 samples from 2010 to early 2016 appears in Table 2, and the time series of the factor strengths appear in Table 3.

The bootstrap runs on the 10 factor, 21 species, 774 sample run had excellent bootstrap reproducibility, with 200 out of 200 correct match-ups for all 10 factors using a 0.8 correlation required for a match. The default correlation for match-ups is 0.6. An FPEAK rotations of -0.5 provided a simpler final result. Fingerprints for the 10 factors are found in Figure 5 through Figure 14. These graphs illustrate the best tracer species for each factor, but should not be interpreted to suggest which species comprise the highest mass in each factor. For example, although Zinc is a good tracer for light duty vehicles, the Zinc concentrations are much lower than, say, EC and OC, which actually comprise most the mass in the LDV factor.

Figure 15 shows the approximate apportionment of factors to total mass at Clinton Dr. This is approximate, given the fact that the mass of crustal factor derived does not take into account the mineral formulae associated with elements, and some organic carbon and nitrate may be underestimated in the masses reported. Overall, however, in the range of 1 $\mu\text{g}/\text{m}^3$ of total mass is added by crustal material that has its largest impact in the summer, and evidence is provided in Section 3.1.6 North African Dust Affecting Clinton Dr. of this report that much if not most of this crustal material is of North African origin.

Table 2. Factors found from using 2010 – 2016 Clinton Dr. data excluding special events and some outliers

Factor number	Suspected Factor	Key species
1	Oil Combustion	Vanadium, Nickel
2	Heavy duty motor vehicle (HDV)	EC, OC, Manganese, Nickel, Iron, Copper
3	Calcium mineral	Calcium
4	Sea Salt	Chlorine, Sodium ion
5	Sodium Sulfate	Sodium, Sulfate ion
6	Fires	Potassium, Potassium ion, OC, EC, Bromine
7	Crustal	Silicon, Aluminum, Iron, Titanium
8	Ammonium Sulfate	Sulfate ion, Ammonium ion
9	Ammonium Nitrate	Nitrate ion, Ammonium ion
10	Light duty motor vehicle (LDV)	Zinc, OC, EC

Figure 5. Oil combustion fingerprint, 774 samples, % of species attributed to this factor

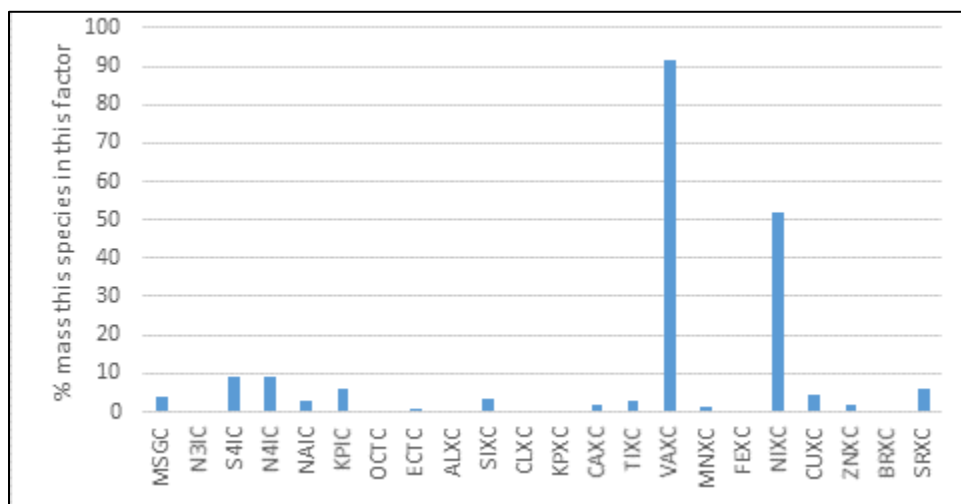


Figure 6. Heavy duty vehicle (HDV) fingerprint, 774 samples, % of species attributed to this factor

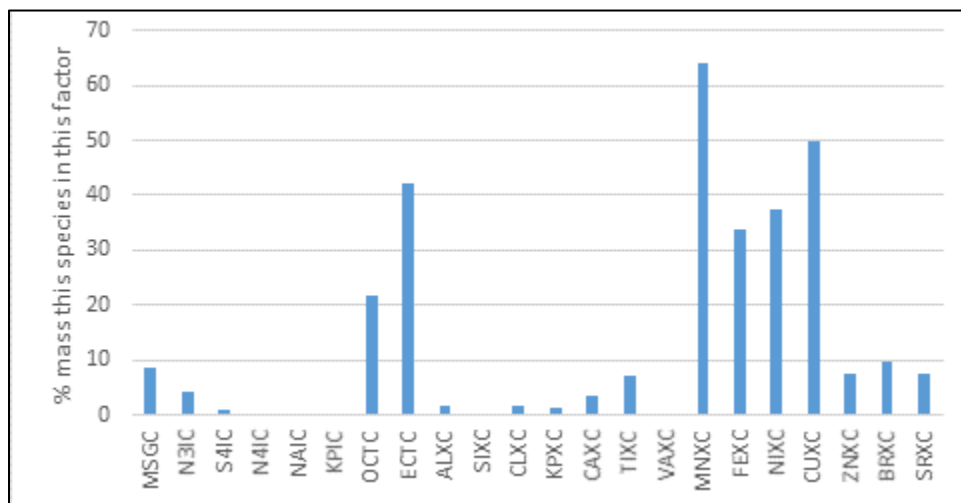


Figure 7. Calcium fingerprint, 774 samples, % of species attributed to this factor

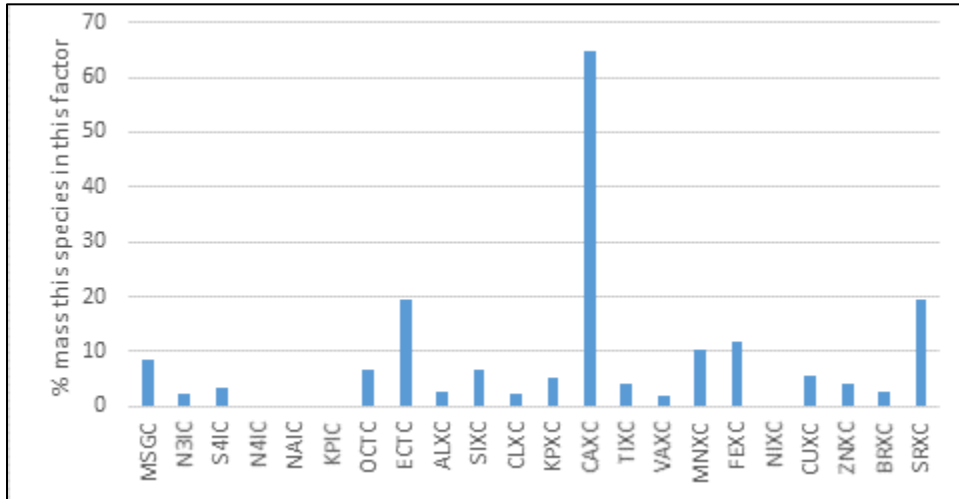


Figure 8. Sea Salt fingerprint, 774 samples, % of species attributed to this factor

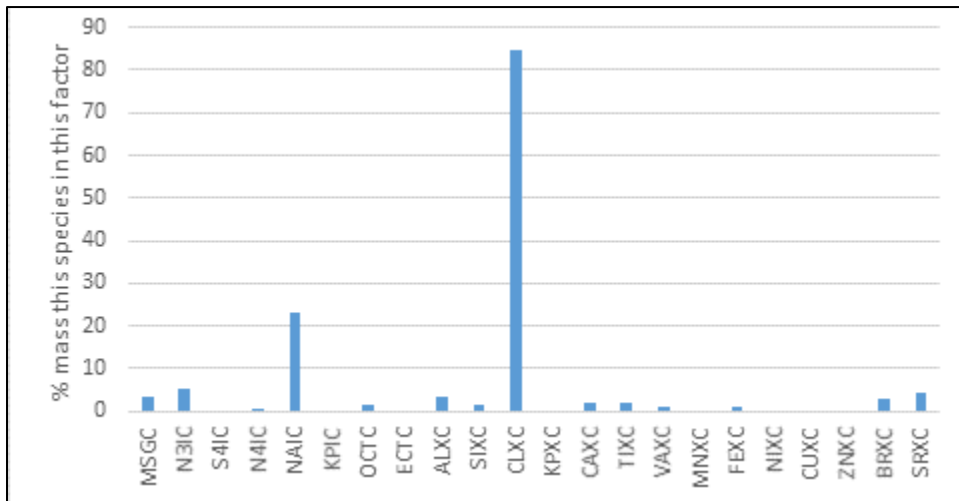


Figure 9. Sodium Sulfate fingerprint, 774 samples, % of species attributed to this factor

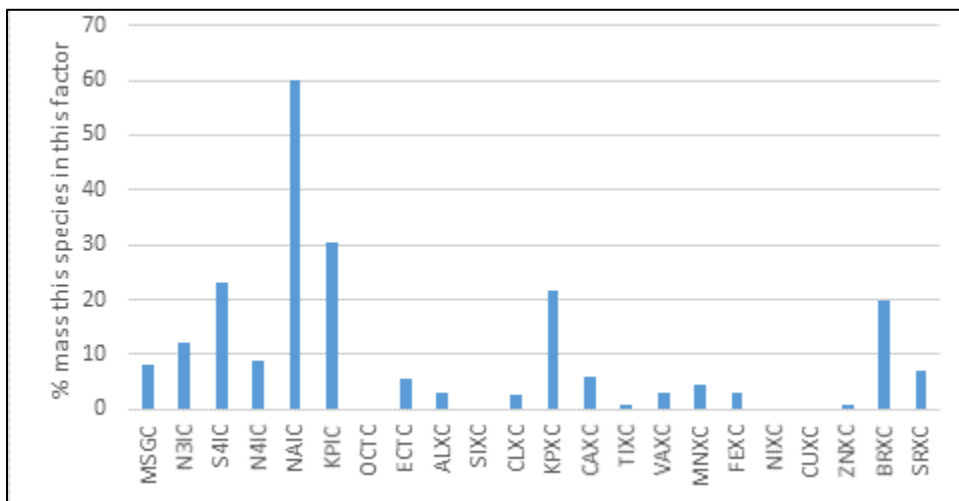


Figure 10. Fire fingerprint, 774 samples, % of species attributed to this factor

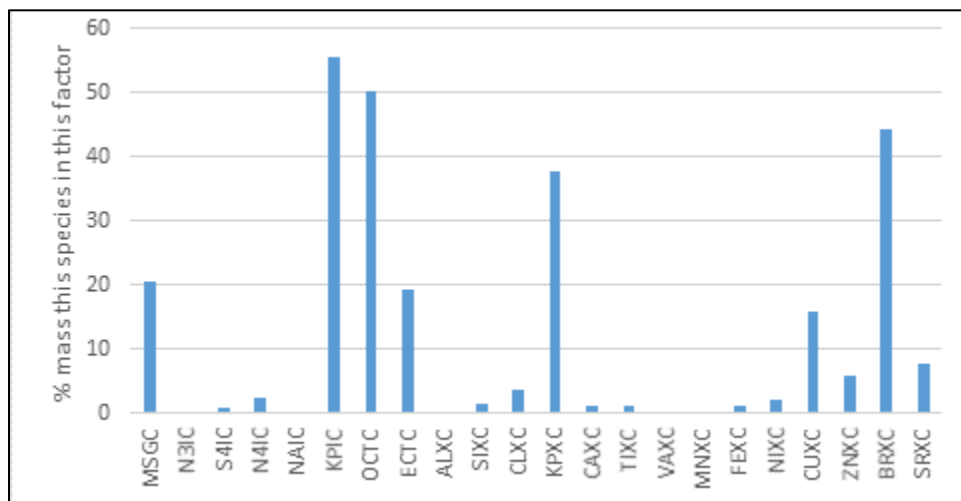


Figure 11. Crustal fingerprint, 774 samples, % of species attributed to this factor

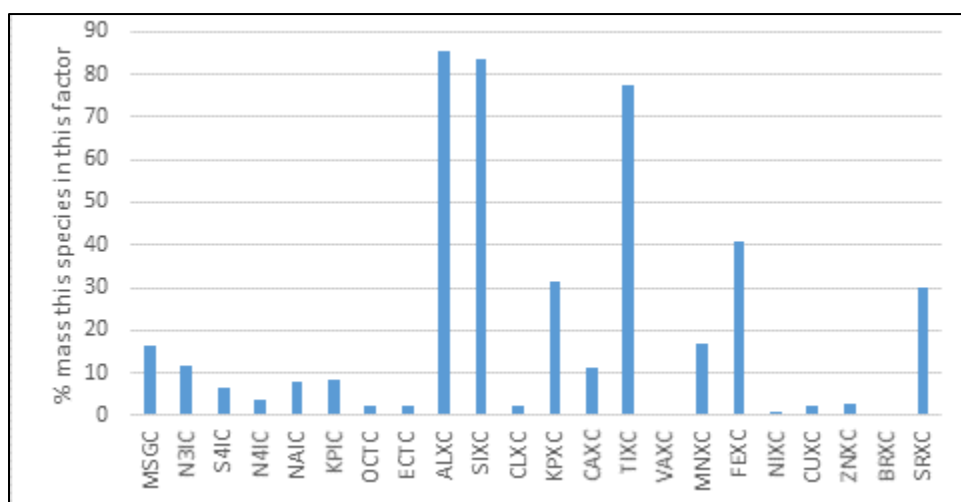


Figure 12. Ammonium Nitrate fingerprint, 774 samples, % of species attributed to this factor

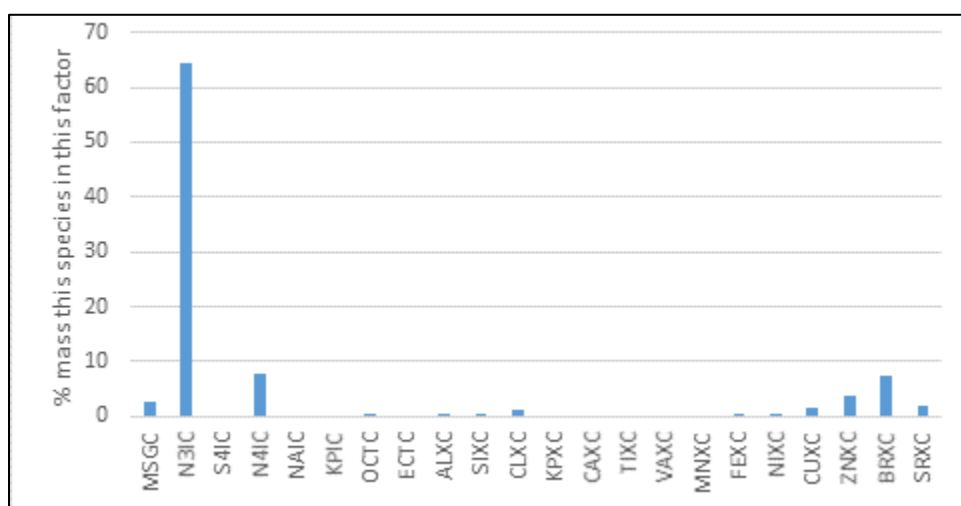


Figure 13. Ammonium Sulfate fingerprint, 774 samples, % of species attributed to this factor

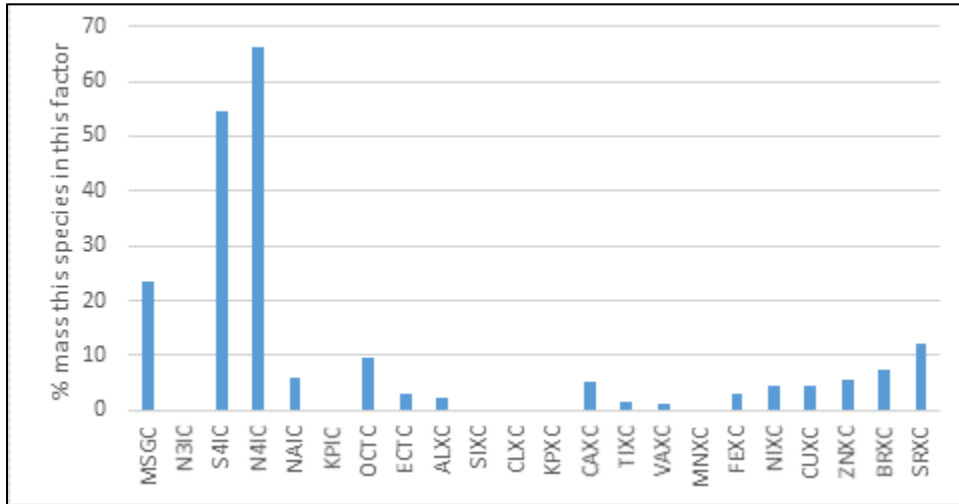


Figure 14. Light duty vehicle (LDV) fingerprint, 774 samples, % of species attributed to this factor

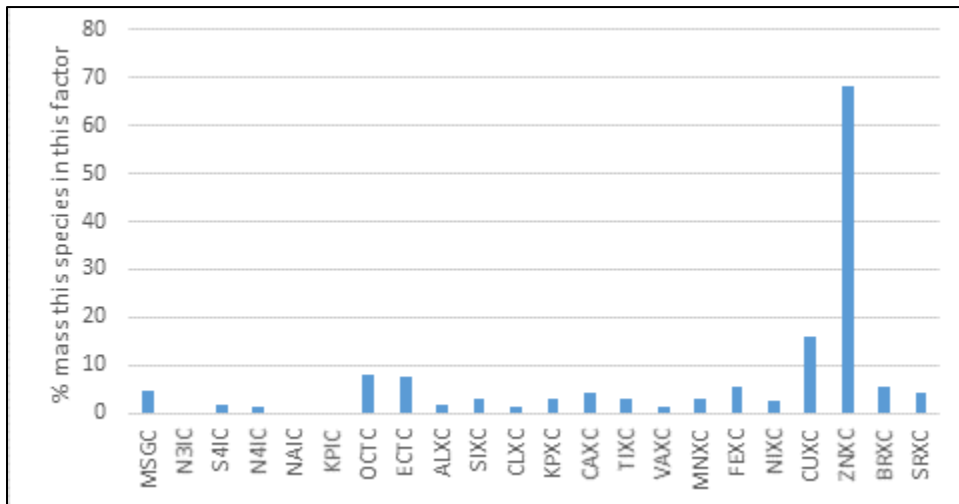
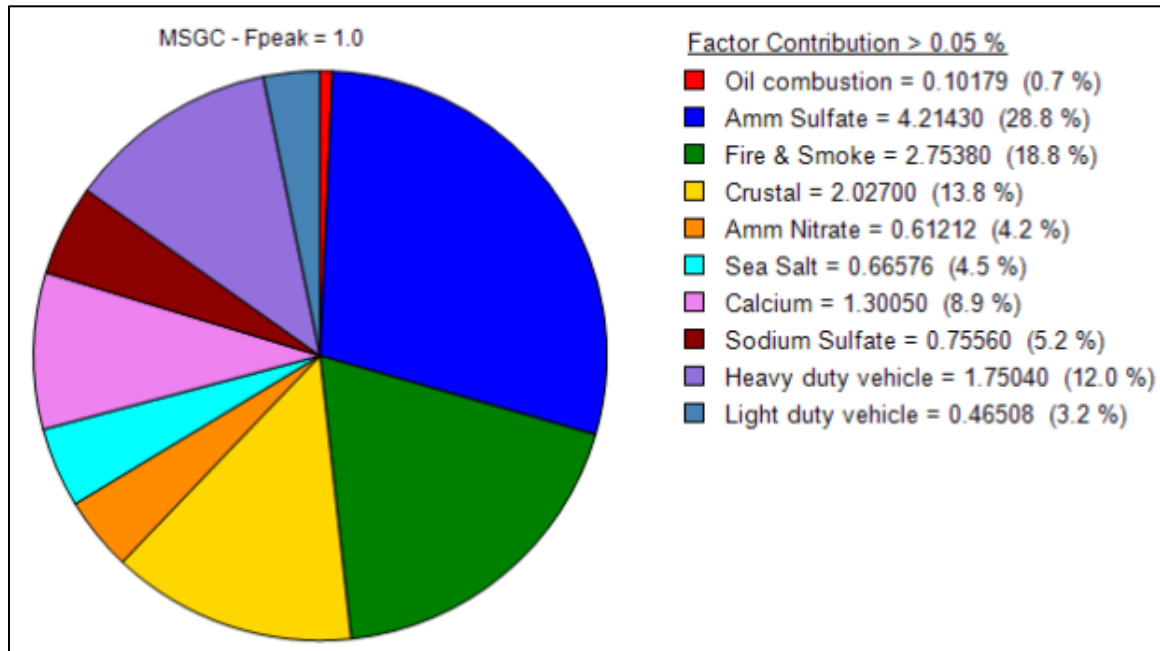


Figure 15 Approximate apportionment of factors to total mass at Clinton Dr.



3.1.2 Characterization of factors by wind direction and day of week

In order to look at the typical sets of days, as opposed to days known to have higher than average concentrations, analysis was performed on every-6th day samples, which basically creates a random selection of the total PM_{2.5} concentration distribution. As was noted earlier, between January 1, 2010 and July 1, 2016 there are 395 every-6th day samples.

Figure 16 shows the average total PM_{2.5} mass from every-6th day samples by wind direction in a radar plot. A radar plot shows the x-variable as the points around the circumference of a circle, as are distributed the hours on the face of a traditional analog clock or the directions on the face of an analog compass. The y-variables are distributed along the hands of the analog clock, so that the y-value is the distance from the center of the graph as a function of the x-value around the circumference.

The PM_{2.5} samples are taken over a 24-hour period, whereas wind direction speed are measured nearly continuously, with five-minute time scale values stored and rolled up to one-hour averages. To perform this analysis of PM_{2.5} mass and factors by wind direction, the following steps were taken.

1. Hourly wind direction data were merged with daily PM_{2.5} mass and factors data, so that each day's PM_{2.5} and factor record was matched to 24 wind direction records.
2. For each hourly record, a kernel smoothing algorithm was applied to increase the number of data records, in effect, spreading out the wind direction with many (20) observations tagged with the actual measurement, and other observations added in linearly decreasing totals at one-degree steps out to +/- 20 degrees around each observation.
3. The data were sorted by integer wind direction and averaged by integer wind direction, with results plotted as in Figure 16.
4. Radar plots were also made without the kernel smoothing, and were compared to the kernel smoothed for a qualitative check on the method.

In Figure 16, the total PM_{2.5} mass associated with east-northeasterly winds average about 13 µg/m³ compares to only 9 µg/m³ under northerly winds. Note that in this analysis, wind speeds are not considered.

In addition to the directional analysis, this report also looks at day of the week effects. Data were categorized as "weekday" for Monday through Friday samples, and "weekend" for Saturday and Sunday samples. Recall that with every-sixth day samples, sequential samples are largely uncorrelated based on having been taken days apart. Figure 17 shows a comparison of the quantile-quantile plots for weekday and weekend samples, and the results of a Student's t-test assuming unequal variances for the null hypothesis that there is no difference between mean weekday and mean weekend values. Figure 17 shows that for total PM_{2.5} mass, weekday mean mass is statistically significantly higher than weekend mean mass.

Following Figures 15 and 16 are figures for the 10 factors. The wind directions associated with maximum average factor value are summarized in Table 3. The day-of-the-week effects are summarized in Table 4.

For the "Oil Combustion" factor, a map is also provided on which rays are laid corresponding to peak directions. A preliminary hypothesis is that ships operating or docked in the Houston Ship

Channel may be significant contributors to this factor. Heavy duty and light duty vehicle factors may be associated with nearby major roads to the west. Factors associated largely with natural sources (sea salt, sodium sulfate) or relatively distant sources (ammonium sulfate) show no significant day of the week effect. The oil combustion factor also shows no day of the week effect.

Figure 16. Clinton Dr. total mass factor by wind direction 2010 – 2016, every 6th day sampling

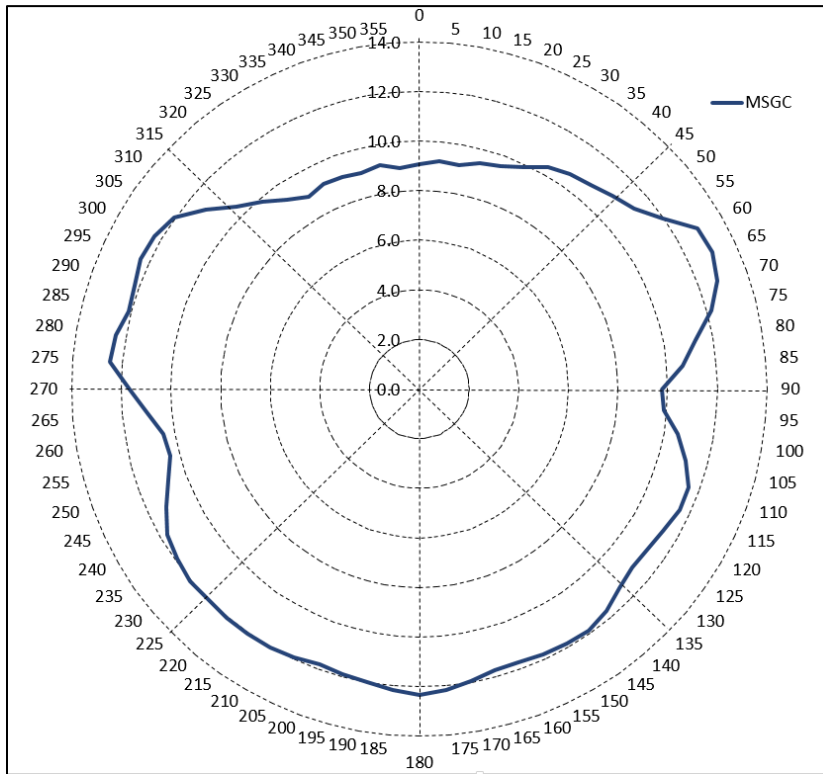


Figure 17. Total mass Student's t-test assuming unequal variances for weekend vs weekend, and weekend-weekday quantile plot → weekdays statistically significantly higher than weekends

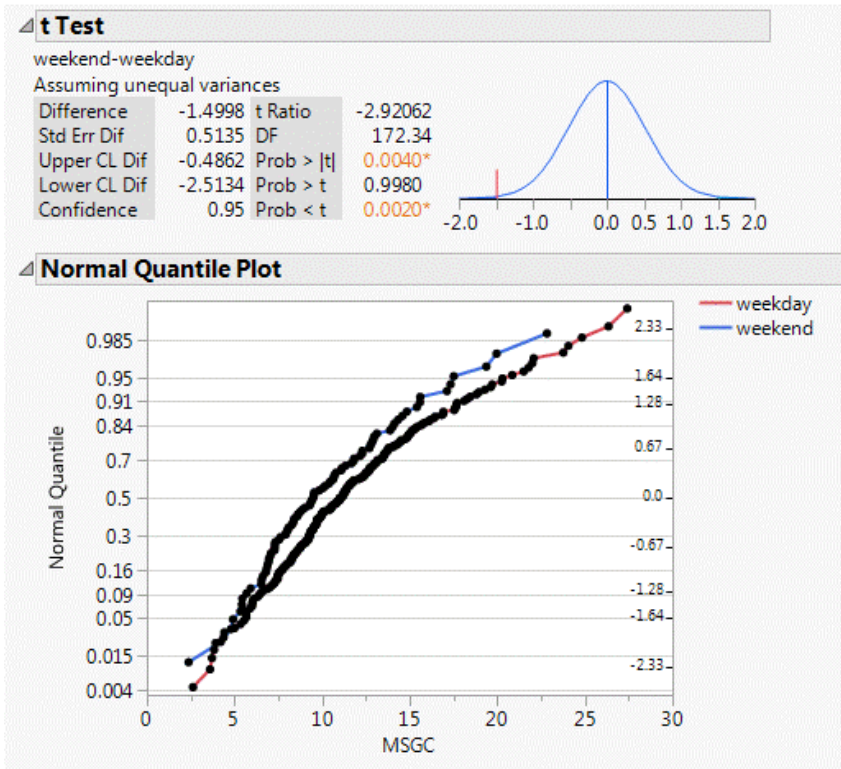


Figure 18. Clinton Dr. Oil-Combustion factor by wind direction 2010 – 2016, every 6th day sampling

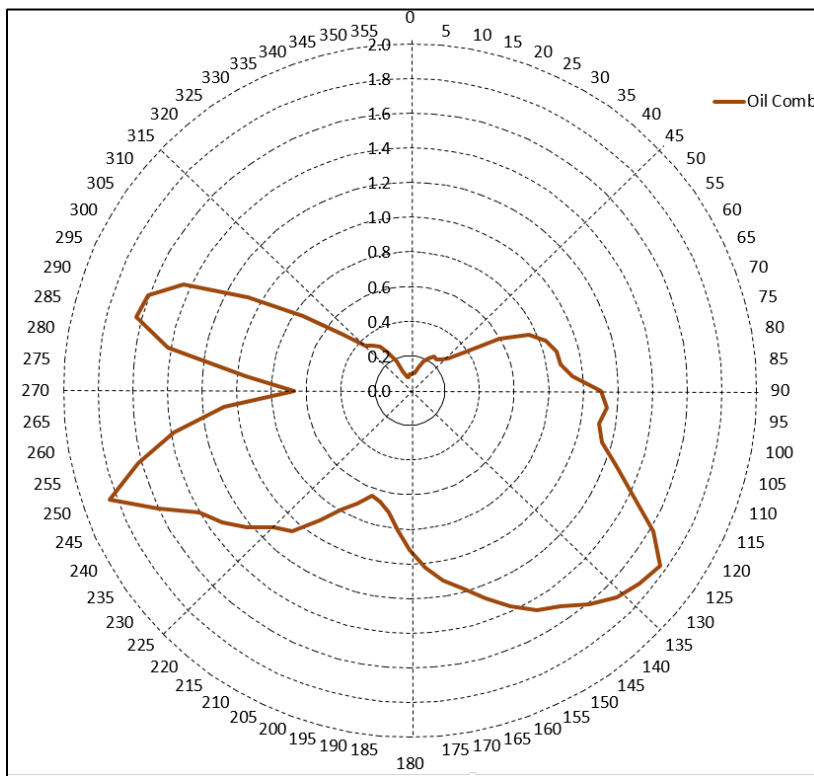


Figure 19. Directional rays for the highest contributions to the oil combustion factor at Clinton Dr.

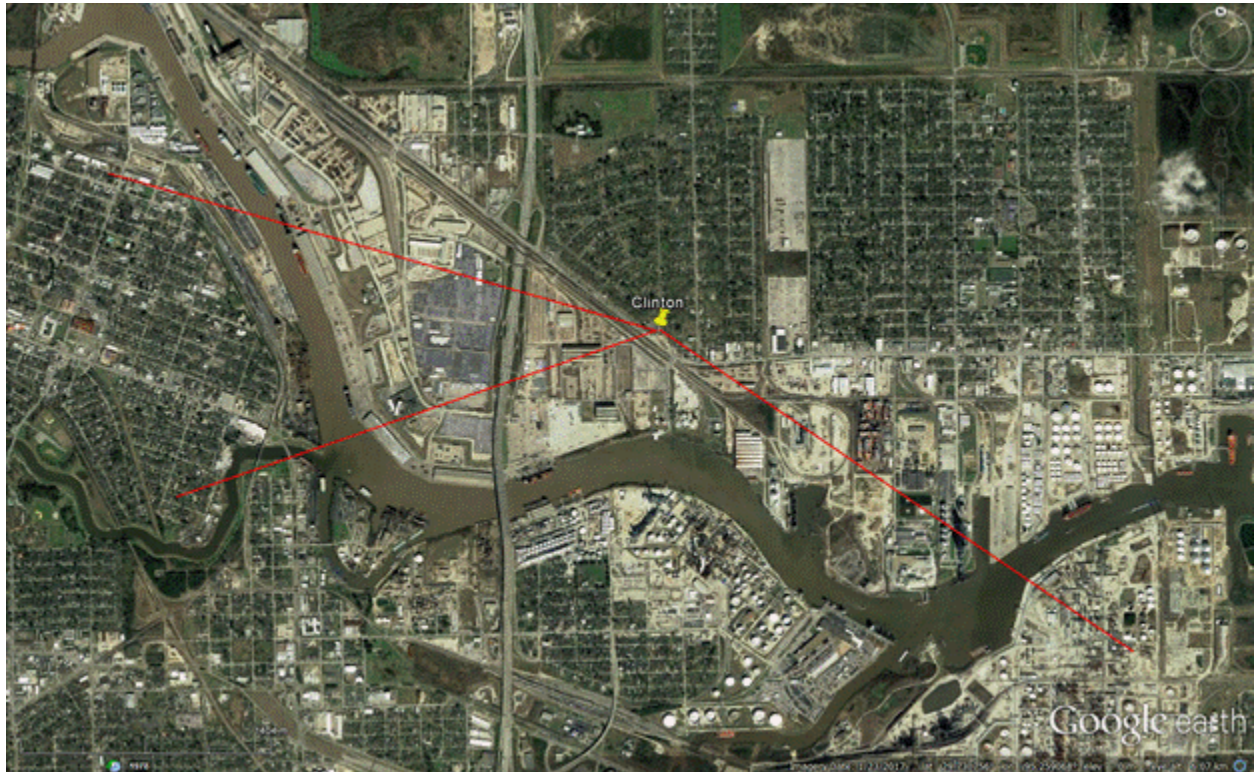


Figure 20. Oil Combustion every 6th day sampling factor t-test assuming unequal variances for weekend vs weekend, & weekend-weekday quantile plot → no statistically significantly difference weekdays vs weekends

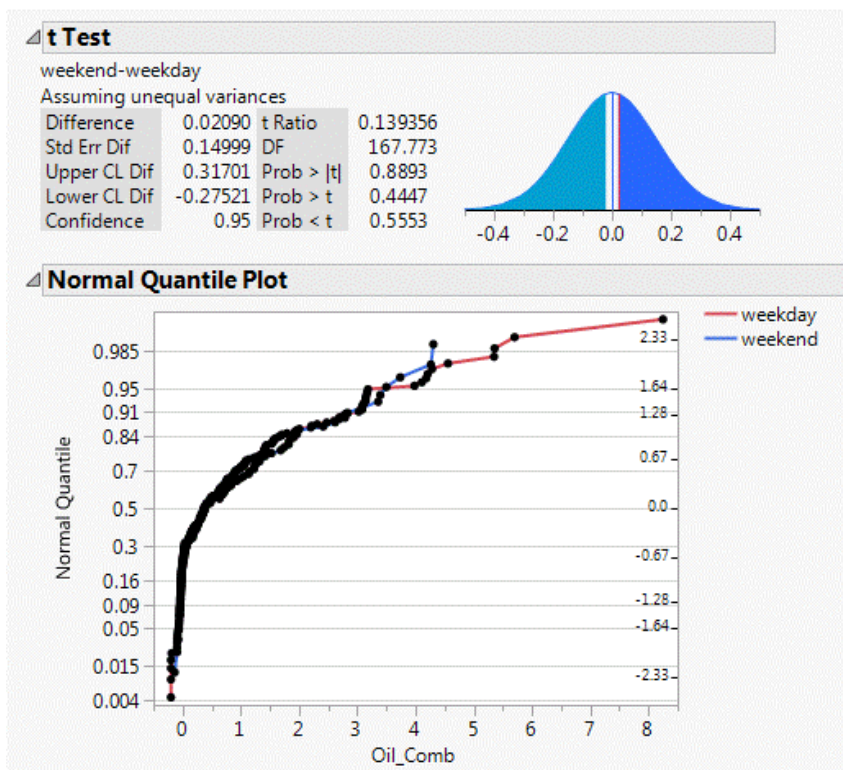


Figure 21. Clinton Heavy-duty Vehicle factor by wind direction 2010 – 2016, every 6th day sampling

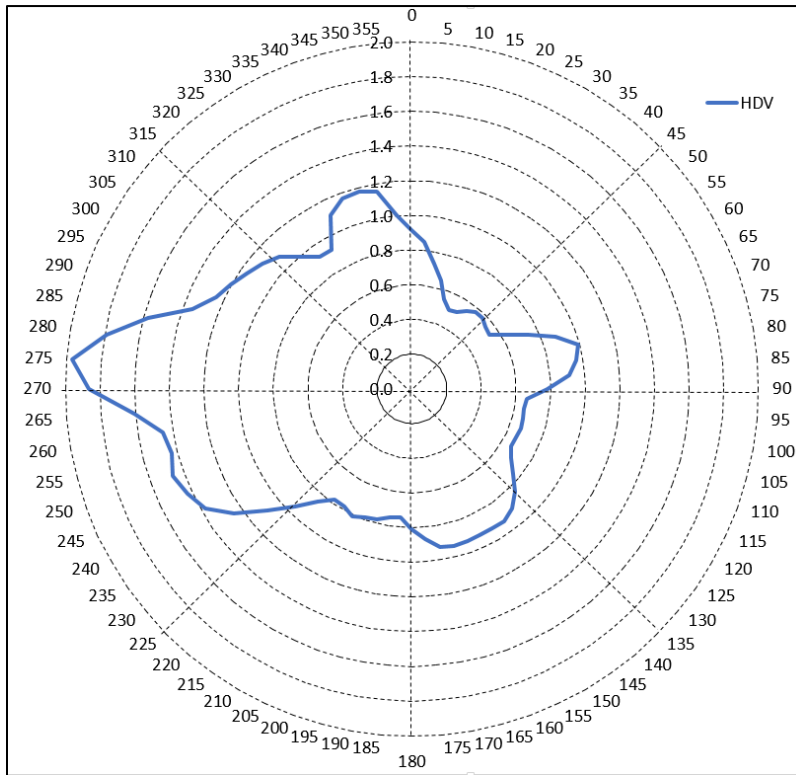


Figure 22. Heavy-duty Vehicle every 6th day sampling factor t-test assuming unequal variances for weekend vs weekend, & weekend-weekday quantile plot → weekdays statistically significantly higher than weekends

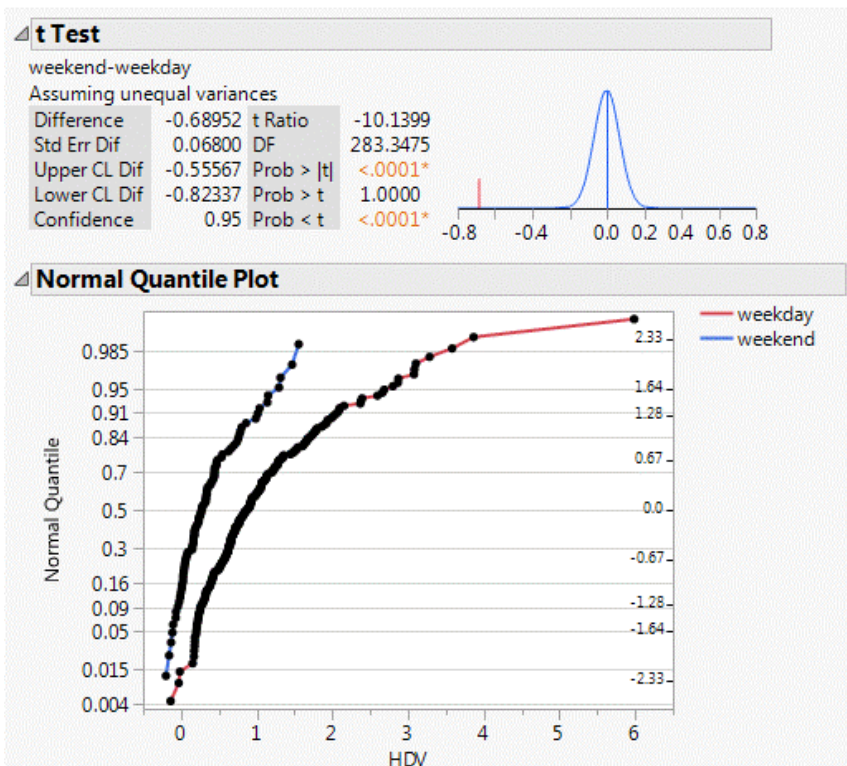


Figure 23. Clinton Dr. Calcium factor by wind direction 2010 – 2016, every 6th day sampling

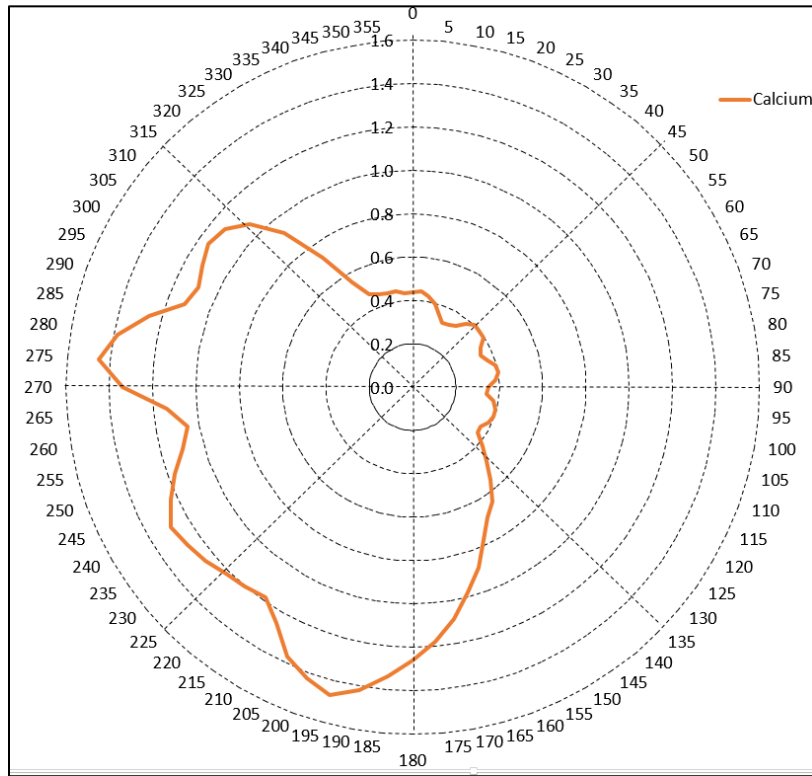


Figure 24. Calcium every 6th day sampling factor t-test assuming unequal variances for weekend vs weekend, & weekend-weekday quantile plot → weekdays statistically significantly higher than weekends

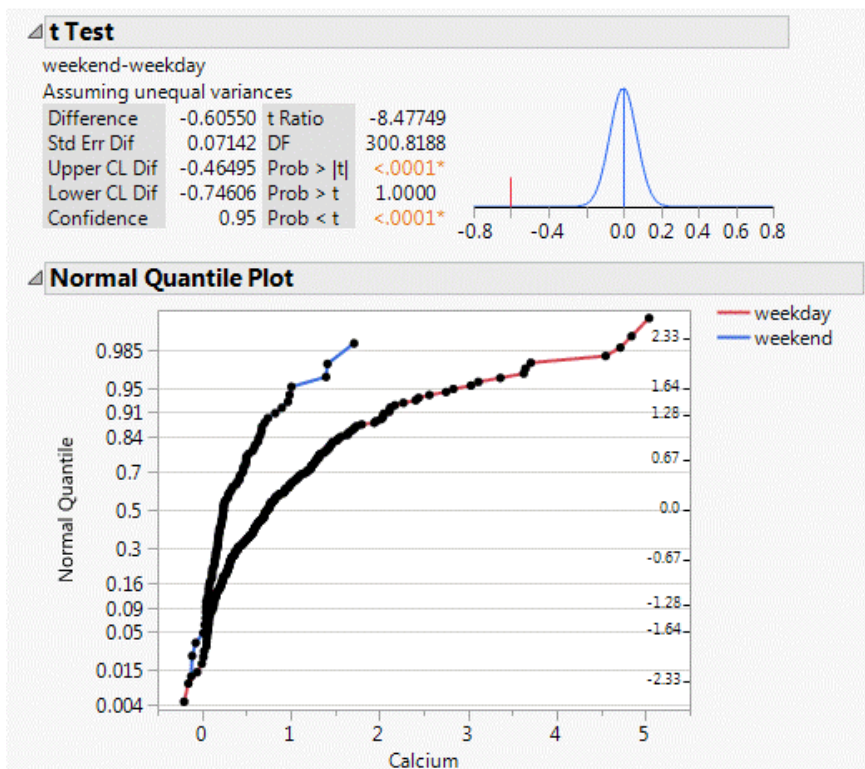


Figure 25. Clinton Dr. Sea Salt factor by wind direction 2010 – 2016, every 6th day sampling

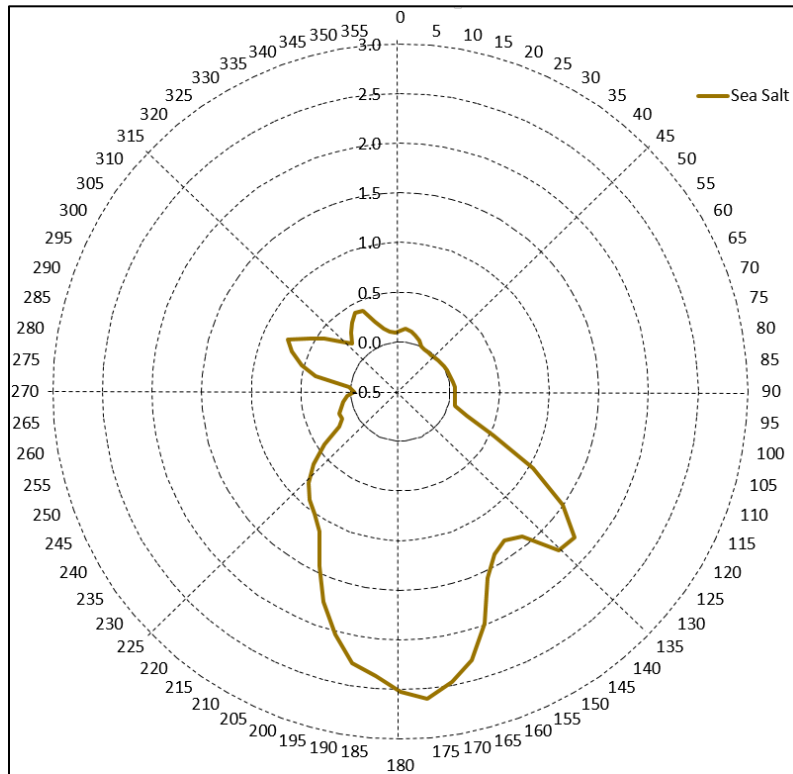


Figure 26. Sea Salt every 6th day sampling factor t-test assuming unequal variances for weekend vs weekday, & weekend-weekday quantile plot → no statistically significantly difference weekdays vs weekends

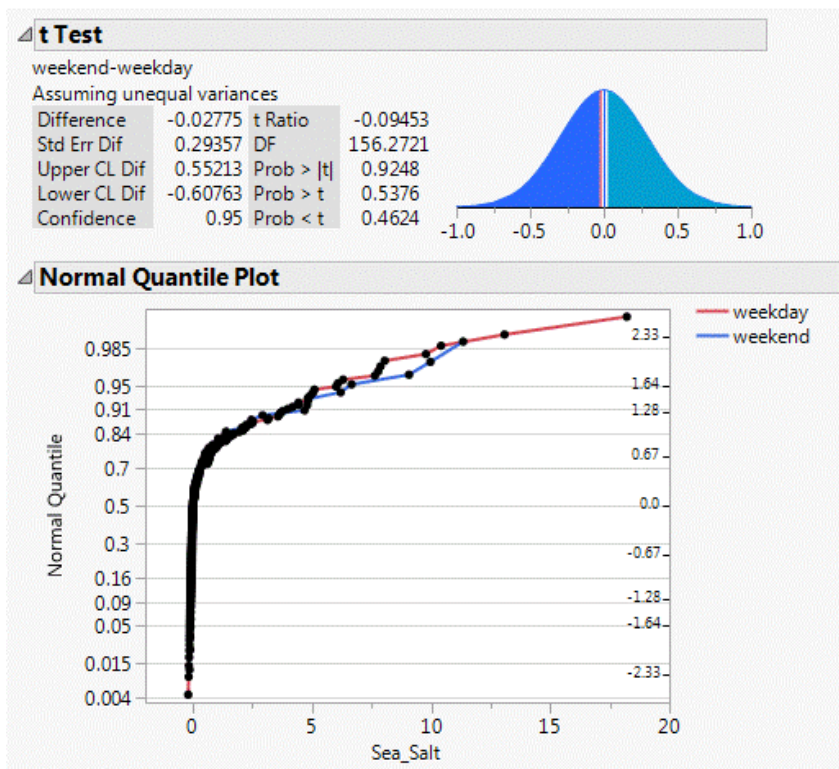


Figure 27. Clinton Dr. Sodium Sulfate factor by wind direction 2010 – 2016, every 6th day sampling

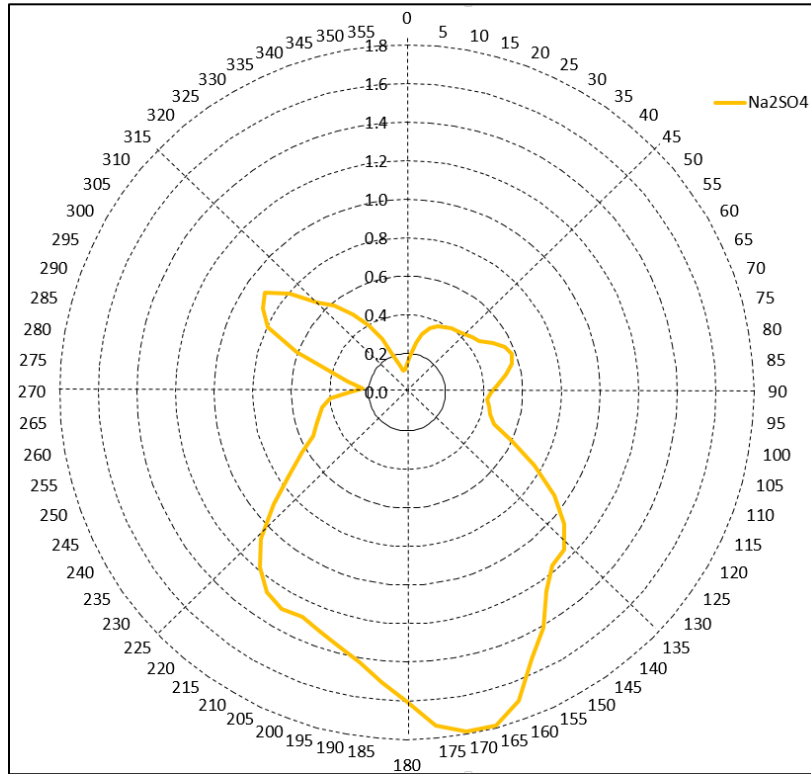


Figure 28. Sodium Sulfate every 6th day sampling factor t-test assuming unequal variances for weekend vs weekend, & weekend-weekday quantile plot → no statistically significantly difference weekdays vs weekends

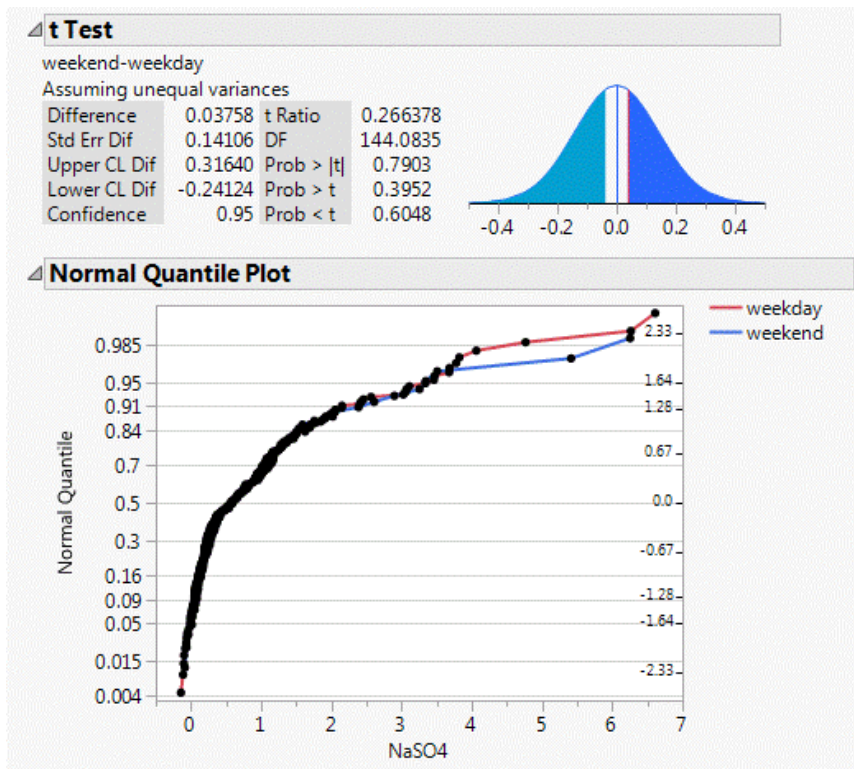


Figure 29. Clinton Dr. Fires factor by wind direction 2010 – 2016, every 6th day sampling

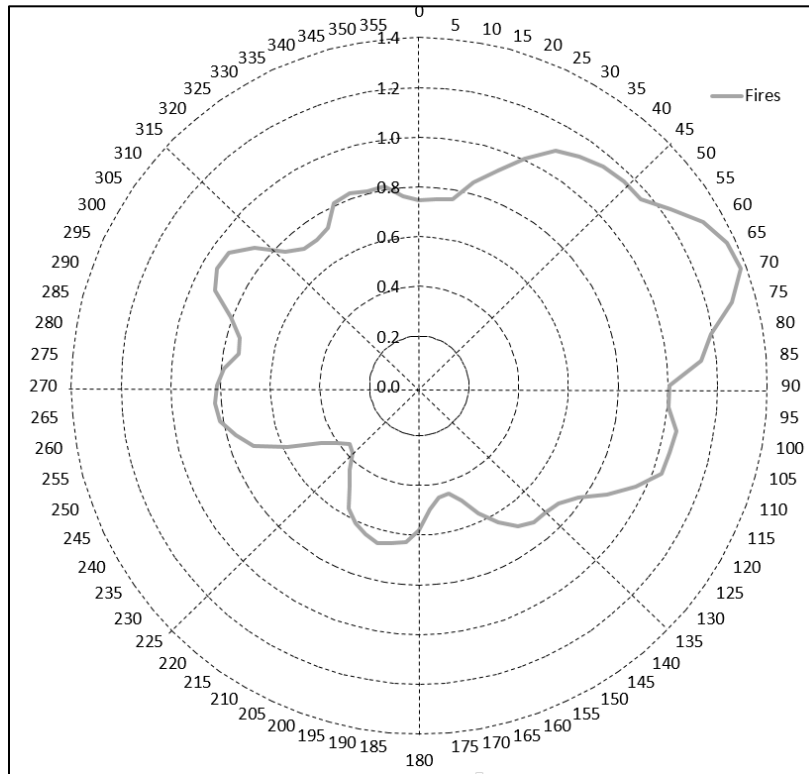


Figure 30. Fires every 6th day sampling factor t-test assuming unequal variances for weekend vs weekday, & weekend-weekday quantile plot → weekdays statistically significantly higher than weekends

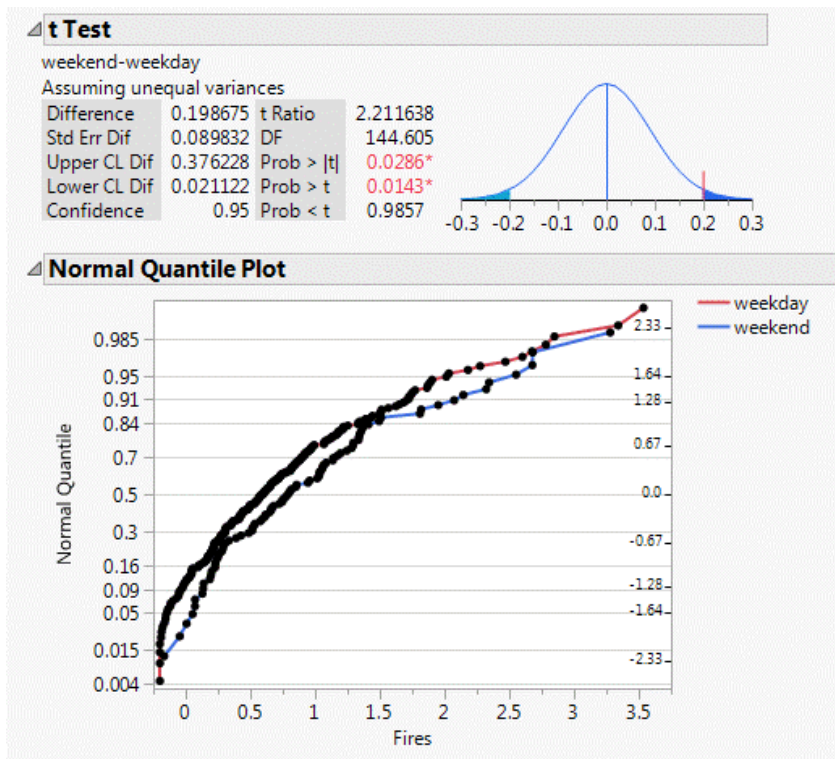


Figure 31. Clinton Dr. Crustal factor by wind direction 2010 – 2016, every 6th day sampling

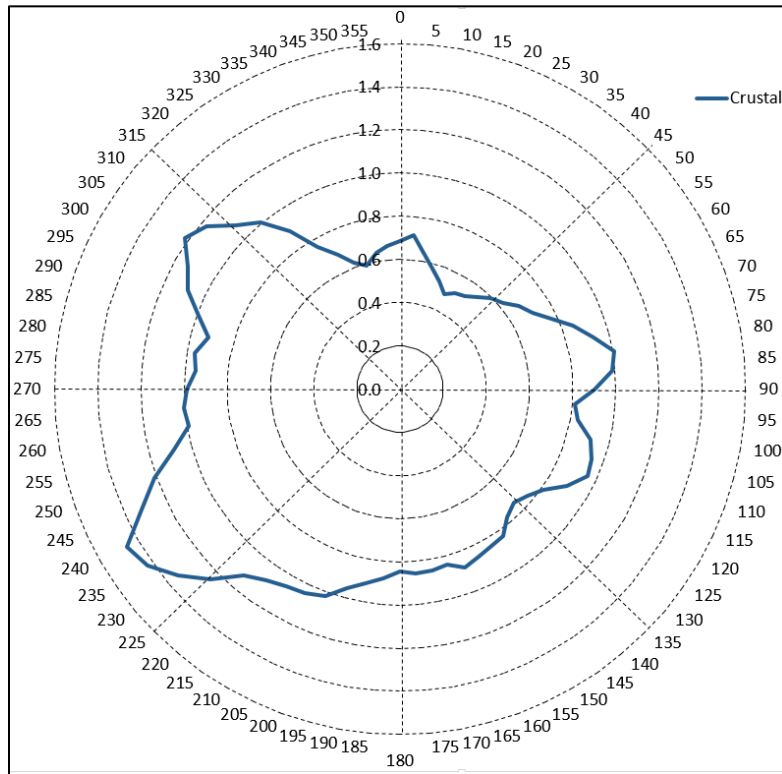


Figure 32. Crustal every 6th day sampling factor t-test assuming unequal variances for weekend vs weekday, & weekend-weekday quantile plot → weekdays statistically significantly higher than weekends

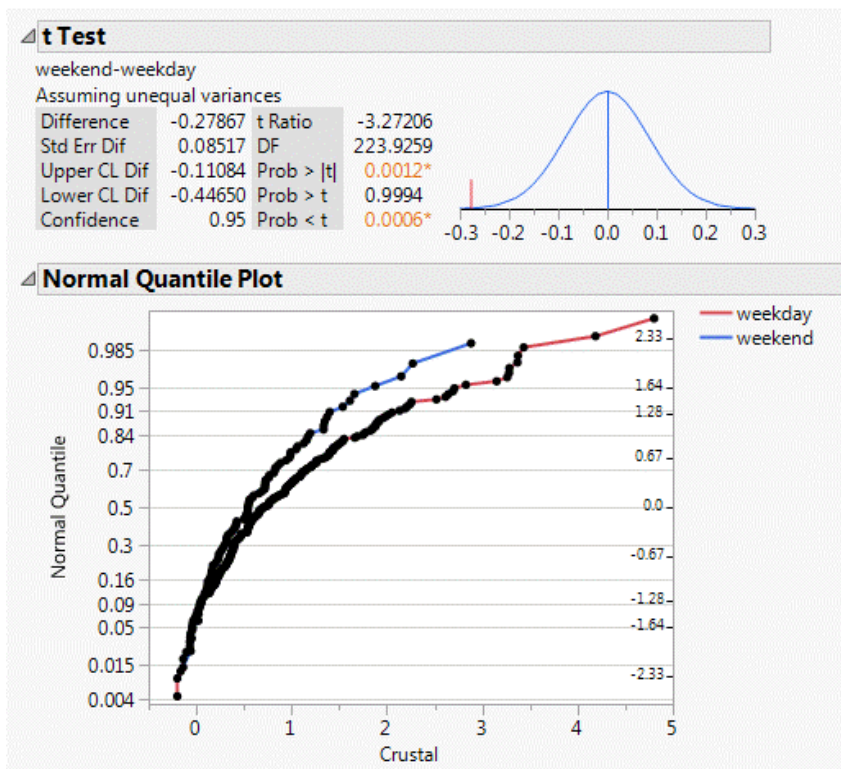


Figure 33. Clinton Ammonium Sulfate factor by wind direction 2010 – 2016, every 6th day sampling

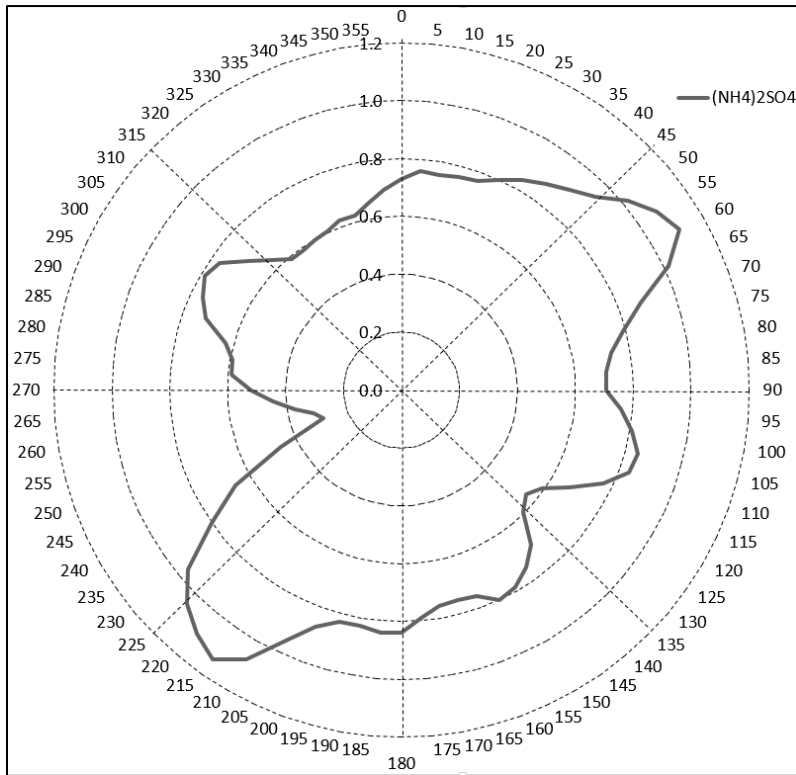


Figure 34. Ammonium Sulfate every 6th day sampling factor t-test assuming unequal variances for weekend vs weekend, & weekend-weekday quantile plot → no statistically significantly difference weekdays vs weekends

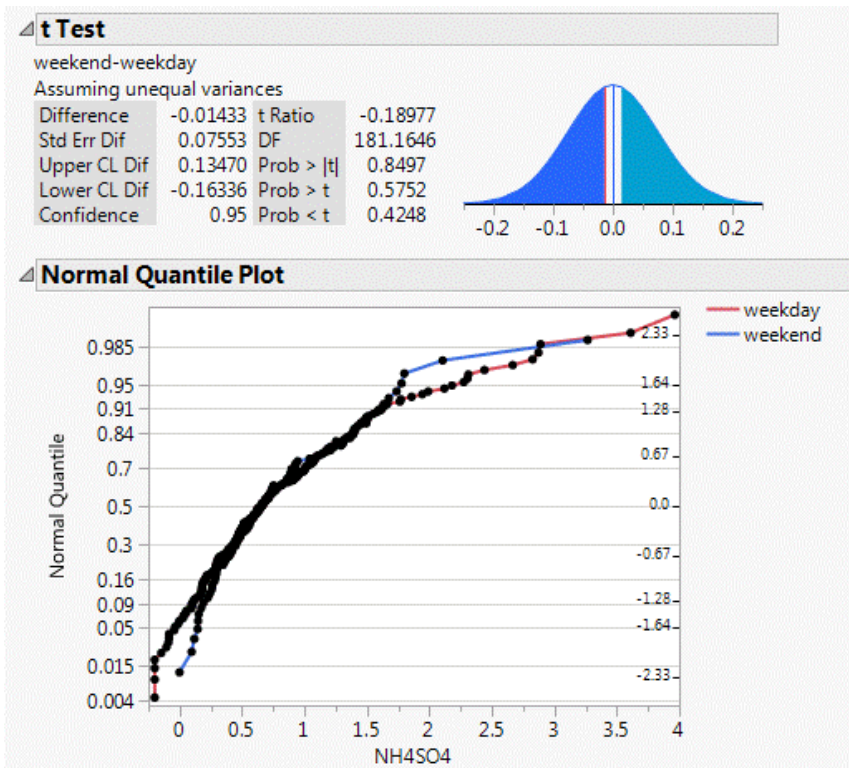


Figure 35. Clinton Ammonium Nitrate factor by wind direction 2010 – 2016, every 6th day sampling

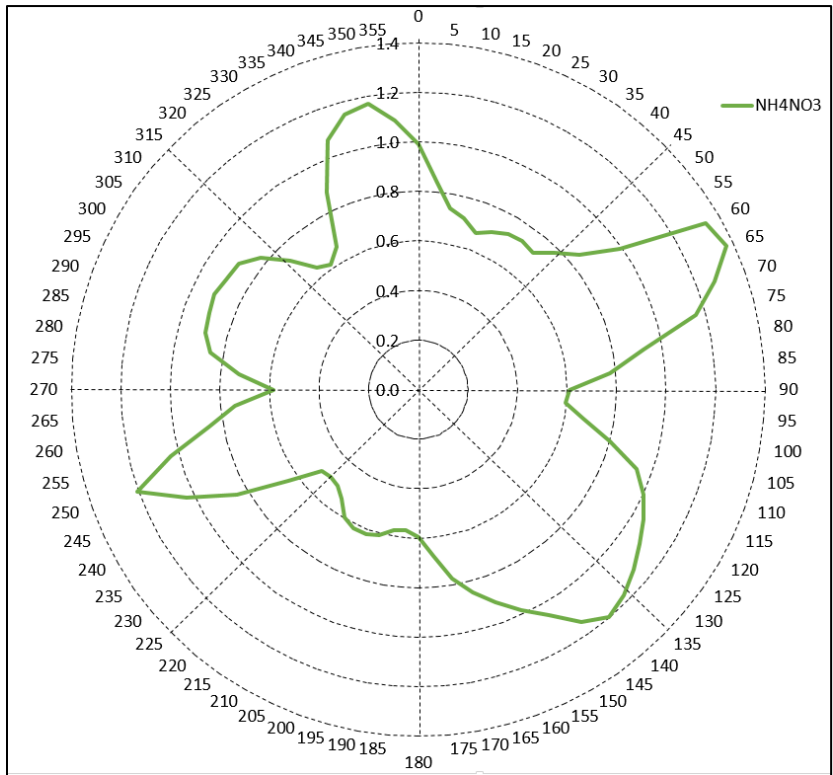


Figure 36. Ammonium Nitrate every 6th day sampling factor t-test assuming unequal variances for weekend vs weekend, & weekend-weekday quantile plot → weekdays statistically significantly higher than weekends

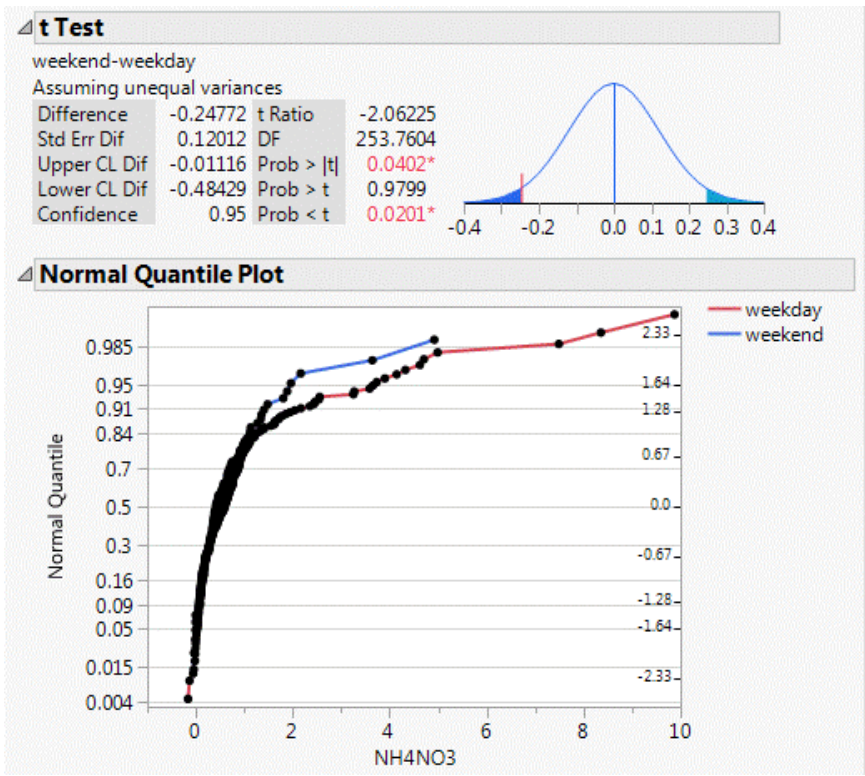


Figure 37. Clinton Dr. Light-duty Vehicle factor by wind direction 2010 – 2016, every 6th day sampling

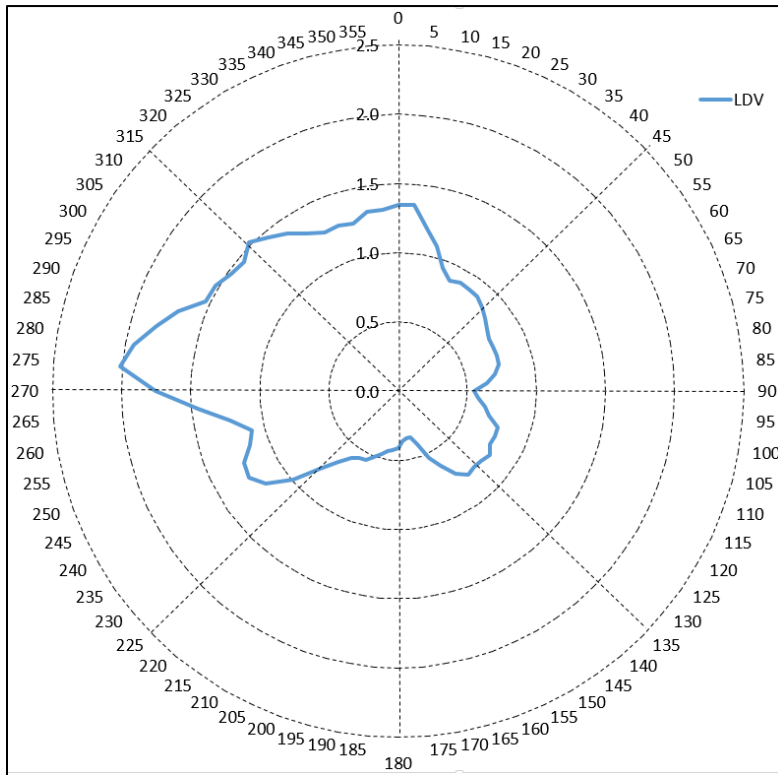


Figure 38. Light duty Vehicle every 6th day sampling factor t-test assuming unequal variances for weekend vs weekend, & weekend-weekday quantile plot → weekdays statistically significantly higher than weekends

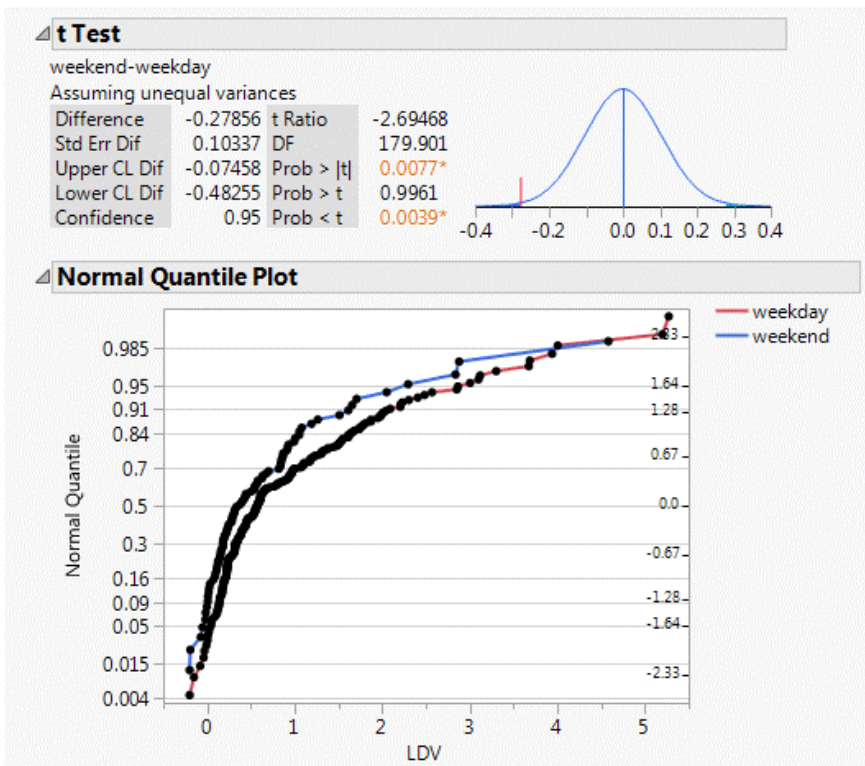


Table 3. Wind directions associated with peak factor averages

Factor	Species	Peak 1	Peak 2	Peak 3
	Total mass	61°		
1	LDV	277°		
2	Calcium	195°	275°	
3	Fires	69°		
4	NaSO4	167°		
5	HDV	273°		
6	NH4NO3	61°	and several others	
7	Crustal	238°		
8	Oil Comb	250°	124°	286°
9	(NH4)2SO4	214°	60°	
10	Sea Salt	175°		

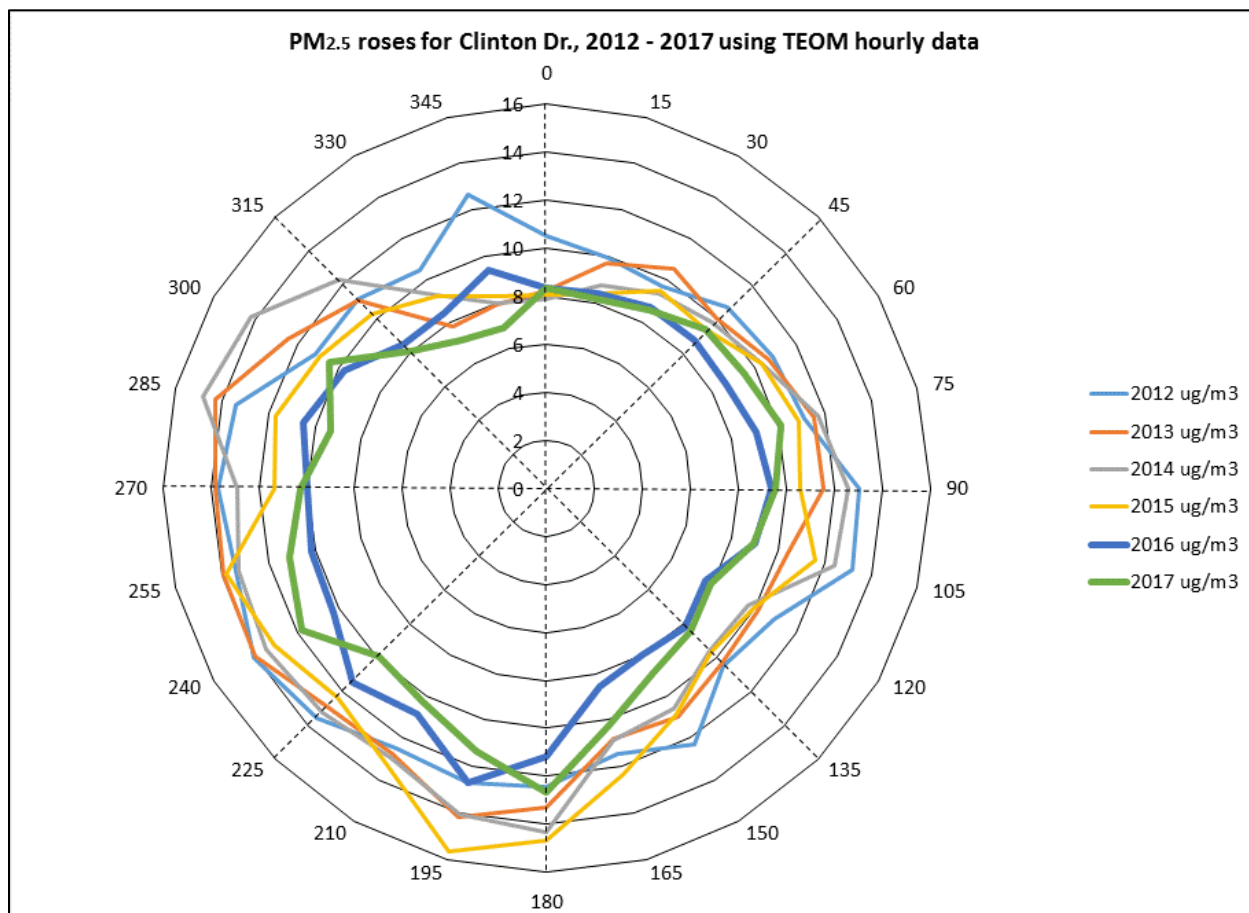
Table 4. Day of the week effect by factor using only every 6th day sampling

Factor	Species	Weekday > weekend	p-value
	Total mass	yes	0.0040
1	Oil Comb	no	
2	HDV	yes	<0.0001
3	Calcium	yes	<0.0001
4	Sea Salt	no	
5	NaSO4	no	
6	Fires	Yes	0.0286
7	Crustal	yes	0.0012
8	(NH4)2SO4	no	
9	NH4NO3	yes (marginally)	0.0402
10	LDV	yes	0.0077

3.1.3 Trends in Houston Using TEOM Data

Figure 39 shows the mean concentration by wind direction for PM_{2.5} mass as measured by the tapered element oscillating microbalance (TEOM) at the Clinton Dr. site. This image allows an assessment of the changes in concentration by wind direction. Overall there have been downward trends since 2012 in most wind directions, with 12 out of 24 wind direction bins have statistically significant downward slopes ($p < 0.05$) and all 24 bins had net negative slopes over the six year period, although several direction bins had an uptick in 2017 following 2016. The steepest rate of decline has been in the 282.5 to 287.5 degrees range labeled as 285 degrees, in which the mean dropped from 14.8 $\mu\text{g}/\text{m}^3$ in 2014 to 9.3 $\mu\text{g}/\text{m}^3$ in 2017. The least significant change is from due south, with values randomly varying between 11.2 and 14.7 $\mu\text{g}/\text{m}^3$.

Figure 39. Pollution roses made with hourly PM_{2.5} at Clinton Dr. by calendar year, 2012 – 2017



3.1.4 Sulfate at Clinton Dr.

A major component of PM_{2.5} mass at the Clinton Dr. sampling site is the sulfate ion (SO₄). In earlier work on this project, UT created Figure 40, for gas phase sulfur dioxide by wind direction by year, which showed that west southwest and southeast winds were associated with higher SO₂, and that concentrations were shrinking over time.

Figure 41 is a graph of 24-hour SO₂ averaged concentrations in Harris County from January 2005 through December 2017, which shows a general decline in concentrations over the past 15 years. Also shown in Figure 41 is a linear regression line for the SO₂ 24-hour averages at Clinton Dr., which shows a statistically and practically significant downward slope that predicts negative concentrations by 2018. Following, in Figure 42, is a time series for every 6th day sulfate ion at Clinton Dr. from January 2005 to June 2016. These data also show a downward slope of 0.006 µg/m³ per day, which is only one half the rate of decrease for SO₂ (0.0013 ppb per day). Thus, SO₂ concentrations have been shrinking at a much faster rate than SO₄ ion concentrations. Combined, this information suggests different sources for sulfate and SO₂ at Clinton Dr.

Figure 40. Slide prepared for an earlier talk on this project, mean hourly sulfur dioxide by surface wind direction by year at Clinton Dr.

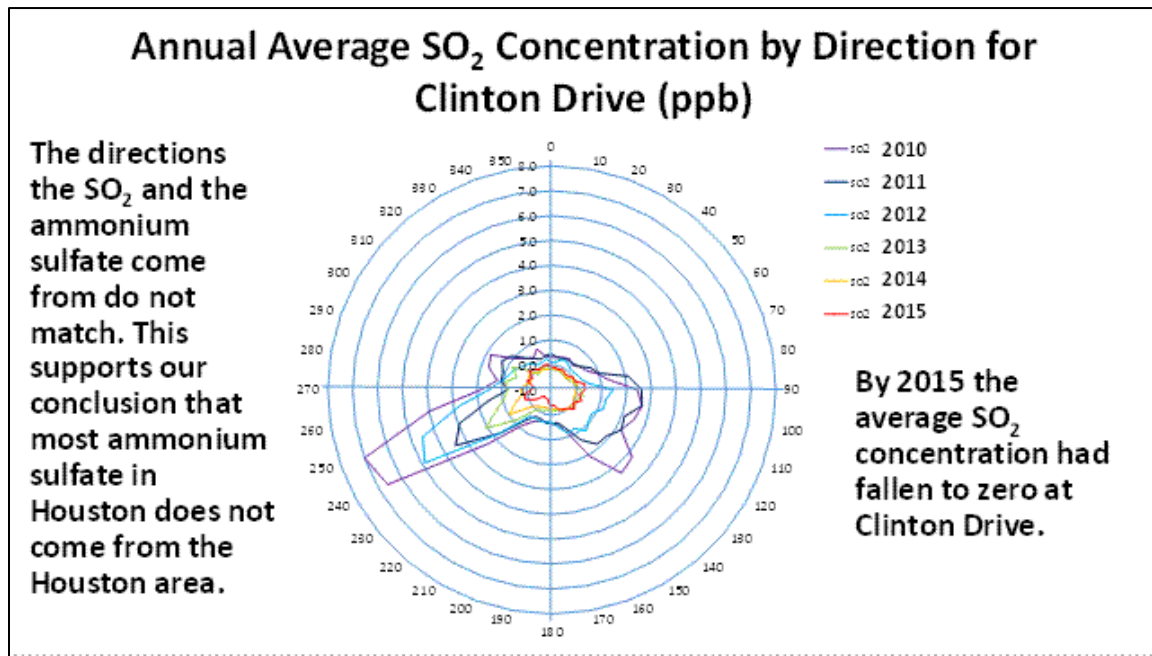


Figure 41. Hourly SO₂ data from Harris County, averaged by day, from 2005 - 2017

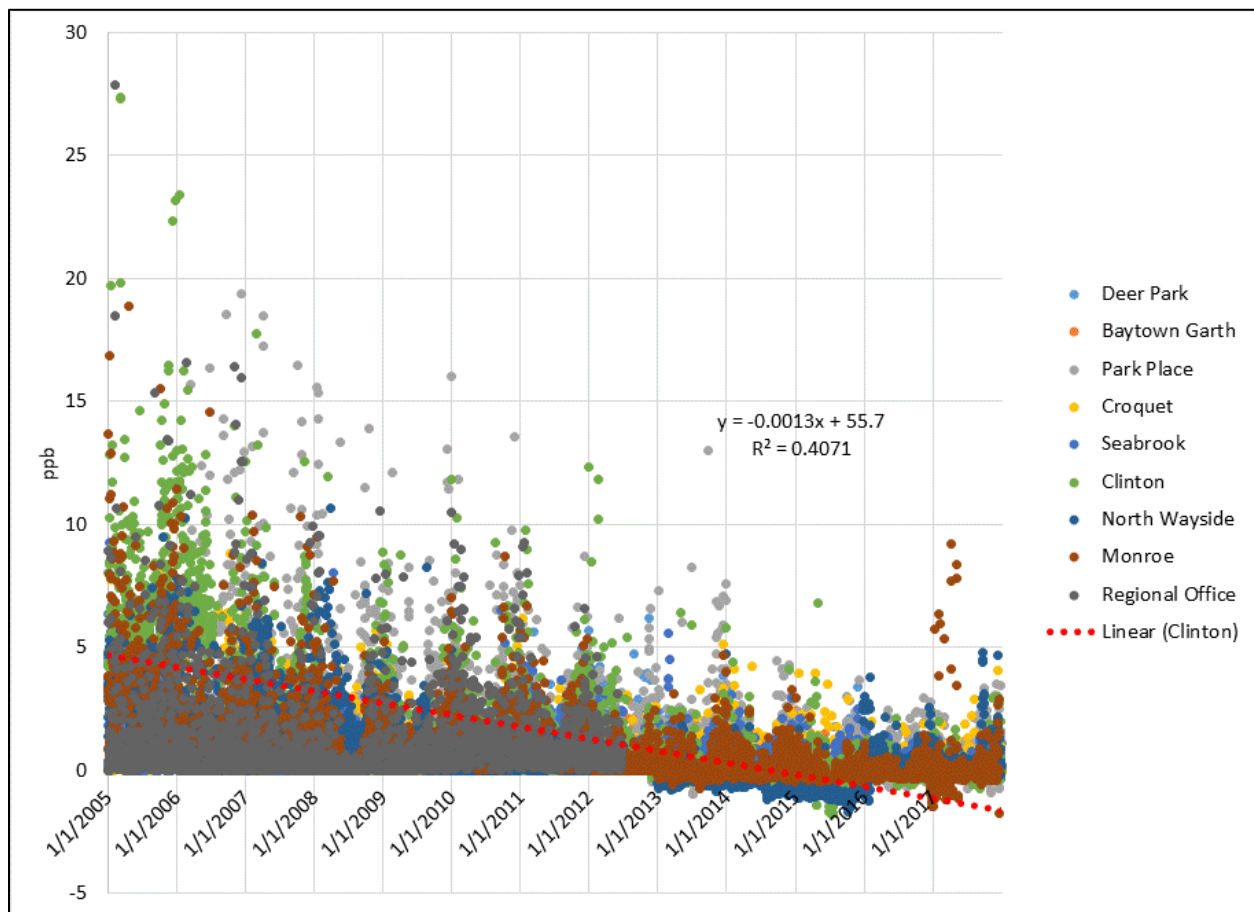
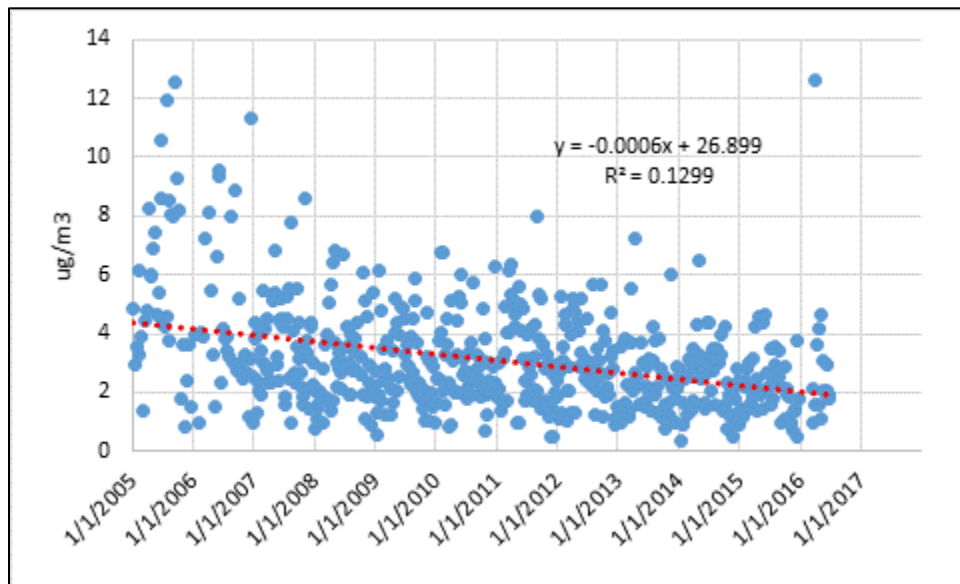


Figure 42. Every-6th day sulfate ion data from Clinton Dr., from January 2005 – June 2016



3.1.5 HYSPLIT Back-Trajectory Cluster Analysis for Clinton Dr. Sulfate Source Apportionment

UT ran 120 hour HYSPLIT³ back-trajectories from Clinton Dr. using EDAS 40km datasets, starting each run from 500 meters above ground level (AGL) at 12 noon CST (18 UTC) for dates from May 1 through September 30 for years 2010 – 2015. In order to balance the decreased certainty associated with longer back trajectories with the desire for increased spatial differentiation of upwind regions, only the first 72 hours of the trajectories were used in a cluster analysis. In cluster analysis, each trajectory is originally considered to be its own cluster. Because of the large number of clusters likely spread out over a wide spatial area, the spatial variance calculated among the data is relatively low. At each step in the algorithm, the closest clusters are joined, and the spatial variance starts to grow, until in the end there is only one encompassing cluster. At each step, there is a calculation of the increase in spatial variance, and at some point there are discrete clusters, which, when joined, cause a larger increase in spatial variance in one step. One can detect the presence of distinct clusters by graphing the step to step change in spatial variance as a function of the number of clusters. Figure 43 shows the change in spatial variance by cluster count from the use of the data set described above. The two circled points indicate where the spatial variance increased from 11 to 10 clusters, and from 5 to 4 clusters. The latter model was selected, to increase the likelihood that many observations would be in each cluster, and that the different clusters would be more qualitatively and visually distinct.

³ Draxler, R.R. and Rolph, G.D., 2003. HYSPLIT (HYbrid Single-Particle Lagrangian Integrated Trajectory) Model access via NOAA ARL READY Website (<http://www.arl.noaa.gov/ready/hysplit4.html>). NOAA Air Resources Laboratory, Silver Spring, MD.

Rolph, G.D., 2003. Real-time Environmental Applications and Display sYstem (READY) Website (<http://www.arl.noaa.gov/ready/hysplit4.html>). NOAA Air Resources Laboratory, Silver Spring, MD. MD.

Figure 44 shows the resulting 5 cluster averaged back trajectories. Clusters found were as follows:

1. Relatively short fetch with net transport only a few hundred km to the northeast (25 percent of trajectories)
2. Long fetch to the north through central North America (5 percent of trajectories)
3. Modest fetch to the east across the Gulf of Mexico and Florida (18 percent of trajectories)
4. Relatively long fetch to the southeast across the Gulf of Mexico past the Yucatan Peninsula (10 percent of trajectories)
5. Relatively short fetch to the southeast across the Gulf of Mexico approaching the Yucatan Peninsula (42 percent of trajectories)

Cluster 5 was the most common cluster, followed by cluster 1. Cluster 2 was the least common.

Illustrations of the trajectories in each of the five clusters appear in Figure 45 through Figure 49. In examining these “spaghetti” plots of the back trajectories, one can note that individual trajectories could have ended up in a different cluster under slight variations in the clustering algorithm. However, the five clusters are qualitatively distinct.

The sulfate ion and organic carbon (OC) daily concentrations from the Clinton Dr. sampler were merged with the records of each day’s trajectory-to-cluster assignment. The average concentrations for both sulfate and OC by cluster are shown in Table 5, along with an approximate 95 percent confidence interval around each mean concentration. For sulfate, cluster 1 has the highest average concentration, at $4 \mu\text{g}/\text{m}^3$. For OC, cluster 2 has the highest average concentrations. Tests of statistical significance have not been performed, but it is clear the confidence intervals overlap.

Figure 43. Change in total spatial variance (TSV) with decreasing number of clusters, significant steps at 11 and 5

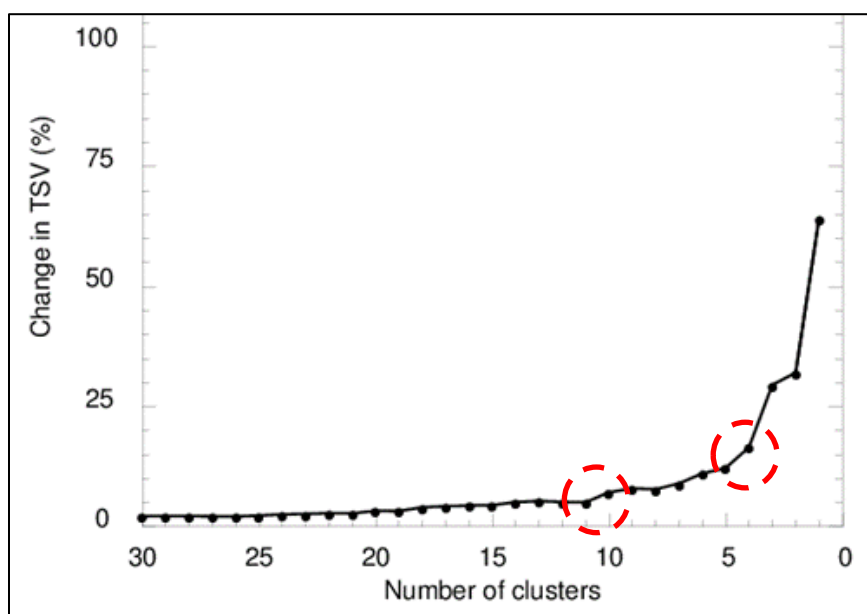


Figure 44. Cluster means for 5 clusters with 831 backward trajectories from Clinton Dr., 500 m, 18 UTC start, 72 hour fetches, EDAS meteorological data.

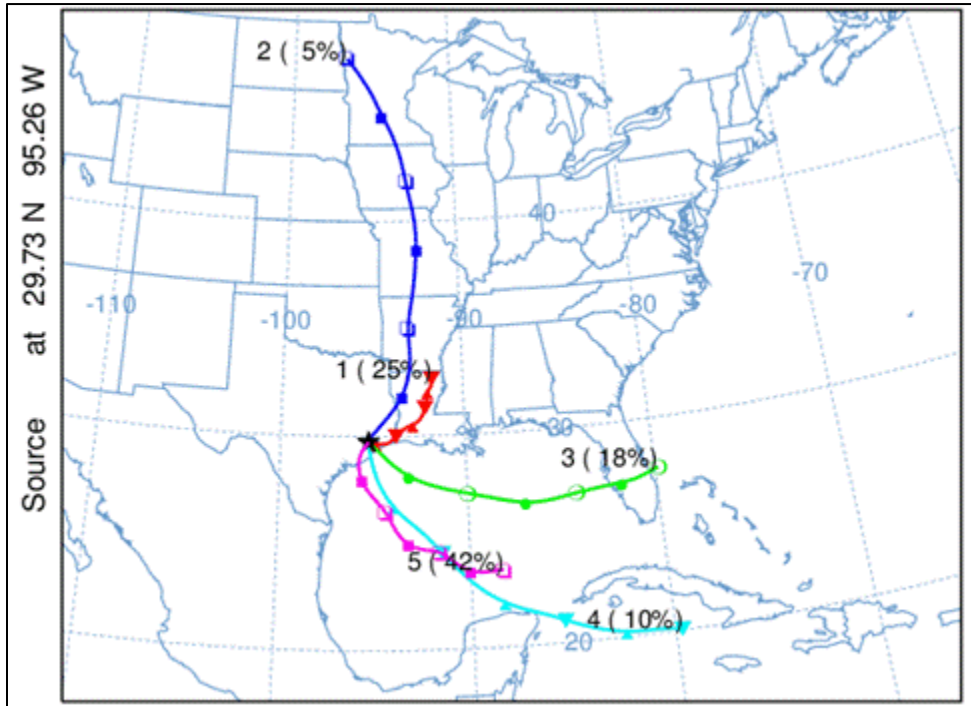


Figure 45. Cluster 1 of 5 with 204 trajectories, slow moving and disorganized

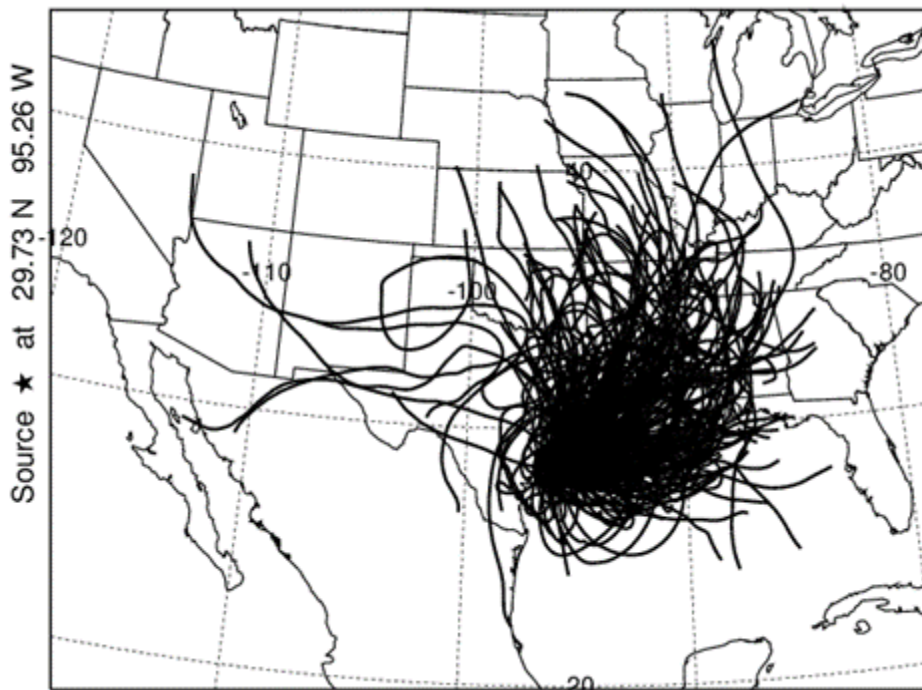


Figure 46. Cluster 2 of 5 with 40 trajectories to the north

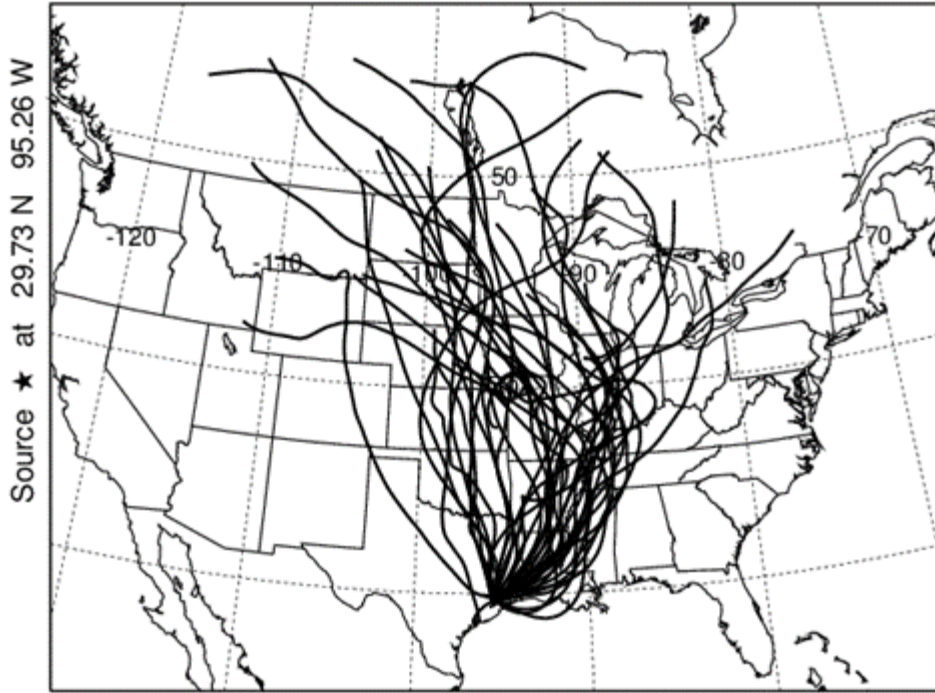


Figure 47. Cluster 3 of 5 with 149 trajectories to the east

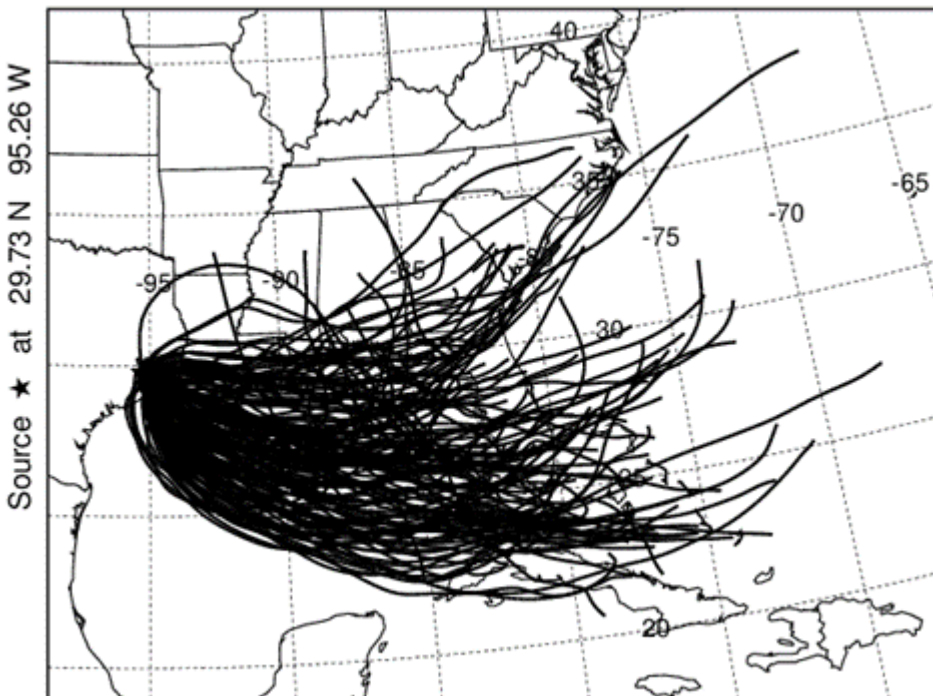


Figure 48. Cluster 4 of 5 with 86 trajectories fast moving to the southeast

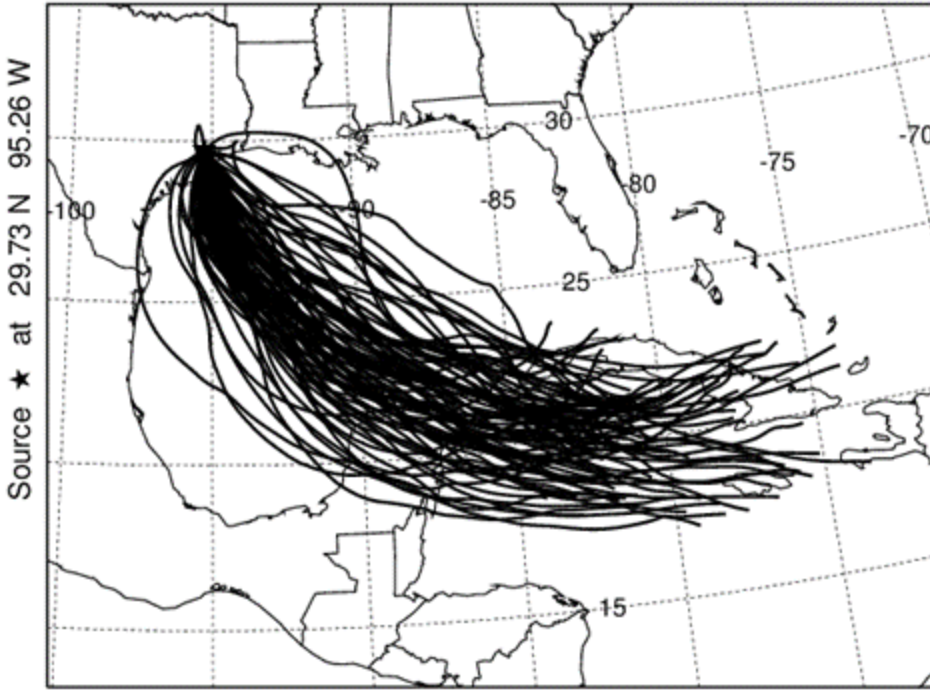


Figure 49. Cluster 5 of 5 with 352 trajectories slow moving to the southeast

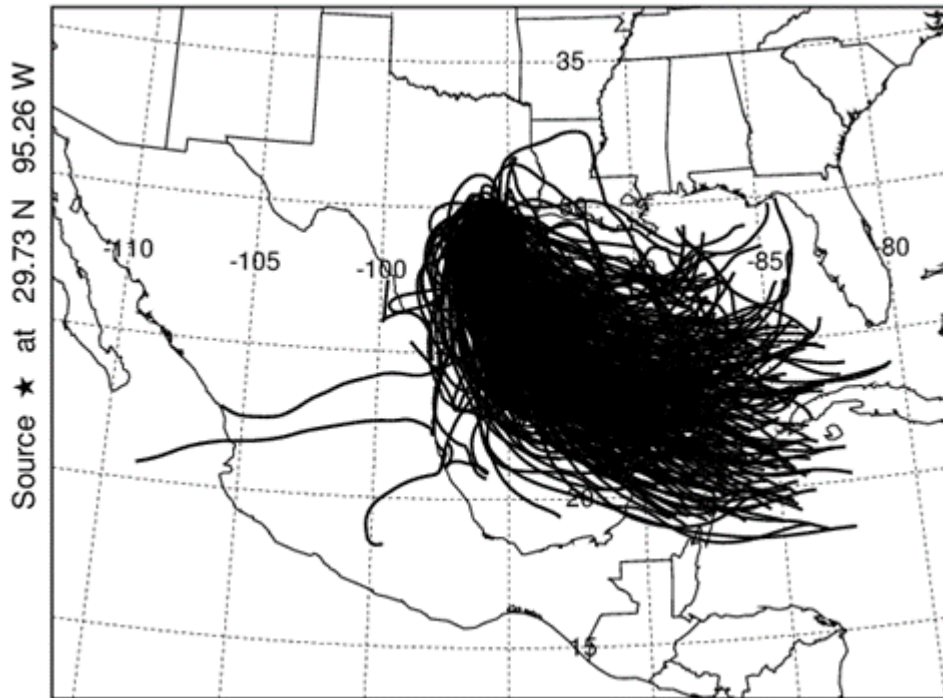


Table 5. Mean sulfate ion, organic carbon ion, standard deviations, and mean plus/minus two standard errors (approx. 95% confidence interval)

CL#	FREQ	SO4 mean	SO4 stdev	SO4±2s.e.	OC	OC stdev	OC±2s.e.
1	100	4.01	1.51	(3.71,4.31)	3.80	1.37	(3.71,4.31)
2	18	3.05	1.72	(2.21,3.88)	4.55	1.69	(3.73,5.37)
3	46	3.10	1.27	(2.73,3.48)	2.35	1.27	(1.97,2.73)
4	42	3.41	1.12	(3.06,3.76)	1.84	0.86	(1.57,2.11)
5	141	2.96	1.16	(2.77,3.16)	1.97	0.95	(1.81,2.13)

3.1.6 North African Dust Affecting Clinton Dr.

Similarly, UT related HYSPLIT back-trajectories to the crustal PM_{2.5} factor at Clinton Dr. The Global Data Assimilation System (GDAS) data sets for global meteorological trajectory or plume modeling were downloaded from the National Oceanic and Atmospheric Administration (NOAA) Air Resources Laboratory website (<https://ready.arl.noaa.gov>, accessed May 2018) for the months April – September 2015 and 2016. Other years/months data may be downloaded for late reports. For each data from May 1 through September 30, 2015, back-trajectories were run from 500 meters (m) altitude above the location for the Clinton Dr. monitoring station, starting at 18 UTC (12 CST) each day. The back-trajectories were run for 240 hours, or 10 days. The end points (each hourly step in space back in time) has increasing uncertainty with increasing time backwards, so that the uncertainty associated with 10 day back trajectories is large. However, on this time scale there are large spatial differences in the 153 days’ worth of back-trajectories. HYSPLIT has a built in clustering algorithm that has been explained in past reports. In running the 153 back-trajectories for 2015 the delta variance graph that depicts the loss of similarity as clusters are joined, shown in Figure 50, suggested there are 7 or 4 clusters. This is based on the relatively large increase in total variance from 7 to 6 clusters, and another in shrinking from 4 to 3 clusters. In this report, only the 7 cluster result has been considered, and the preliminary conclusion is that the 4 cluster model may be better, as the maps in Figure 3 through Figure 10 suggest some clusters could be joined. The figures of the clusters show the following:

- Figure 51 for cluster #1 shows air masses that are more or less slow moving over the Gulf of Mexico and the eastern half of North America.
- Figure 52 for cluster #2 shows air masses that are more or less slow moving the central and eastern parts of North America.
- Figure 53 for cluster #3 shows air masses that move more or less north along the Mississippi River and the central part of North America into Northern Canada.
- Figure 54 for cluster #4 shows air masses that move out over the Atlantic Ocean extending past -40 deg. longitude.
- Figure 55 for cluster #5 shows air masses that move out more slowly over the Atlantic Ocean extending past -60 deg. longitude.
- Figure 56 for cluster #6 air masses that move out still more slowly over the Atlantic Ocean extending past -80 deg. longitude.
- Figure 57 for cluster #7 shows air masses with long fetches through central United States of America and Western Canada.

These figures suggest that a more parsimonious set of clusters may exist in combining some clusters. The mean horizontal traces for the seven clusters is shown in Figure 58. Table 6 lists that 18 dates in 2015 for which the TCEQ forecast predicted elevated North African dust for Southeast Texas, and the corresponding cluster assigned by HYSPLIT to those dates. Much more work must be done on this to confirm the relationship of the elevated crustal factors to the North African source area, and this is considered in in at later section on page 43 of this report. Table 6 shows that

- 9 of 18 dates match to cluster #4, the cluster with strongest proximity to North Africa,
- 6 of 18 dates match to cluster #5, the cluster with the next strongest proximity to North Africa,
- 2 of 18 dates match to cluster #6, the cluster with next strongest proximity to North Africa, but much shorter 10 day fetches.
- 1 date matches with cluster #1.

Figure 50. Change in total variance as cluster are combined, suggesting 7 or 4 clusters

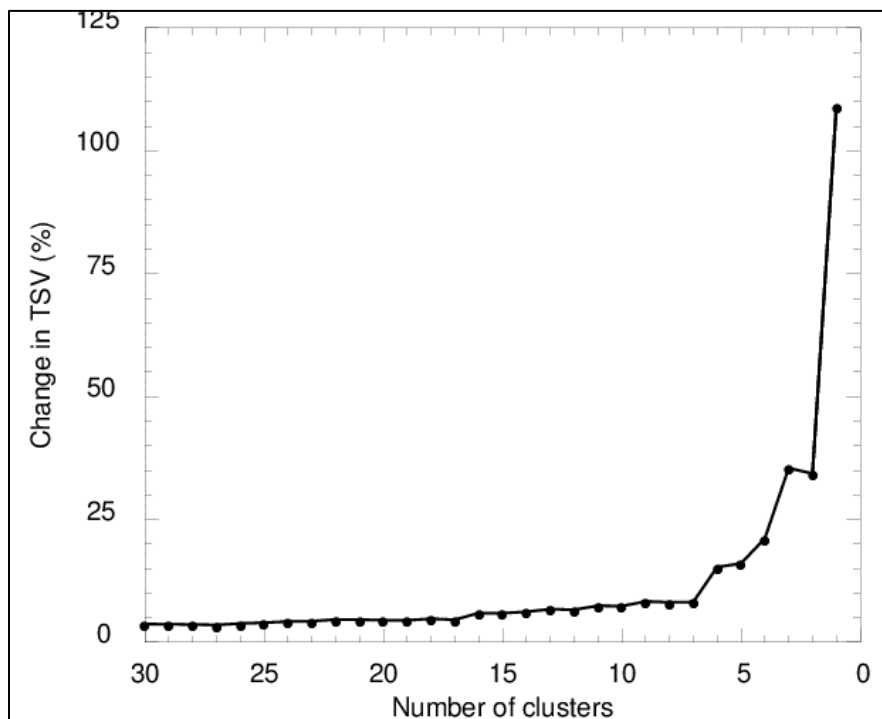


Figure 51. Cluster 1 of 7 Standard 12 back-trajectories ending at 18 UTC at 500 m above Clinton Dr. using GDAS meteorological data sets April – September 2015

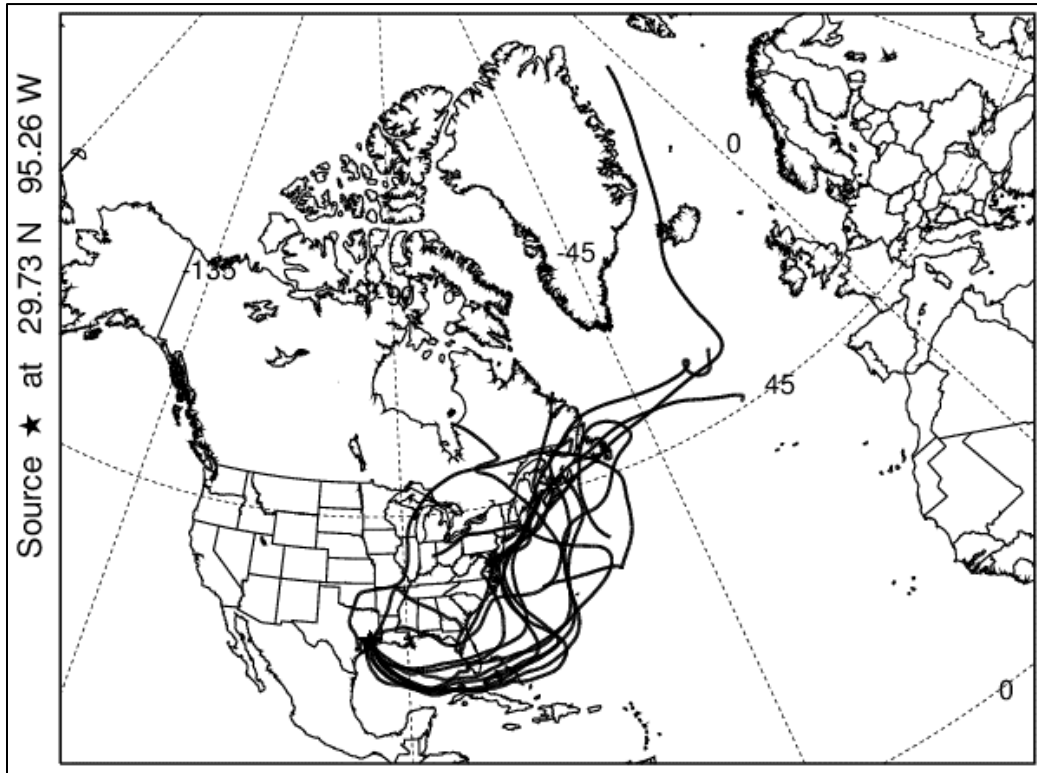


Figure 52. Cluster 2 of 7 Standard 30 back-trajectories ending at 18 UTC at 500 m above Clinton Dr. using GDAS meteorological data sets April – September 2015

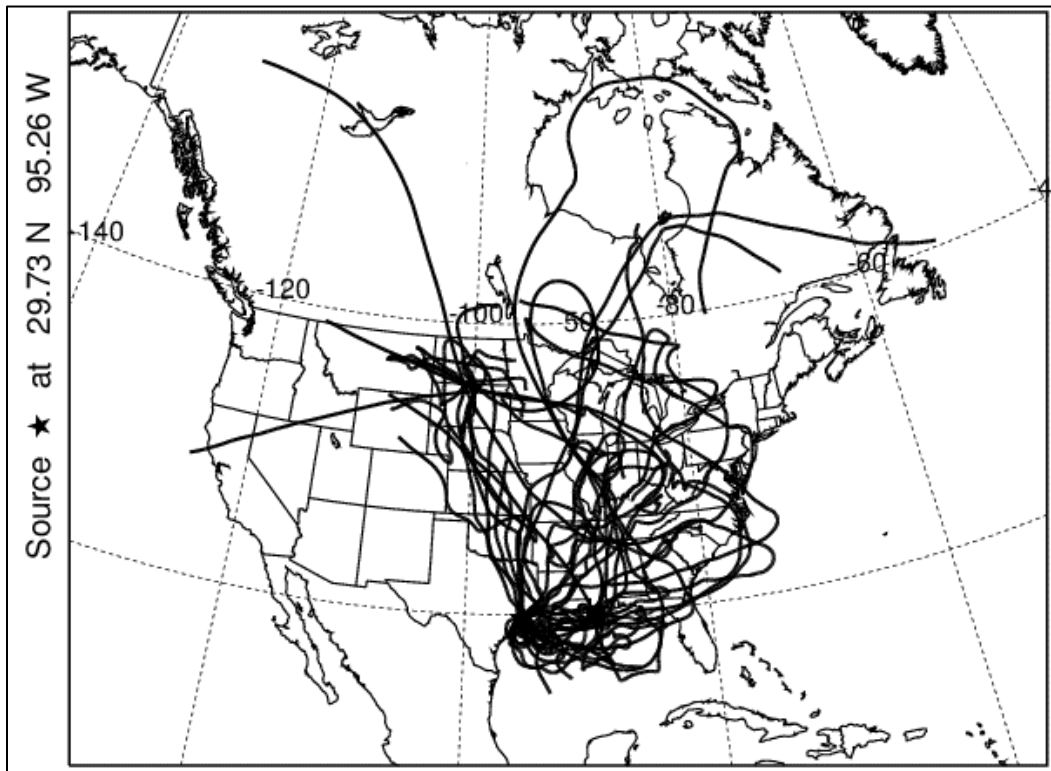


Figure 53. Cluster 3 of 7 Standard 10 back-trajectories ending at 18 UTC at 500 m above Clinton Dr. using GDAS meteorological data sets April – September 2015

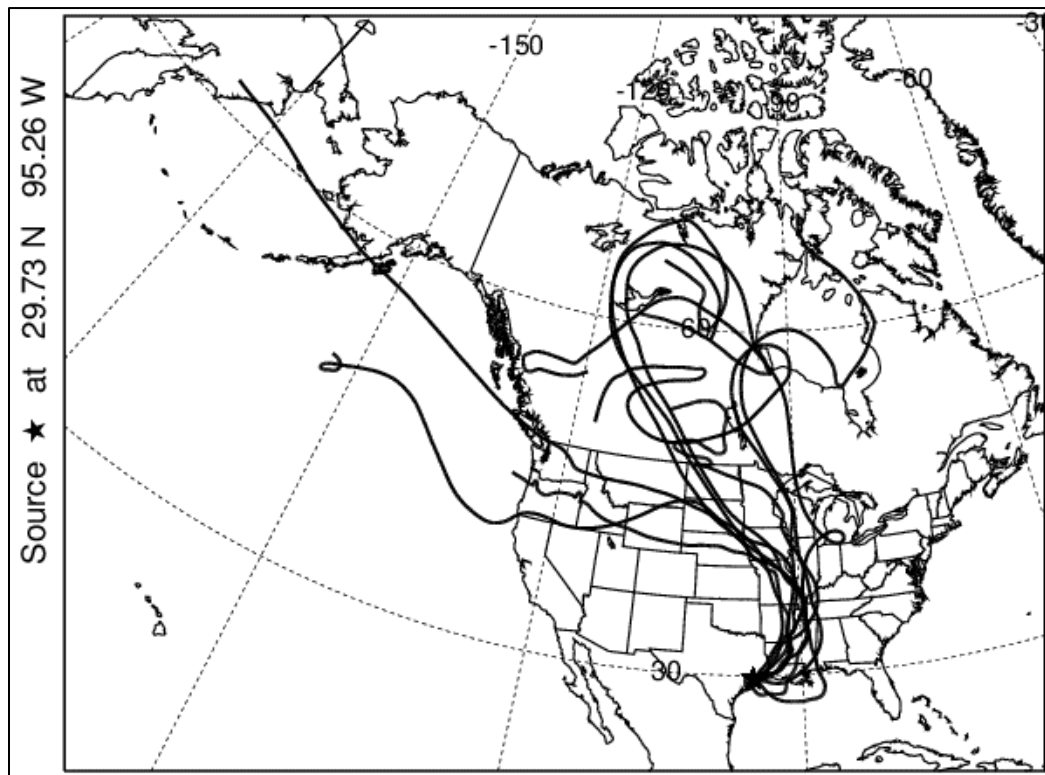


Figure 54. Cluster 4 of 7 Standard 29 back-trajectories ending at 18 UTC at 500 m above Clinton Dr. using GDAS meteorological data sets April – September 2015

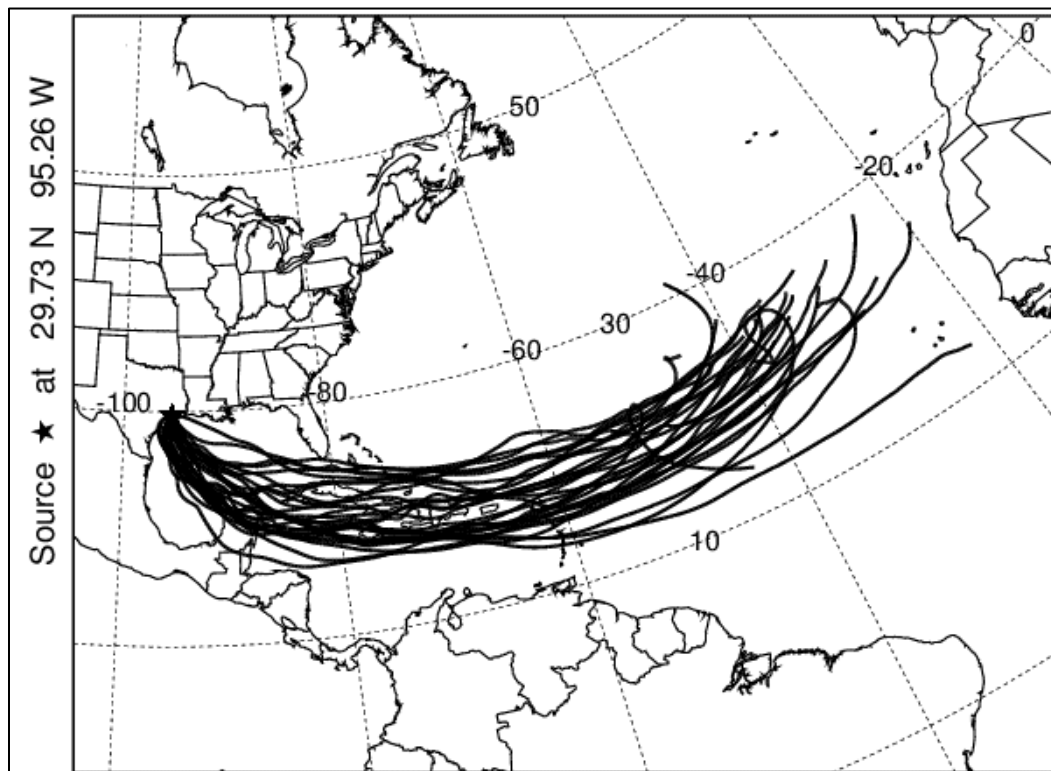


Figure 55. Cluster 5 of 7 Standard 38 back-trajectories ending at 18 UTC at 500 m above Clinton Dr. using GDAS meteorological data sets April – September 2015

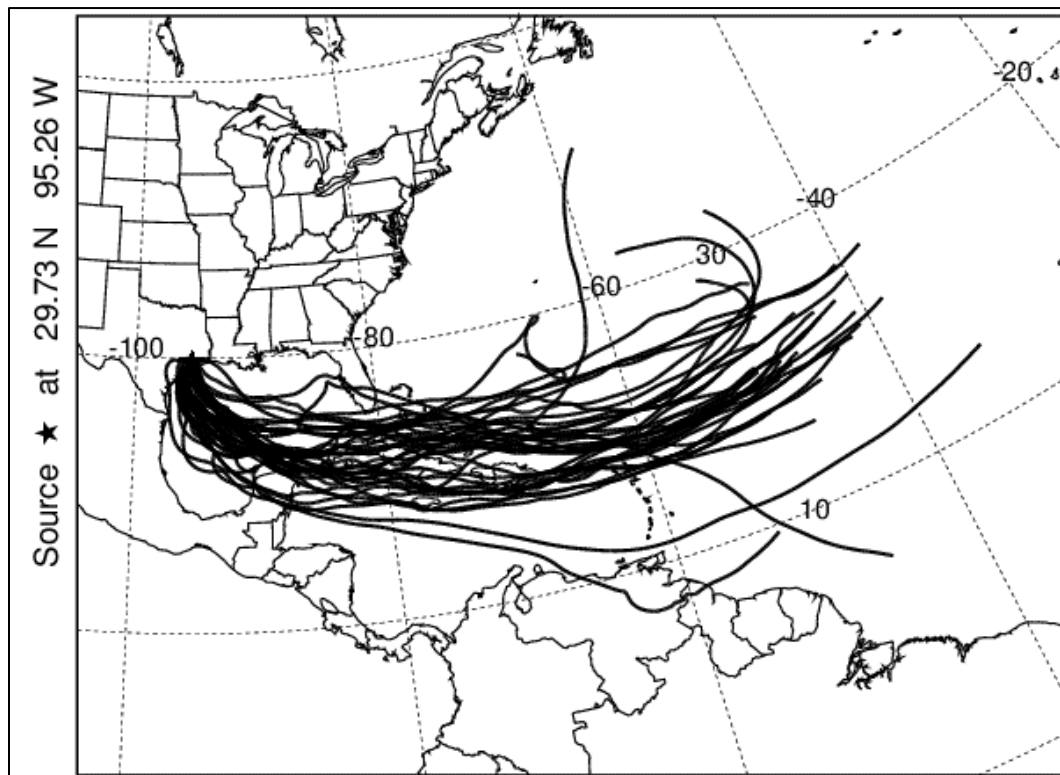


Figure 56. Cluster 6 of 7 Standard 31 back-trajectories ending at 18 UTC at 500 m above Clinton Dr. using GDAS meteorological data sets April – September 2015

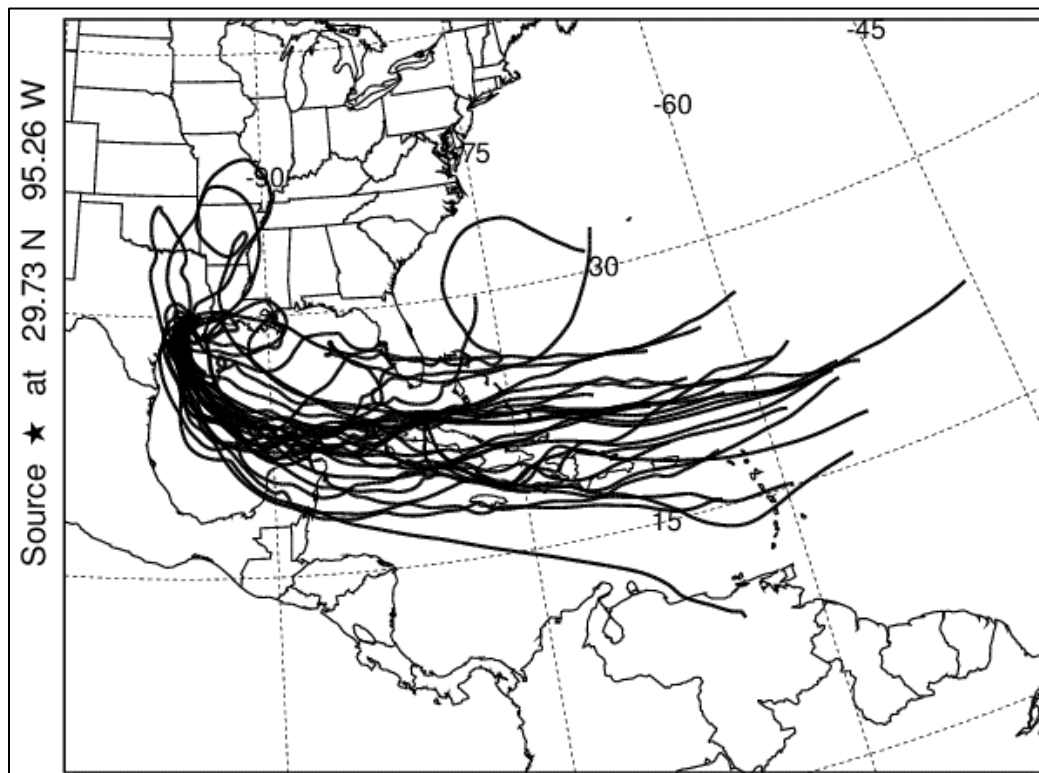


Figure 57. Cluster 7 of 7 Standard 3 back-trajectories ending at 18 UTC at 500 m above Clinton Dr. using GDAS meteorological data sets April – September 2015

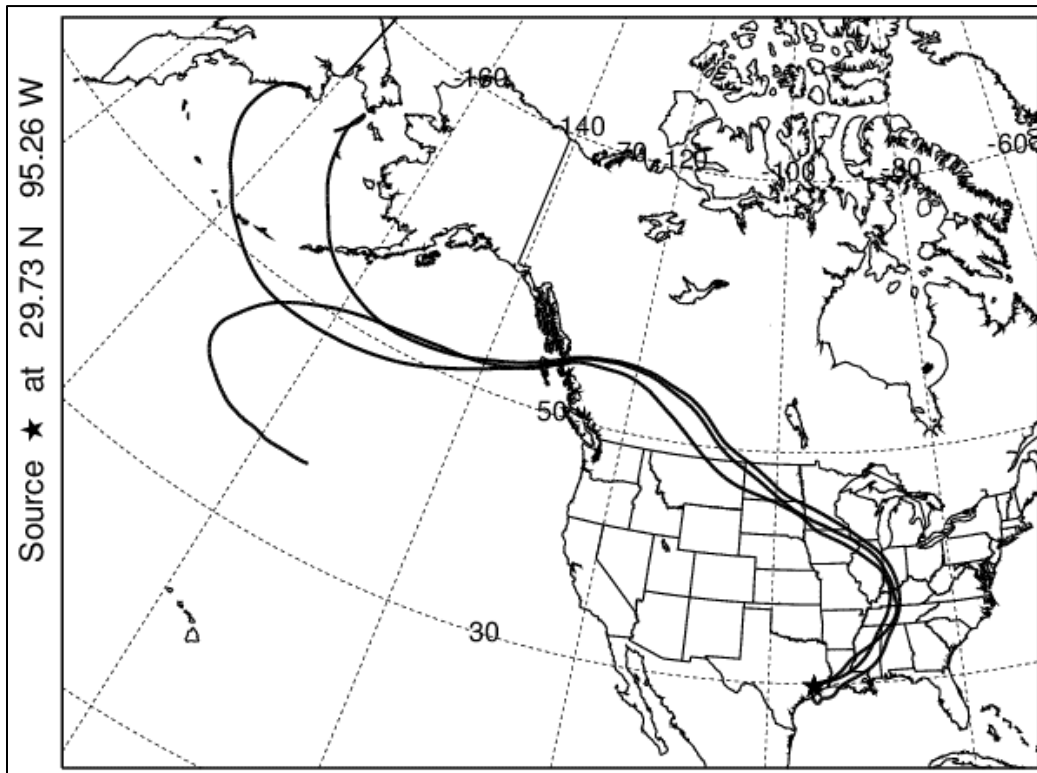


Figure 58. Mean horizontal paths for 7 clusters derived from 153 HYSPLIT back-trajectories starting from 500 m above Clinton Dr. at 18 UTC, May 1 – September 30, 2015.

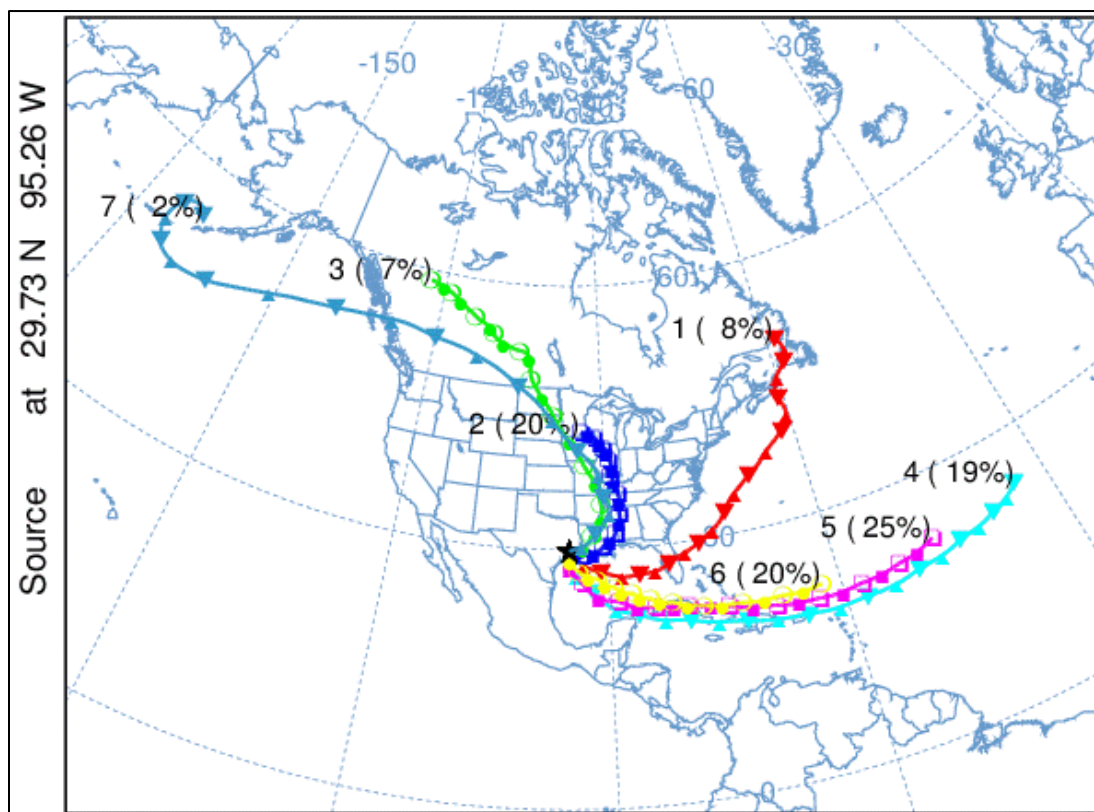


Table 6. Days with forecast North African dust with resulting elevated crustal component $PM_{2.5}$ sample, and cluster for that date

Class	Count in class	Index	Date
1	12	10	5/10/2015
4	29	16	5/16/2015
4	29	49	6/18/2015
5	38	50	6/19/2015
5	38	51	6/20/2015
5	38	52	6/21/2015
6	31	61	6/30/2015
4	29	63	7/2/2015
5	38	64	7/3/2015
4	29	66	7/5/2015
4	29	67	7/6/2015
4	29	68	7/7/2015
4	29	69	7/8/2015
4	29	70	7/9/2015
4	29	71	7/10/2015
6	31	90	7/29/2015
5	38	96	8/4/2015
5	38	100	8/8/2015

3.1.7 Joint Research with Texas A&M & Univ. of Houston into Crustal & Fire Factor Transport

UT began a collaboration with other researchers in 2017 and 2018 into transport of pollutants affecting Houston PM_{2.5} concentrations. UT identified dates for Texas A & M University (TAMU) group (Shankar Chellam and Ayse Bozlaker) to attempt Chemical Mass Balance (CMB) experiments. UT provided PMF results on Clinton Dr. PM_{2.5} speciation data using all data excluding some clear fireworks-related outliers and a couple of other days with unexplained outlier values, leaving 774 observations with complete data from 2010 to mid-2016, from which were extracted 10 factors. It was not practical to easily differentiate African dust from domestic crustal material with EPA PMF 5.0. However, four approaches were used to select African dust samples or Mexican / Central American agricultural burning samples.

1. If PMF results for summer time samples showed an elevated crustal factor composition or the PMF results for spring time showed an elevated fire factor composition, then a sample became a candidate.
2. When transported pollutants reach one region from a distant source, it is generally the case that the effects would be measured at several monitors in the same date, or even monitors in adjacent regions. For candidate dates with elevated crustal or fire composition, the total mass measurements at other monitors in Southeast Texas were also examined.
3. TCEQ meteorologists provide a daily email of PM_{2.5} and ozone forecasts that are based both on meteorological forecasts and review of satellite images that detect smoke and dust clouds, and UT compares these emails with PMF results.
4. The HYSPLIT back trajectory tool is used to assess upwind source areas. It has been the practice for UT to not rely on individual back trajectories over a multi-day period, but to put faith in ensembles of multi-day back-trajectories.

Following this rubric, UT selected the days for fire and crustal factors so as to fill out a data set for CMB testing, as well as a selection of days with highest overall PM_{2.5} mass, then divided the data by calendar year. UT lined up the highest crustal and fire factor dates by year for which there existed a corresponding TCEQ air quality forecast. The dates for crustal and fire factors with a forecast are highlighted in red in tables below to differentiate them from elevated crustal and fire factor dates for which there was not an forecast. UT also selected all the dates for which total PM_{2.5} mass concentration exceeded 20 µg/m³. For each year 2010 to 2015 there are:

- four or five dates provided for days with high crustal factor loading and a corresponding African dust forecast,
- two or three dates in yellow cells for days with high fire factor loading and a corresponding smoke forecast,
- two or three dates in yellow cells for days for which PM_{2.5} exceeded 20 µg/m³

For each year, 10 dates are selected (highlighted in yellow) to represent the dates selected for CMB use.

Table 7 through Table 12 show the dates selected and provided to TAMU by year.

Table 7. Dates from 2010 selected for TAMU

PM2.5 mass	Fire	Crustal
2/1/2010		
3/16/2010		
4/21/2010		
5/1/2010	5/1/2010	
5/7/2010	5/7/2010	
5/29/2010		
6/6/2010	6/6/2010	
6/9/2010		
		7/8/2010
7/10/2010		7/10/2010
		7/12/2010
7/13/2010		7/13/2010
7/15/2010		7/15/2010
7/16/2010		7/16/2010
8/25/2010		
8/26/2010		
8/27/2010		
10/16/2010		
12/7/2010	12/7/2010	
	12/8/2010	

Table 8. Dates from 2011 selected for TAMU

PM2.5 mass	Fire	Crustal
2/12/2011		
2/28/2011		
3/2/2011	3/2/2011	
3/3/2011		
3/10/2011	3/10/2011	
3/29/2011	3/29/2011	
	4/15/2011	
4/16/2011	4/16/2011	
	4/18/2011	
4/19/2011	4/19/2011	
4/20/2011	4/20/2011	
4/26/2011	4/26/2011	
4/27/2011	4/27/2011	
	5/1/2011	
	5/9/2011	
5/10/2011		
5/20/2011	5/20/2011	
5/25/2011		
5/27/2011	5/27/2011	
6/6/2011		
6/7/2011		
7/1/2011		7/1/2011
		7/2/2011
		7/3/2011
7/21/2011		7/21/2011
8/29/2011		
8/30/2011		
8/31/2011		
9/6/2011		
12/28/2011		
12/30/2011		

Table 9. Dates from 2012 selected for TAMU

PM2.5 mass	Fire	Crustal
1/24/2012	1/24/2012	
4/3/2012		4/3/2012
5/17/2012		
6/26/2012		
6/28/2012		
		7/3/2012
7/21/2012		7/21/2012
7/22/2012		7/22/2012
7/26/2012		7/26/2012
7/27/2012		7/27/2012
7/28/2012		7/28/2012
		8/2/2012
8/15/2012		8/15/2012
	10/30/2012	
11/27/2012		

Table 11. Dates from 2014 selected for TAMU

PM2.5 mass	Fire	Crustal
1/12/2014		
2/13/2014		
4/27/2014	4/27/2014	
4/28/2014	4/28/2014	
	4/29/2014	
		6/8/2014
		6/15/2014
6/16/2014		6/16/2014
		6/21/2014
6/22/2014		6/22/2014
6/23/2014		6/23/2014
6/29/2014		6/29/2014
		8/17/2014
8/18/2014		8/18/2014
8/19/2014		8/19/2014
		8/20/2014
8/21/2014		8/21/2014
8/22/2014		8/22/2014
10/10/2014		
	11/19/2014	
12/9/2014		
12/10/2014		

Table 10. Dates from 2013 selected for TAMU

PM2.5 mass	Fire	Crustal
1/22/2013		
3/18/2013		
3/23/2013	3/23/2013	
4/16/2013		
5/17/2013	5/17/2013	
6/11/2013		6/11/2013
6/20/2013		6/20/2013
6/21/2013		6/21/2013
6/25/2013		6/25/2013
7/23/2013		7/23/2013
7/24/2013		7/24/2013
7/25/2013		7/25/2013
7/28/2013		7/28/2013
7/29/2013		7/29/2013
		7/30/2013
8/7/2013		8/7/2013
8/8/2013		8/8/2013
8/30/2013		
12/4/2013		
12/13/2013		
12/16/2013		
12/17/2013		

Table 12. Dates from 2015 selected for TAMU

PM2.5 mass	Fire	Crustal
1/16/2015		
2/11/2015		
	2/12/2015	
	2/13/2015	
	2/14/2015	
	3/1/2015	
3/17/2015		
4/24/2015		
5/9/2015		
5/10/2015		5/10/2015
5/16/2015		5/16/2015
6/18/2015		6/18/2015
6/19/2015		6/19/2015
		6/20/2015
6/21/2015		6/21/2015
6/30/2015		6/30/2015
7/2/2015		7/2/2015
7/3/2015		7/3/2015
		7/5/2015
7/6/2015		7/6/2015
7/7/2015		7/7/2015
7/8/2015		7/8/2015
7/9/2015		7/9/2015
7/10/2015		7/10/2015
		7/29/2015
		8/4/2015
		8/8/2015
	8/27/2015	
	8/28/2015	
	9/27/2015	
	10/7/2015	
10/8/2015	10/8/2015	
	10/16/2015	
12/6/2015	12/6/2015	
12/7/2015	12/7/2015	
12/8/2015	12/8/2015	
	12/9/2015	

An important clue to detecting long range transport using ambient PM_{2.5} data is the near simultaneous occurrence of higher than average concentrations measured at monitoring sites over a relatively large geographic area, say, covering more than one urban area. UT downloaded hourly PM_{2.5} data from the TCEQ's Leading Environmental Analysis and Display System (LEADS) for Texas monitoring sites and examined the data for such clues. In 2016, the Houston/Galveston/ Brazoria (HGB) region, the Beaumont/Port Arthur (BPA) region, Austin and San Antonio regions (CenTx), and the Corpus Christi and Lower Rio Grande Valley regions (SoTx) contained 20 to 22 hourly continuous PM_{2.5} monitoring sites with high data return. The hourly data were averaged into daily mean concentrations, and averages for sites on days with less than 18 hours of data were considered missing data days.

UT looked for days with elevated regional concentrations, on which most monitors within a region and potentially monitors within several regions had concentrations above 12 µg/m³. Table 2 shows the list of dates for which there appears to have been a regional effect, with monitors over a relatively large area measuring PM_{2.5} at or above 12 µg/m³. Region-wide PM_{2.5} could have several sources, such as transported North African crustal material, smoke from agricultural fires in the Southeastern United States or Southern Mexico / Central America, or secondary pollutants that formed under stagnant conditions in a heavily urbanized upwind area in the Eastern United States and then advected to South Texas. Examination of the Clinton and Galveston speciated PM_{2.5} helped to identify the types of sources that caused the regional pollution. As a first step, principal component analysis (PCA) was often used to quickly assess the data for, as certain factors have long been reliably found using this relatively easy technique. However, positive matrix factorization has proven more powerful in qualifying the contributions more precisely and from more source types.

Figure 59, Figure 60, and Figure 61 show the profile and time series for crustal factor on 2010 – early 2016 samples, excluding a few outliers.

Figure 59. Clinton Dr. crustal material factor, % of species mapped to this factor, data 2010 – early 2016, some outliers excluded

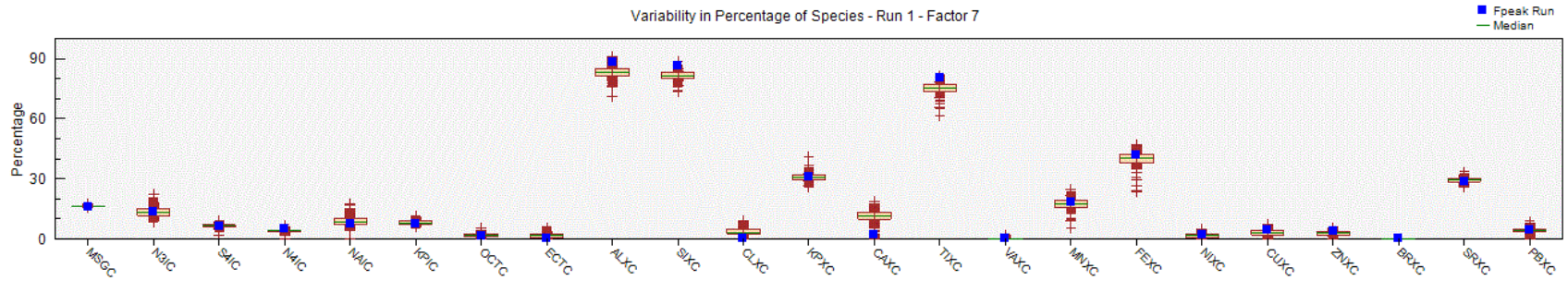


Figure 60. Clinton Dr. crustal material factor, mass contribution to this factor, data 2010 – early 2016, some outliers excluded

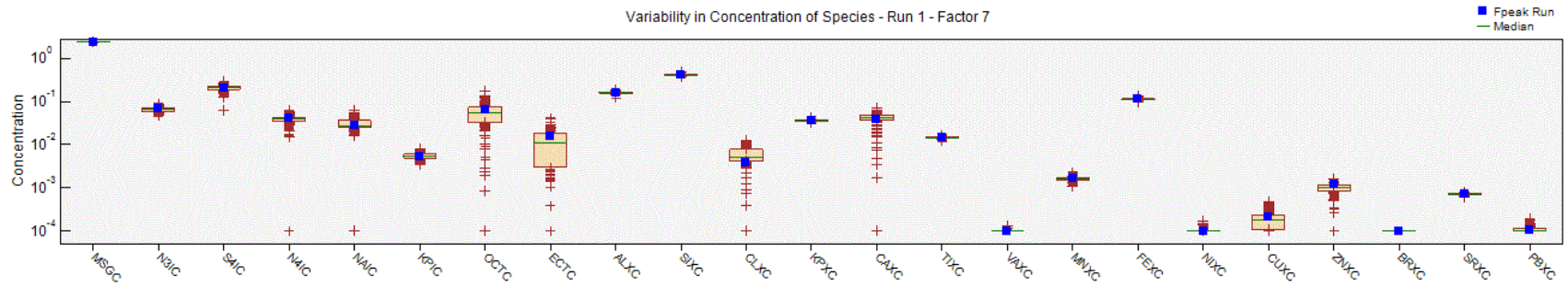
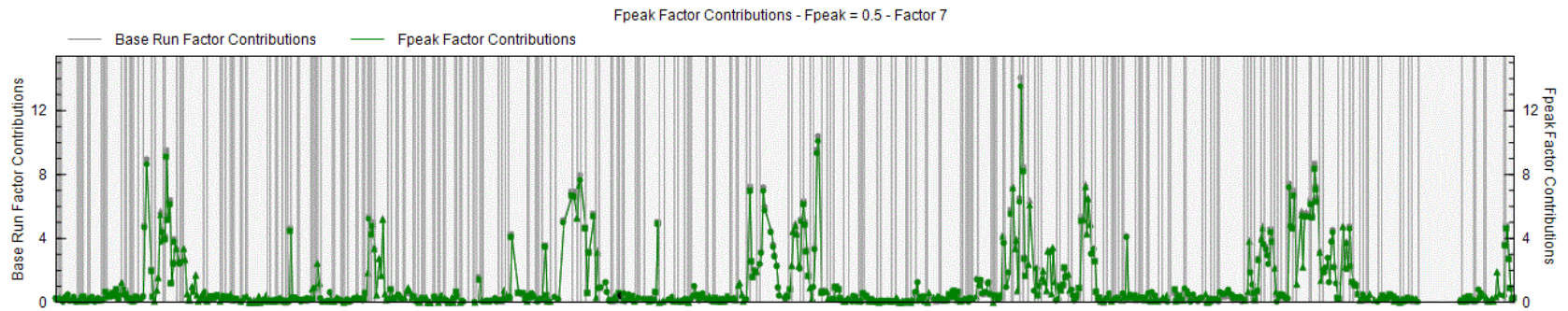


Figure 61. Clinton Dr. crustal material factor, relative contribution (mean=1), data 2010 – early 2016, some outliers excluded



Sixty dates from 2010 to 2016 were suggested as having been heavily influenced by North African crustal material. As described above, part of the evidence comes from examining the TCEQ air quality forecasts which UT archived and later filtered based on references to African dust. TCEQ forecasts use combined meteorological forecasts and satellite imagery. UT also used the PMF results and examination of coincident elevated total mass at other monitoring stations. As part of an independent analysis, UT ran 240-hour (10 day) back-trajectories using HYSPLIT⁴ with data produced by the National Oceanographic and Atmospheric Administration (NOAA) Air Resources Laboratory. For this application, a height of 100 meters (m) above ground level (AGL) over the Clinton Dr. monitoring site was selected to better represent transport winds, and the HYSPLIT 4 desktop application was used with Global Data Assimilation System (GDAS) 1-degree gridded data files to generate four 240-hour back trajectories per day for all dates in June, July, and August, 2010 through 2016. Trajectories were run for 0 UTC, 6 UTC, 12 UTC, and 18 UTC each day, which represent trajectory local Central Standard Times 18 CST (day before), 0 CST, 6 CST, and 12 CST. Figure 62 is an illustration of the last 120 hours of the endpoints from the trajectories on dates selected for African dust. Note that one date shows the air came from northeastern North America as opposed to across the North Atlantic Ocean.

⁴ Stein, A.F., Draxler, R.R., Rolph, G.D., Stunder, B.J.B., Cohen, M.D., and Ngan, F., (2015). NOAA's HYSPLIT atmospheric transport and dispersion modeling system, *Bull. Amer. Meteor. Soc.*, **96**, 2059-2077, <http://dx.doi.org/10.1175/BAMS-D-14-00110.1> 

Rolph, G., Stein, A., and Stunder, B., (2017). Real-time Environmental Applications and Display sYstem: READY. *Environmental Modelling & Software*, **95**, 210-228, <https://doi.org/10.1016/j.envsoft.2017.06.025> . (<http://www.sciencedirect.com/science/article/pii/S1364815217302360>) 

Figure 62 Ensemble of HYSPLIT back trajectories on suspected African dust impact dates, last 120 hours of 240 hour trajectories shown



The map in Figure 62 is not sufficient to explain the transport of African dust, since it is possible that most trajectories on summer days follow similar paths regardless of resulting crustal component at the Clinton Dr. site. Figure 63 and Figure 64 compare the identified African dust days to the other days in the summer months from 2010 – 2016. The figures show the frequency of back trajectory end points rounded and gridded by integer latitude and longitude and contoured with Kriging to illustrate the difference in the distributions of the endpoints for the last 120 hours of the 240 hour back-trajectories. It is clear that the suspected African dust dates have a deeper penetration eastward in the direction of North Africa than all other dates.

Figure 63 Countoring of trajectory endpoints associated with African dust summers 2010-2016

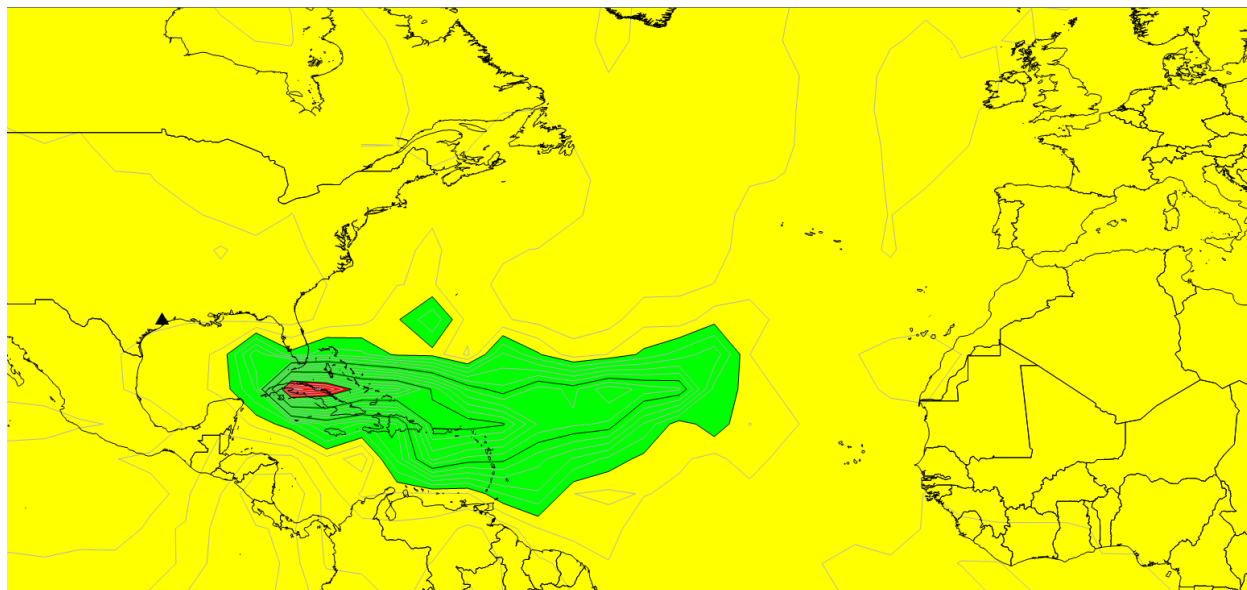
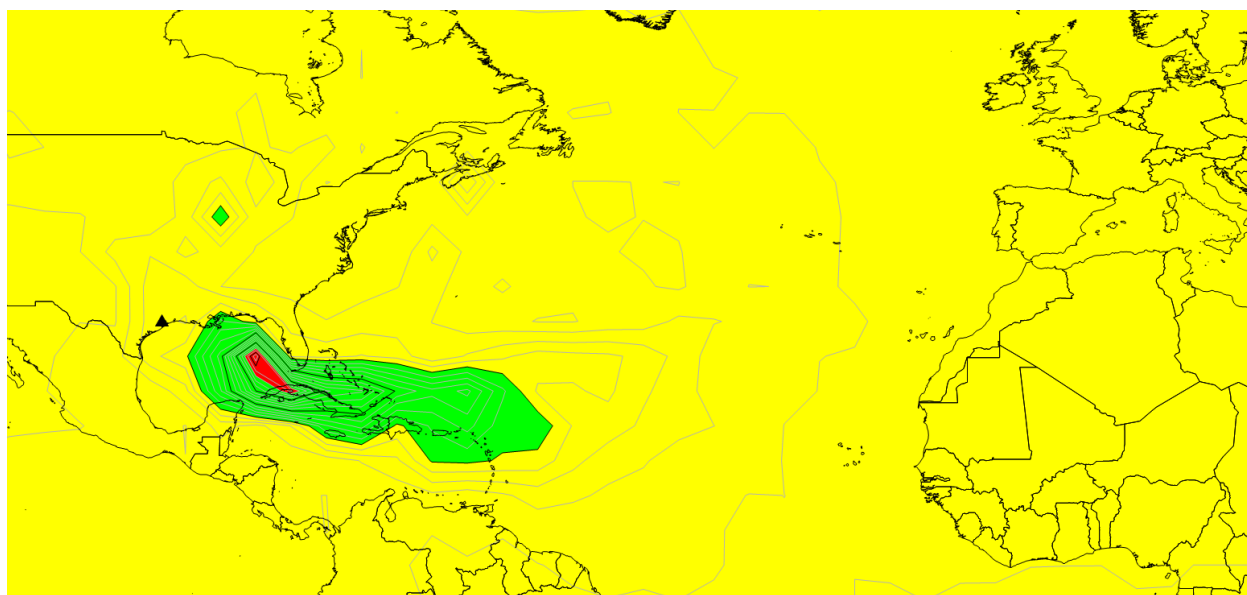


Figure 64 Countoring of trajectory endpoints not associated with African dust summers 2010-2016



3.1.8 Fire back trajectory analysis

HYSPLIT back trajectories from 100 meters AGL were run from the Clinton Dr. site for 120 hours (5 days) backward in time, starting every 6 hours, for all days in March, April, May, and June for 2010 through 2016 (seven years). This produced 3,146 data files. The dates suspected of having been affected by Mexican and Central American fires were identified by both examining the composition of samples for the highest contributions of the fire factor, and by examining the forecasts made by TCEQ staff meteorologists in the Monitoring Division. UT identified 26 dates, 23 of which fell in March (5), April (10), May (7), and June (1). The trajectories for all the other sampled dates in March through June that had been used in the PMF runs were separated from the trajectories on these 23 dates. The trajectory dates in the “fire” and “non-fire” categories were subjected to the following processing:

1. Data from 49 hours to 120 hours back in time were kept.
2. These data points were rounded to the nearest integer latitude and longitude, so as to represent a grid of discrete points.
3. The gridded data points were tabulated for the count of observations at each grid point.
4. The gridded count of data points was contoured with Kriging algorithm in Surfer 13.6, and placed on a color coded map.

Figure 65 shows the density of hourly back trajectory points from between 49 and 120 hours upwind from Clinton Dr., on dates with suspected fire impacts, and Figure 66 shows the density of hourly back trajectory points from between 49 and 120 hours upwind from Clinton Dr. on all other March – June PMF sample dates. A comparison of the two figures suggests that the large majority of upwind tracks traverse the Gulf of Mexico during springtime. However, on suspected fire-impacted days, the tracks pass closer to the Yucatan Peninsula in Southern Mexico and Central America than on other days. On other days the highest frequency of flow is farther east between Cuba and Florida.

Figure 65 Countoring of trajectory endpoints associated with Mex/CenAm fires spring 2010-2016

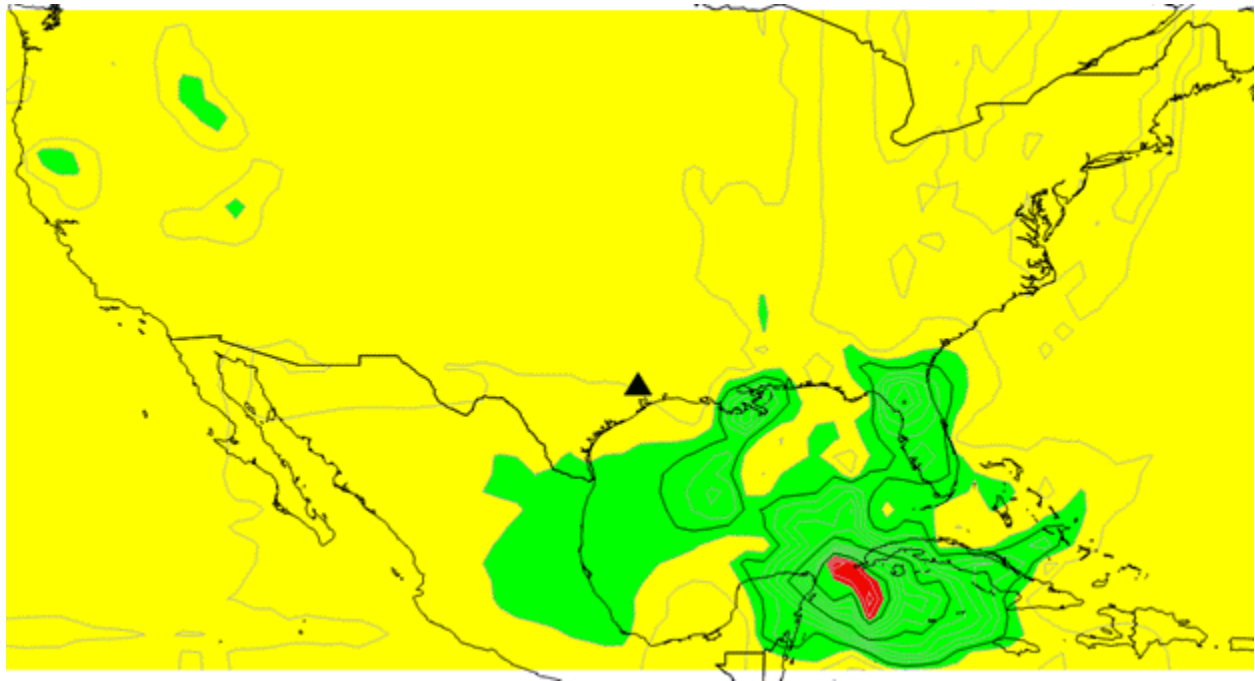
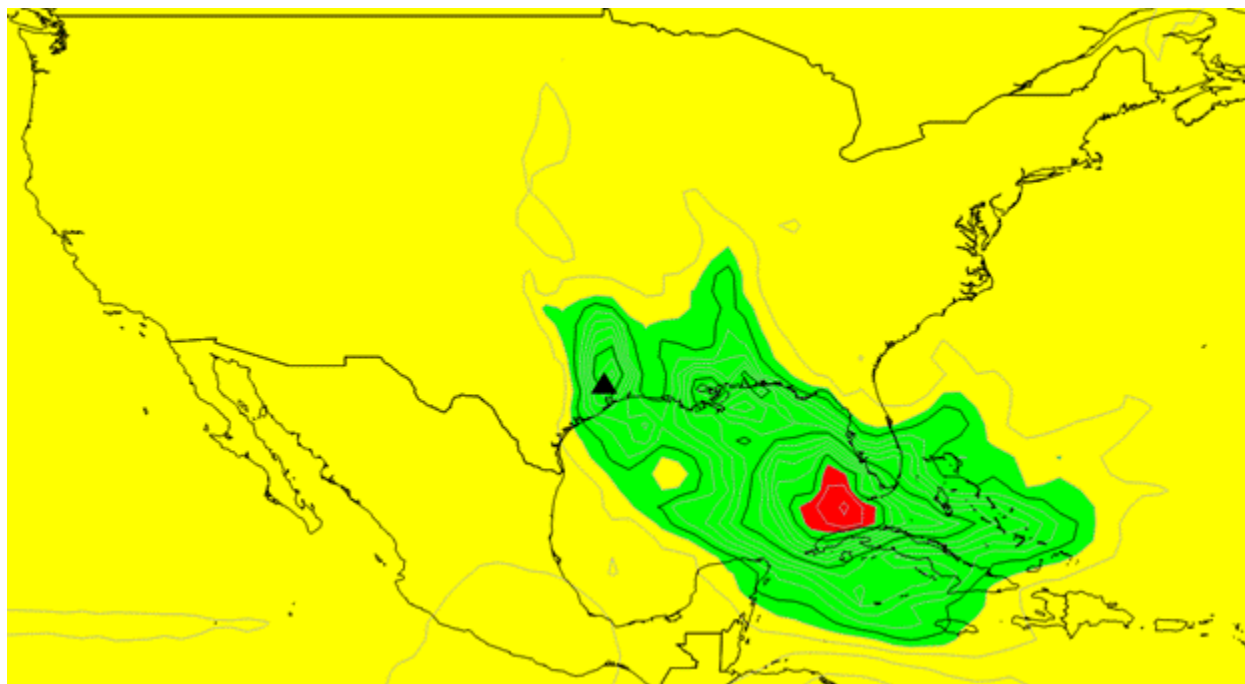


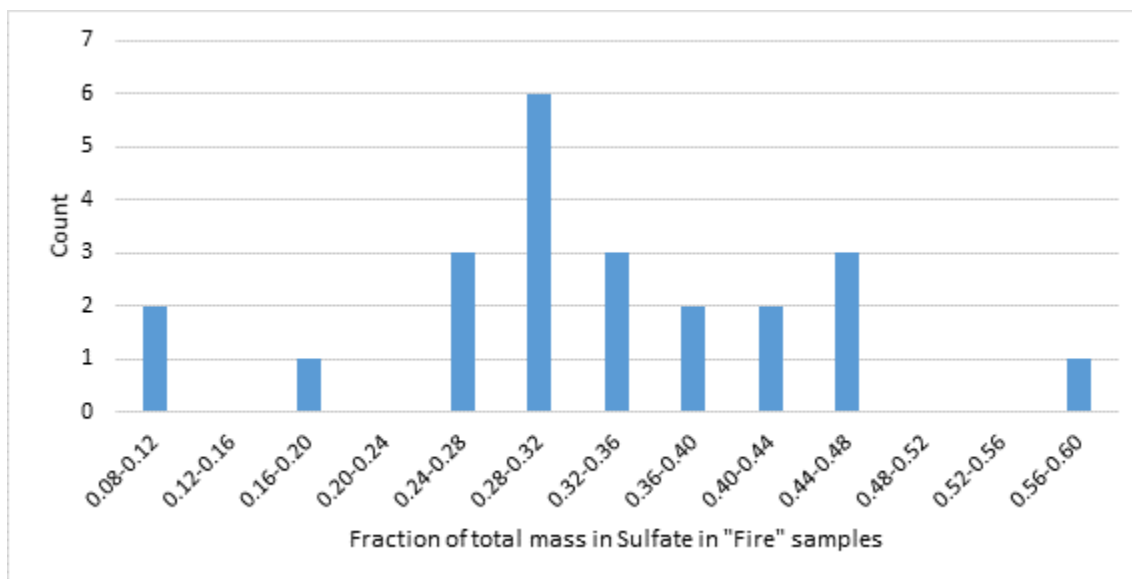
Figure 66 Countoring of trajectory endpoints not associated with Mex/CenAm fires spring 2010-2016



3.1.9 Sulfate in Fire Samples at Clinton Dr.

Sulfate is a large component of mass in the fire samples the range and distribution of percent mass is shown in Figure 67. On average 23% of mass is sulfate ion. In the fire samples it is 30% mass.

Figure 67 Sulfate ion distribution of percent mass on dates identified with fire component springs 2010-2016



3.1.10 2017 Houston Area TEOM and Beta-attenuation Monitor PM_{2.5} Data

PM_{2.5} data are collected by means of 24-hour filter samples and through the use of two continuous instrument technologies – the tapered element oscillating microbalance (TEOM) and the beta-attenuation monitor (BAM). Figure 68 shows the result of averaging hourly data over each 24-hour day, discarding values with less than 18 hours data, for PM_{2.5} collected by continuous instruments in the Houston-Galveston Region in 2017 through late October. In Figure 68, several periods appear with elevated 24-hour concentrations from several monitors. In Figure 68, sites are listed by continuous ambient monitoring station (CAMS) number. “Accept” is a suffix used for the TEOM data, the other monitors being BAMs. East CAMS 1 and Baytown CAMS 148 started 2017 as TEOMs and switched to BAMs. Deer Park CAMS 35 simultaneously hosts several PM_{2.5} measurement methods, and a comparison of the BAM and TEOM appears in Figure 69 and Figure 70. The BAM tends to produce more negative concentrations than the TEOM, as evidenced by the presence of below 0.0 average 24-hour concentrations for two BAMs in Figure 68. Figure 69 shows CAMS 35 BAM vs TEOM data for 2017 and Figure 70 shows only days on which both instruments measured values greater than 10 µg/m³, excluding the single highest concentration date on July 1, 2017 (TEOM measured 30.3 and BAM measured 31.7 µg/m³).

Figure 68 Daily averaged 24-hour PM_{2.5} BAM and TEOM data in the Houston-Galveston Region in 2017 through late October

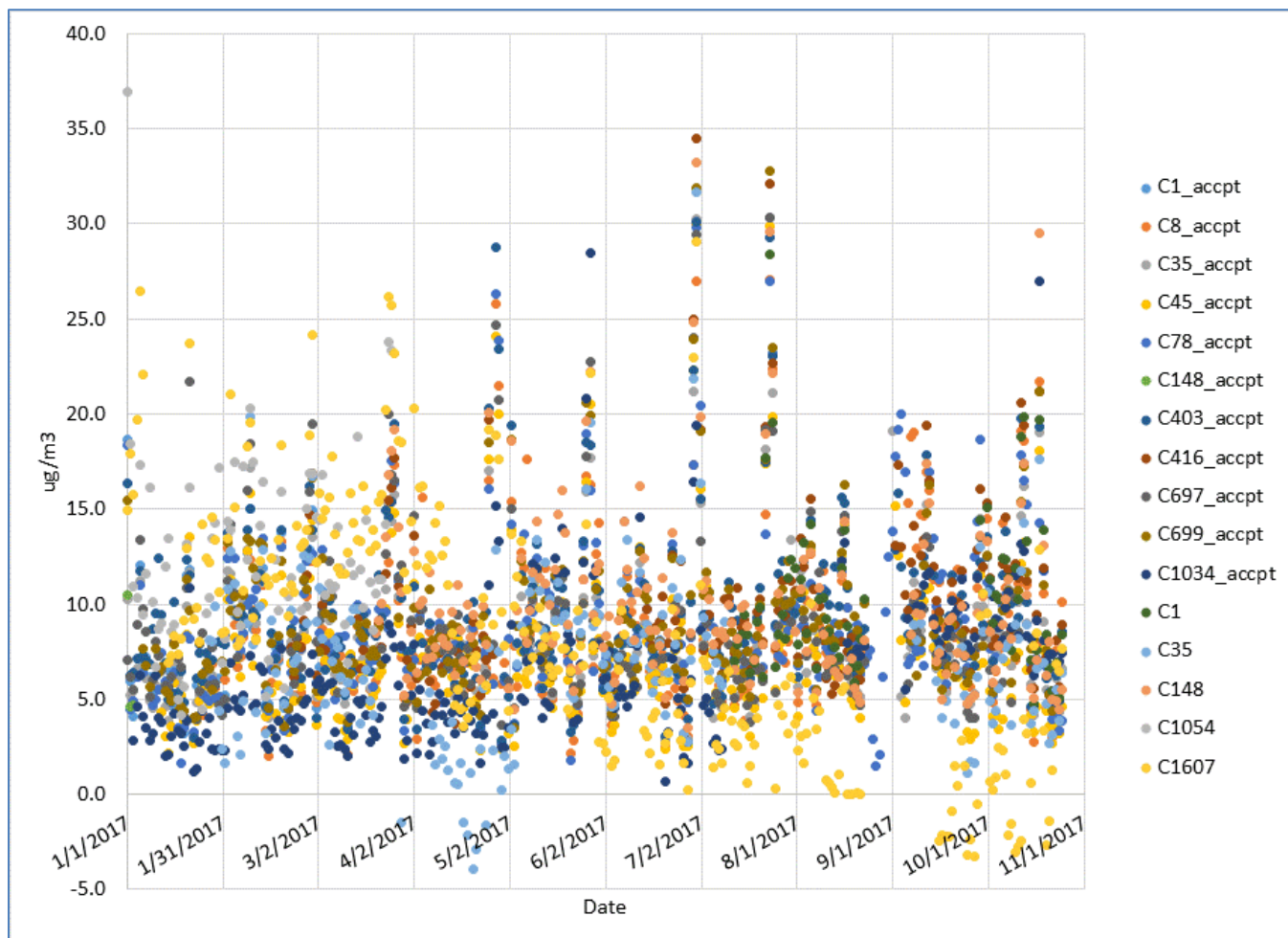


Figure 69. CAMS 35 BAM vs TEOM 2017 averaged 24-hour data

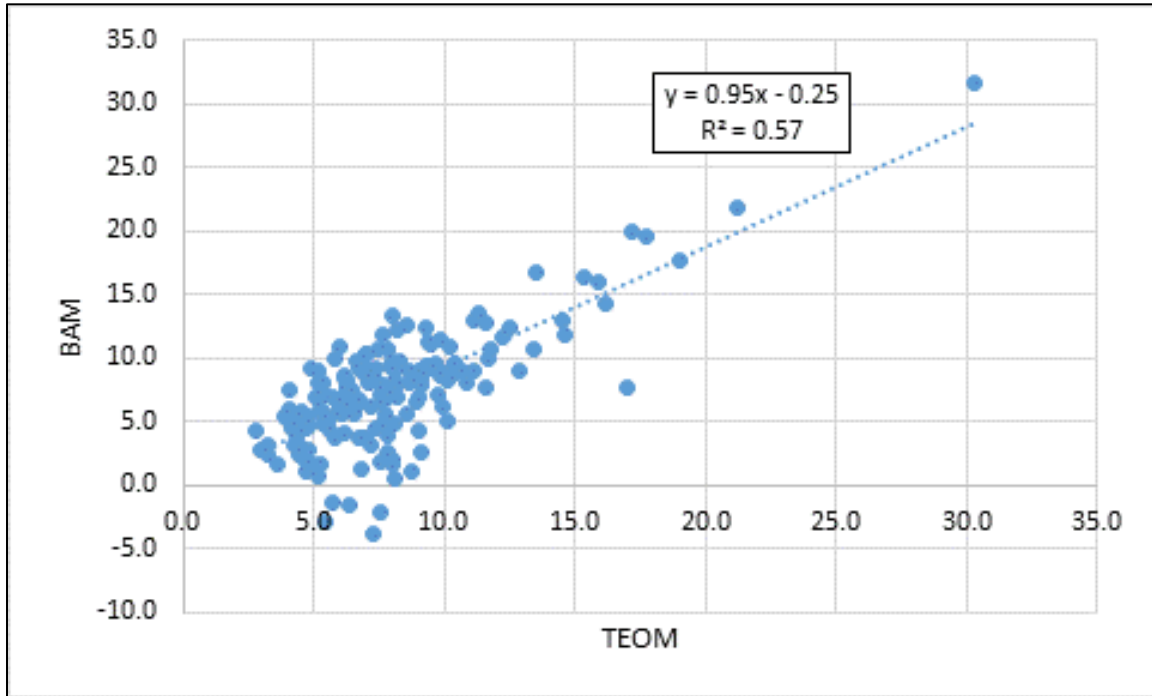


Figure 70. CAMS 35 BAM vs TEOM 2017 averaged 24-hour data when both measure $> 10 \mu\text{g}/\text{m}^3$, one value excluded

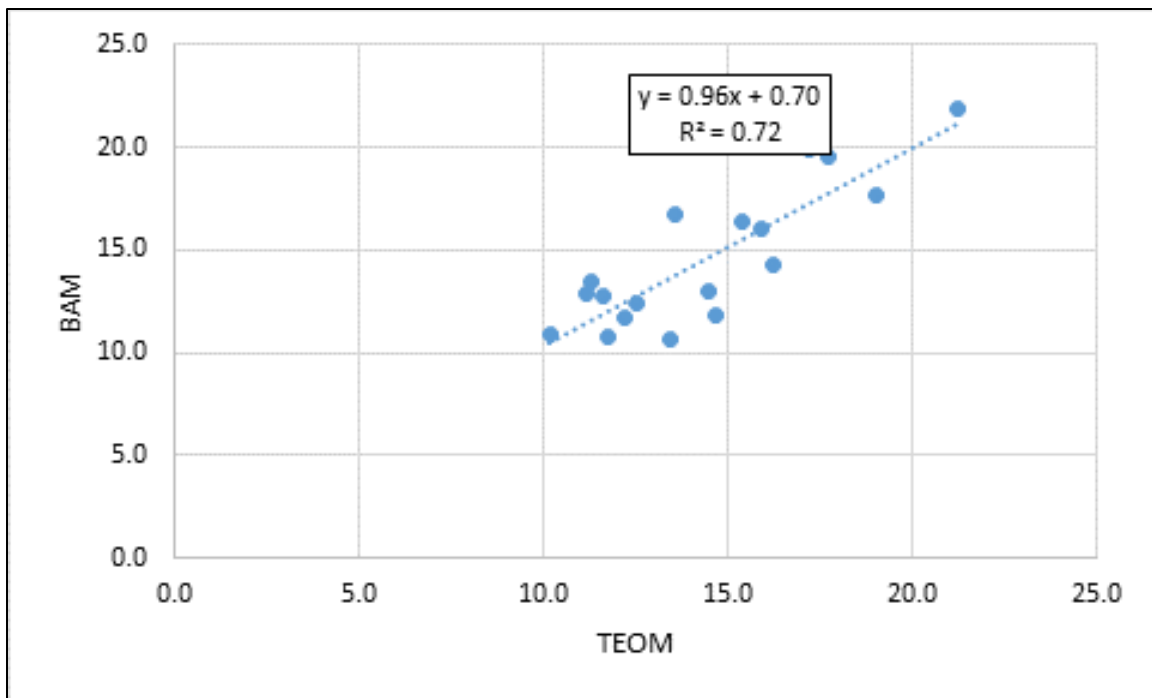
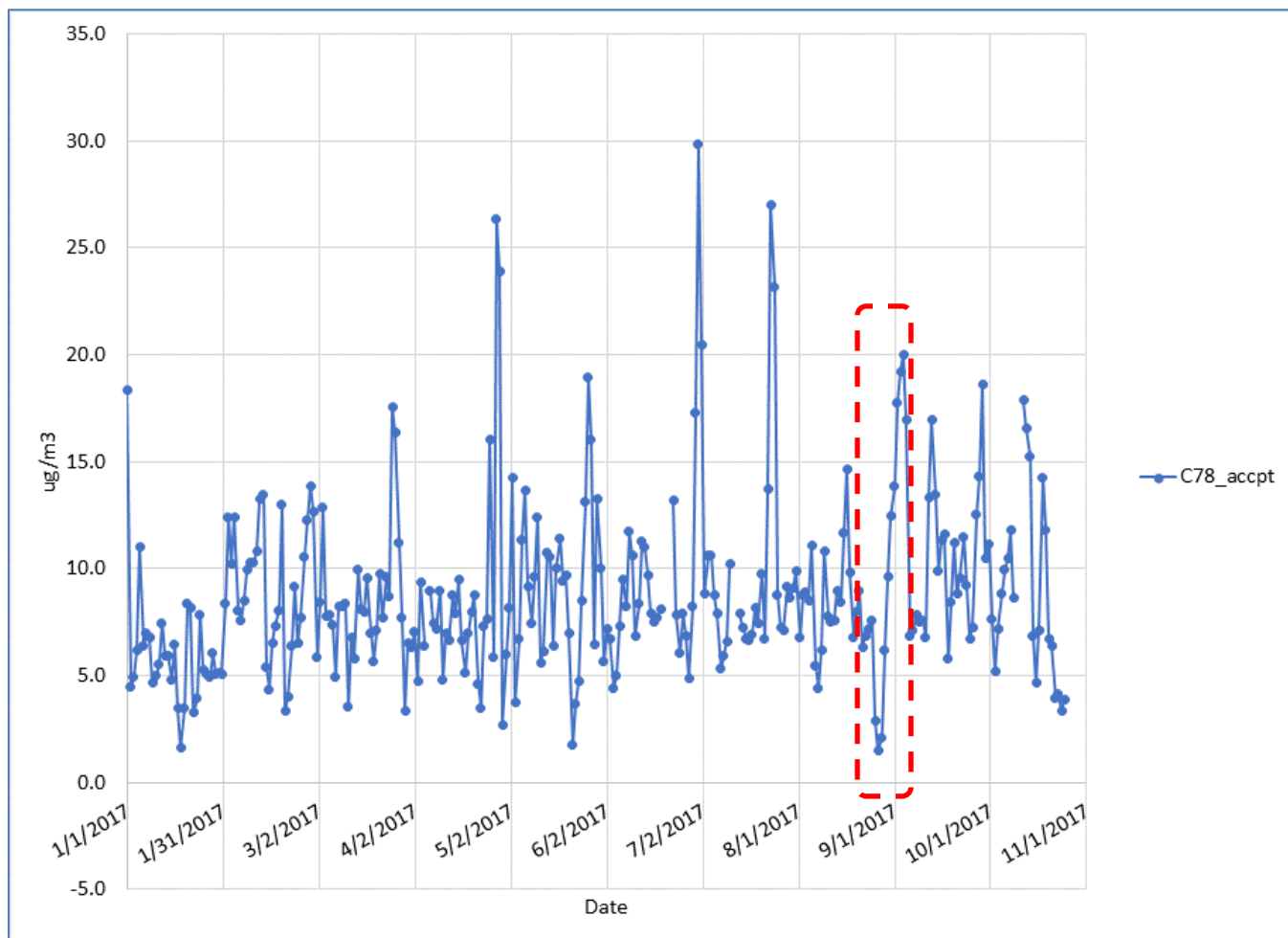


Figure 68 shows a break in the data in late August and early September corresponding to the equipment shut down during Hurricane Harvey. However, Figure 68 also shows that one monitor collected data over the period during which other sites did not. The CAMS 78 Conroe Relocated site in Montgomery County just north of Harris County was not shut down, and had continuous data collection over the late August – early September period. Figure 71 shows the daily average 24-hour concentrations for CAMS 78 for 2017, with the Hurricane Harvey period highlighted. Concentrations during the storm were low, most likely owing in large part to rain. However, the figure shows concentrations climbing in the ensuing days.

Figure 71. Daily averaged 24-hour PM_{2.5} TEOM data for Conroe CAMS 78 in 2017 through late October



3.1.11 Effect of Hurricane Harvey on PM_{2.5}

As mentioned above, all of the TCEQ and City of Houston PM_{2.5} monitoring/sampling sites were temporarily shut down in late August 2017 owing to Hurricane Harvey; with an exception being CAMS 78 Conroe Relocated site in Montgomery County adjacent to Harris County, which had continuous data collection over the Hurricane Harvey period. In addition, the nearby National Weather Service site CAMS 5008 also kept running during the storm period providing meteorological data. Figure 72 shows the annotated ground track of the hurricane/tropical storm during late August while the storm approached and passed over Texas and Louisiana. Data were

accessed from <https://www.wunderground.com/hurricane/atlantic/2017/hurricane-harvey?map=history> (October 2017). Figure 73 shows the hourly time series from the CAMS 78 Conroe site for 2017 through late October, with the period of August 25 through 29 highlighted. Figure 74 shows the data from CAMS 78 for the two month period August and September 2017. Figure 75n shows the hourly time series from the CAMS 5008, the National Weather Service Conroe site for August and September 2017, also with the period of August 25 through 29 highlighted.

During the storms' passage, wind speed rose and significant rain fell, as would be expected. Interestingly, ozone concentrations, solar radiation, and temperature were flat, showing no diurnal pattern and ozone hovered around 30 ppb, while NOx concentrations were close to 0.0. As mentioned earlier, PM_{2.5} concentrations were low during the storm, but rose for several days after the rain ended. Note that no problems are cited in the operator log and these data have been validated.

Figure 72. Ground track color coded for wind speed for Hurricane Harvey from Weather Underground data, relative to CAMS 78 in Montgomery County

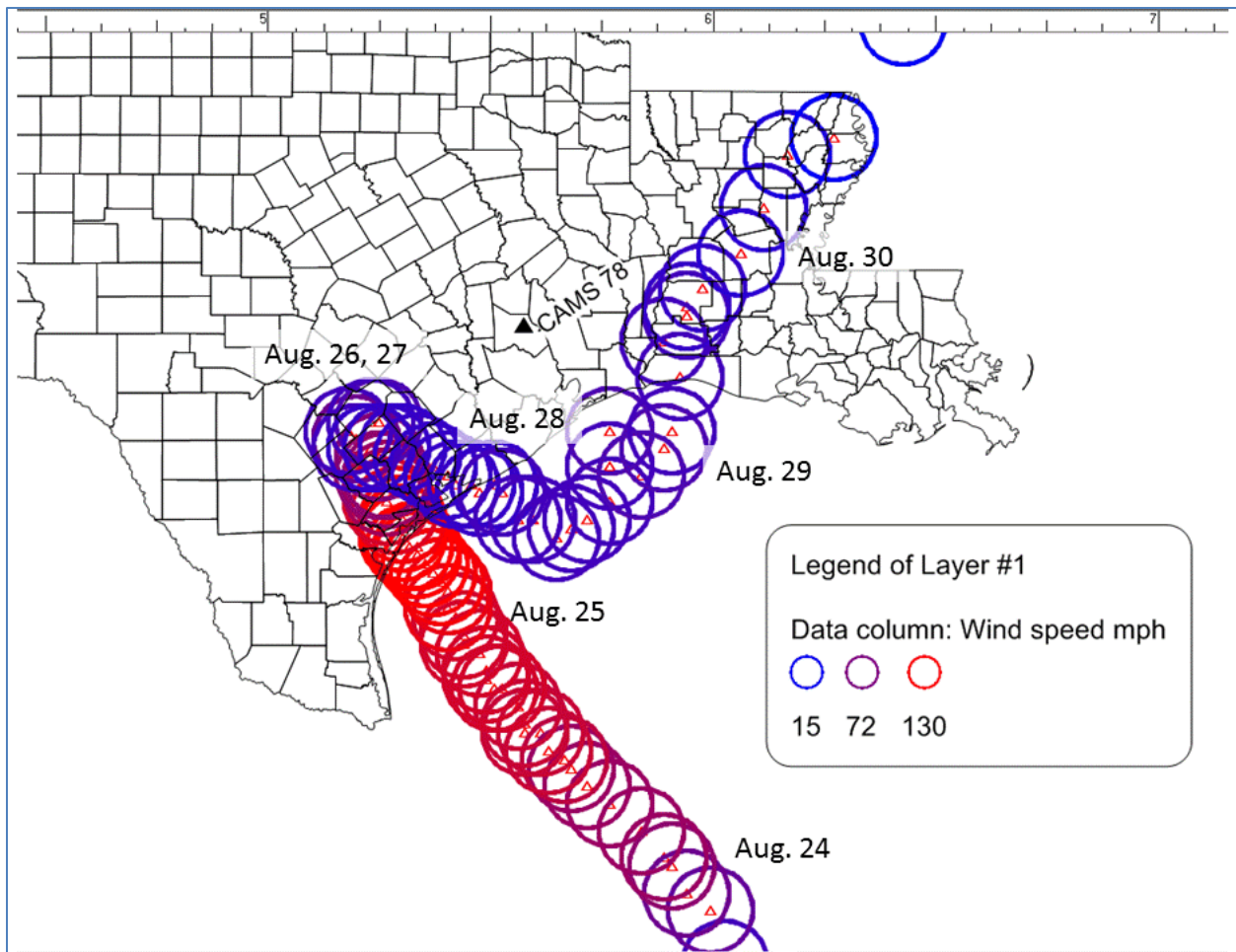


Figure 73. Hourly time series from the CAMS 78 Conroe Relocated site for 2017 through late October, Aug. 25 – Aug. 29 highlighted

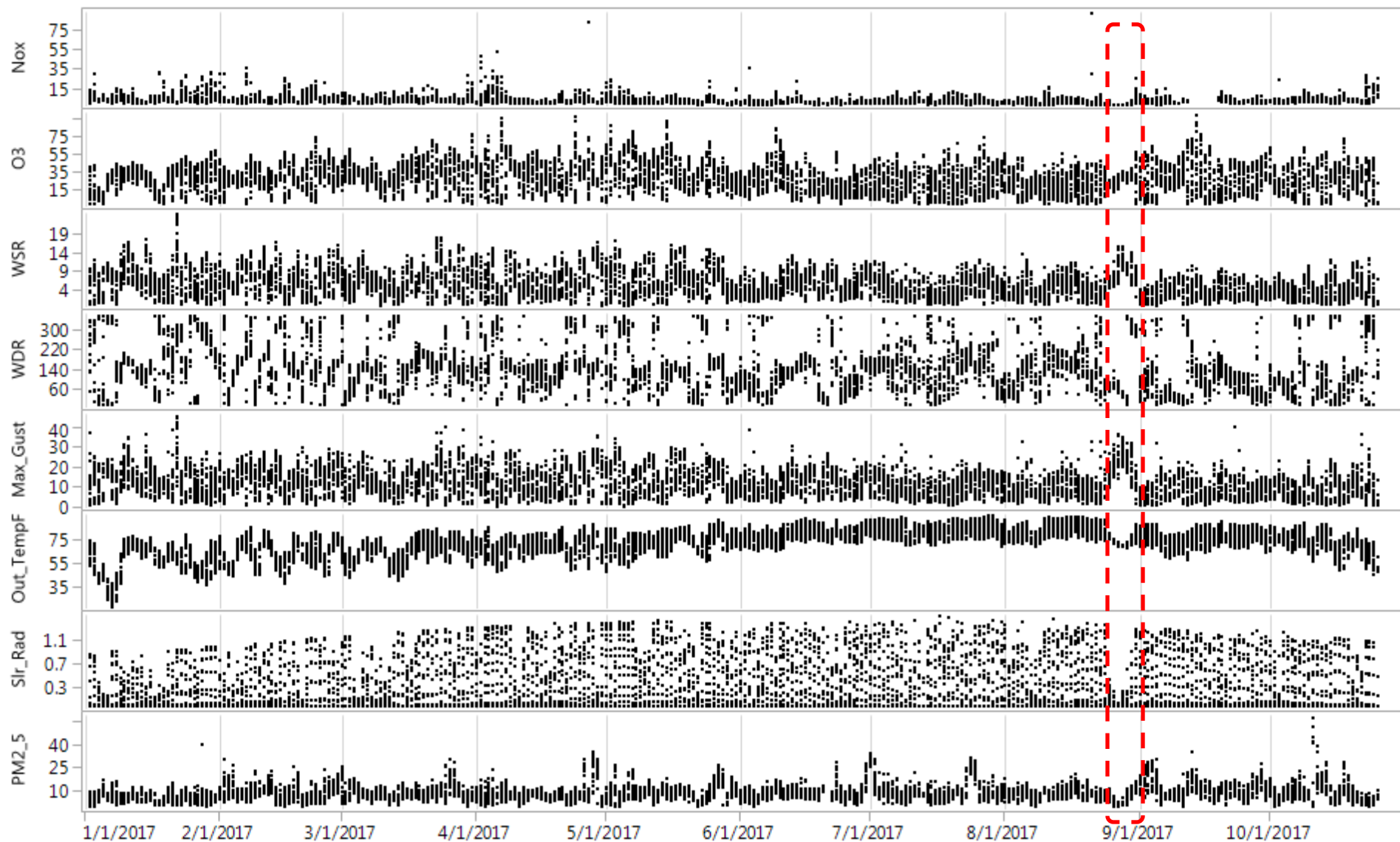


Figure 74. Hourly time series from the CAMS 78 Conroe Relocated site for August and September 2017, Aug. 25 – Aug. 29 highlighted

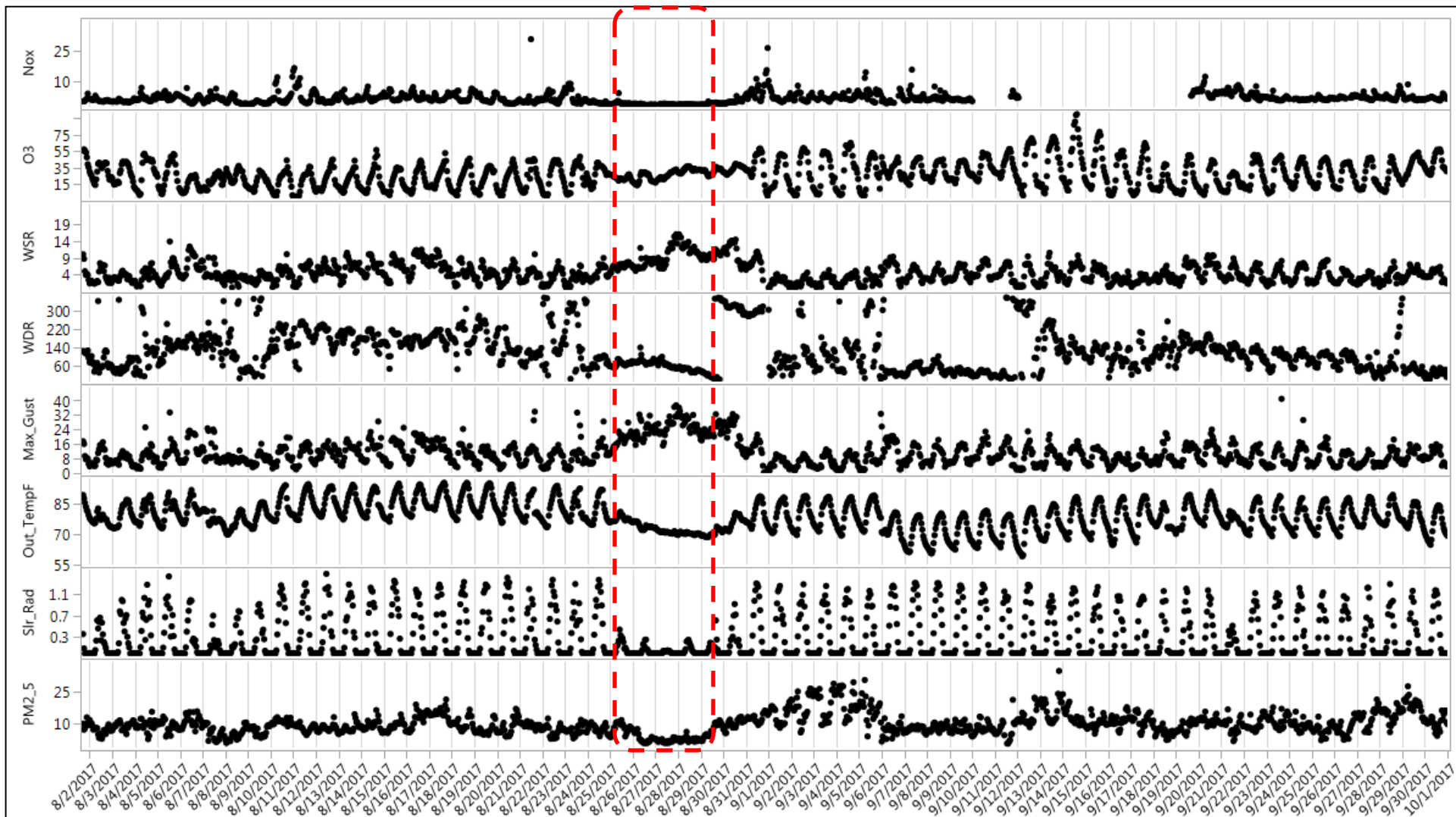
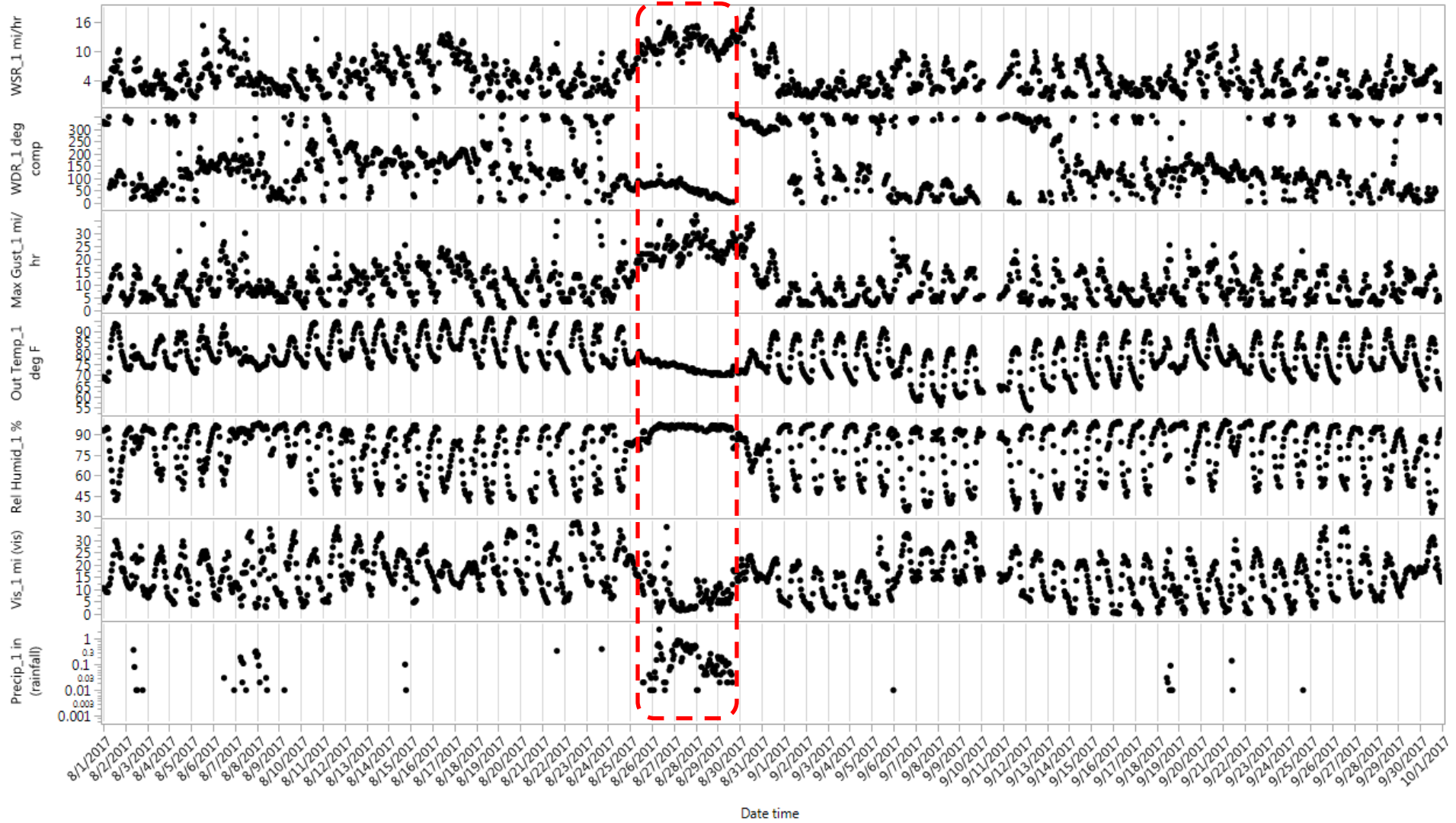


Figure 75. Hourly time series from the CAMS 5008 Conroe National Weather Service site for August and September 2017, Aug. 25 – 29 highlighted



3.2 Galveston Sampling Results

3.2.1 PMF Analysis for Galveston

Most of these PM_{2.5} species used for PMF were also used in the Clinton Dr. PMF analysis. However at Galveston the signal to noise ratios for organic and elemental carbon were significantly lower. A total of 316 elemental samples are available for analysis from 2013 through 2015 (no data received since then). Only 278 ion and carbon samples are available, so a complete data total is 278 samples.

Eight factors are identifiable from the Galveston data. Only 277 samples were used, as one day was disqualified owing to unusual data. With only three years of data there is less information available for accurate assessments. The PMF analysis showed relatively poor reproducibility through bootstrap runs, and a 0.5 FPEAK rotation appeared to produce the best bootstrap matches. The resulting factor profiles appear in Figure 76 with approximate apportionment to total mass in Figure 77.

Figure 76 FPEAK rotation (0.5) resulting Galveston PMF factors

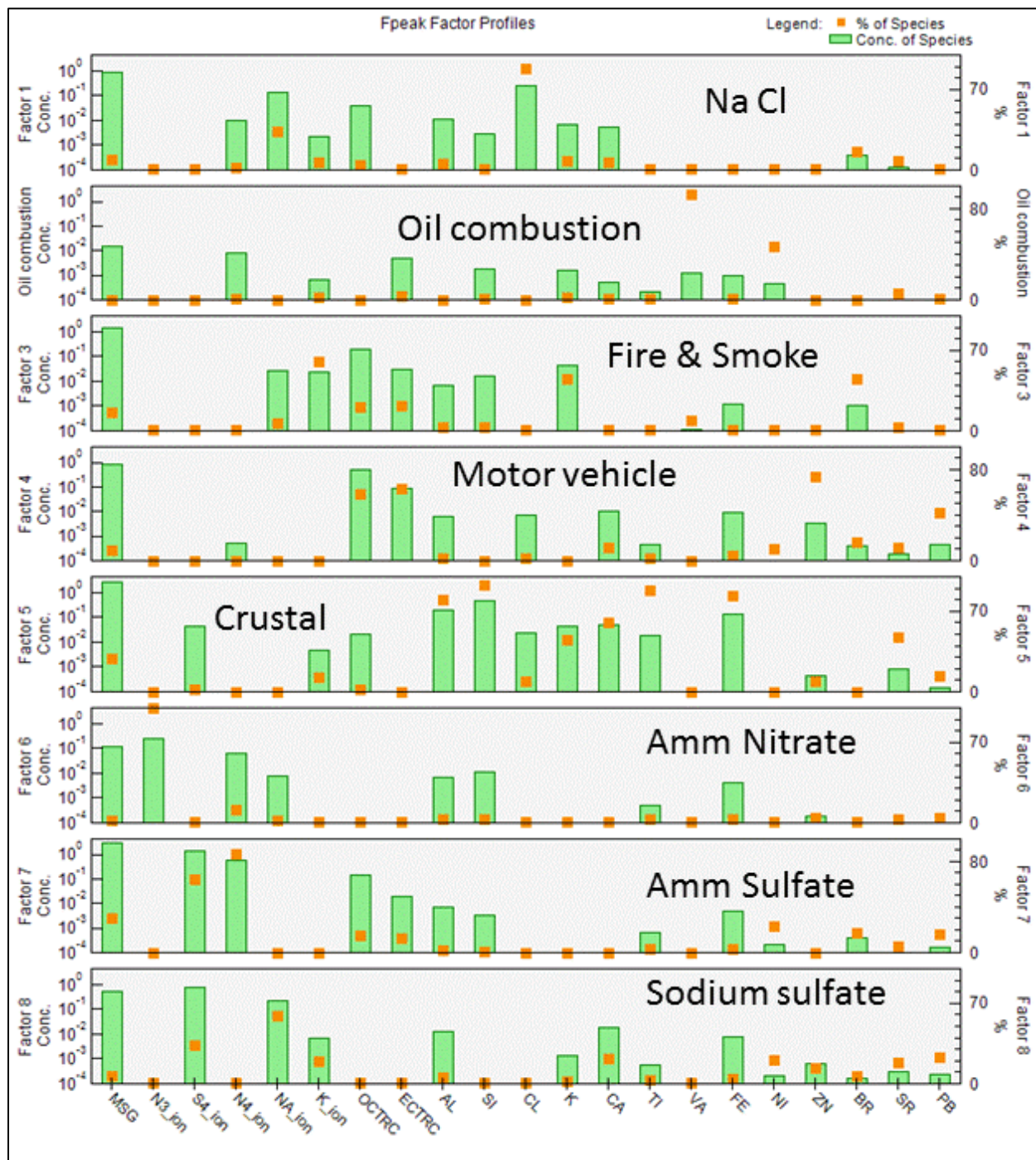
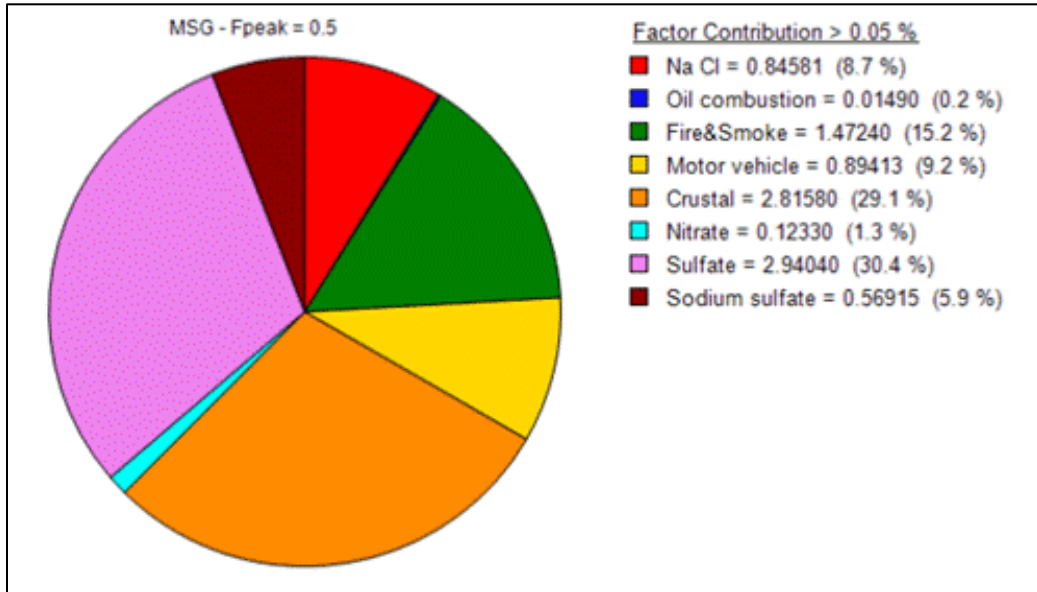


Figure 77 Approximate apportionment of factors and total mass at Galveston



3.3 Chamizal Sampling Results

3.3.1 PMF Analysis for Chamizal

PMF Analysis was conducted on the Chamizal speciated PM_{2.5} data. The speciation data were very closely examined. Earlier work on this project has included principal component analysis (PCA) work that identified five sources. The most recent PMF work identifies seven sources, although one which is dominated by a few elements may be associated with industry and is not readily identifiable. Figure 78 shows the source fingerprints from a rotated solution (FPEAK=0.5) that included a fixed constraint to get closure on matching the Chlorine ion with elemental sodium as a factor (mass ratio chlorine ion = 1.54 x sodium). Figure 79 shows a pie chart summarizing the contribution in terms of mass of each factor to total mass. This is very approximate, as crustal material is expressed in elemental as opposed to mineral form, and the sum of the speciated variables used in the model is less than the total mass. Nevertheless, the results fall in line with other finding that factors associated with motor vehicle emission sources, transported ammonium sulfate, and wind-blown crustal material comprise the majority of total PM_{2.5} mass.

Figure 78 FPEAK rotation (0.5) resulting Chamizal PMF factors

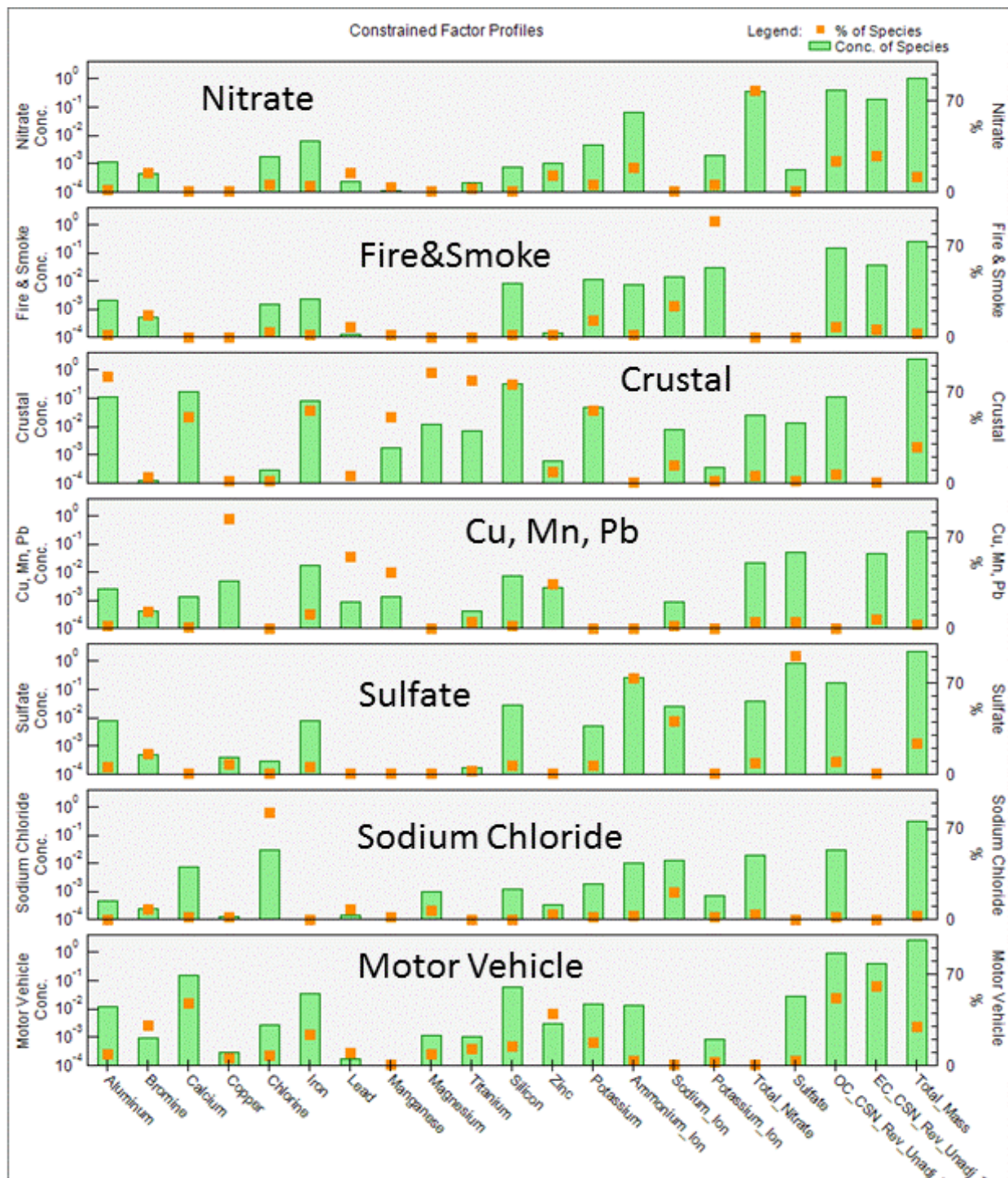
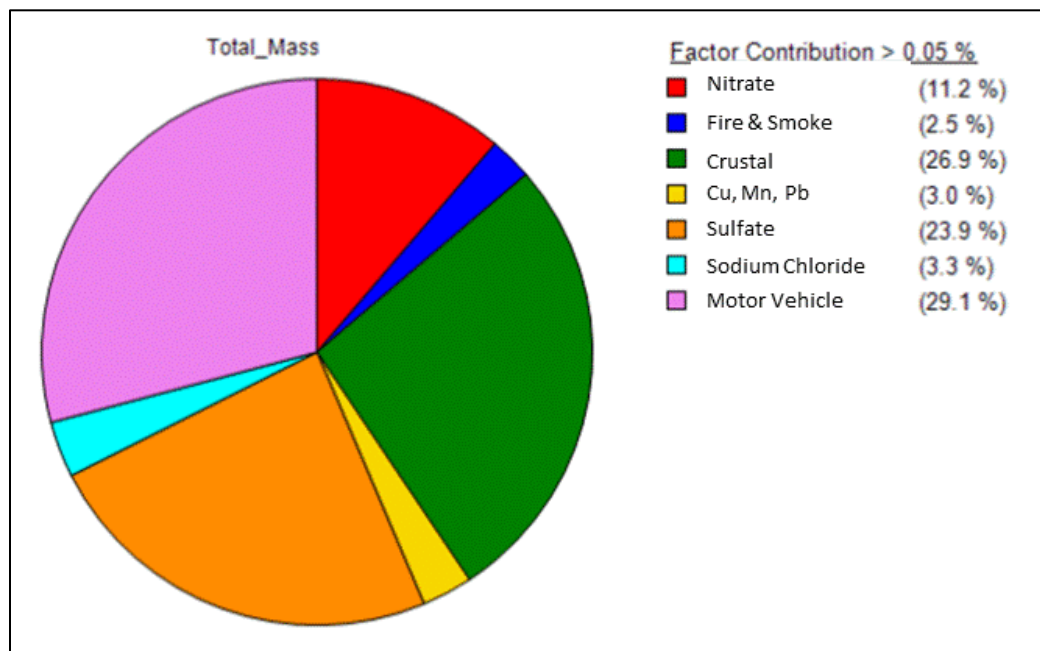


Figure 79 Approximate apportionment of factors and total mass at Chamizal



3.3.2 PM_{2.5} Case Study May 16, 2017

A shorter version of this case study appeared in the August 31, 2017 Quarterly Report on the Maintenance, Data Validation, and Data Analysis of El Paso Radar Wind Profiler Project (Umbrella Contract 582-16-560422; Internal TCEQ PCR#: 61800; Work Order 6). More detail has been added for this report.

Figure 80 shows the time series from May 10 to May 22, 2017, for hourly fine particulate matter for tapered element oscillating microbalance (TEOM) instruments at Ascarate Park CAMS 37 and UTEP CAMS 12, along with the beta-gauge instrument at Chamizal CAMS 41. The day of May 16 is a clear outlier, with all three sites measuring elevated concentrations. Figure 81 is a closer look at May 15 – 17, 2017. The local news media in El Paso reported on a high dust event in the area in the May 16, 2017 forecast (<http://kfoxtv.com/news/local/winds-blowing-dust-back-in-the-borderland>). The TCEQ weather forecast on Tuesday May 16 said:

Strong afternoon winds are expected to generate and transport patchy blowing dust in parts of West Texas and the Panhandle, including in the El Paso area, where the daily PM₁₀ AQI could reach "Moderate" or possibly higher levels, and in the Lubbock and Midland-Odessa areas, where the duration, intensity, and associated precipitation is not expected allow the daily PM₁₀ AQI to rise beyond the "Good" range.

Figure 80. El Paso County PM_{2.5} monitor (TEOM & Beta-gauge) concentrations May 10 – 22, 2017

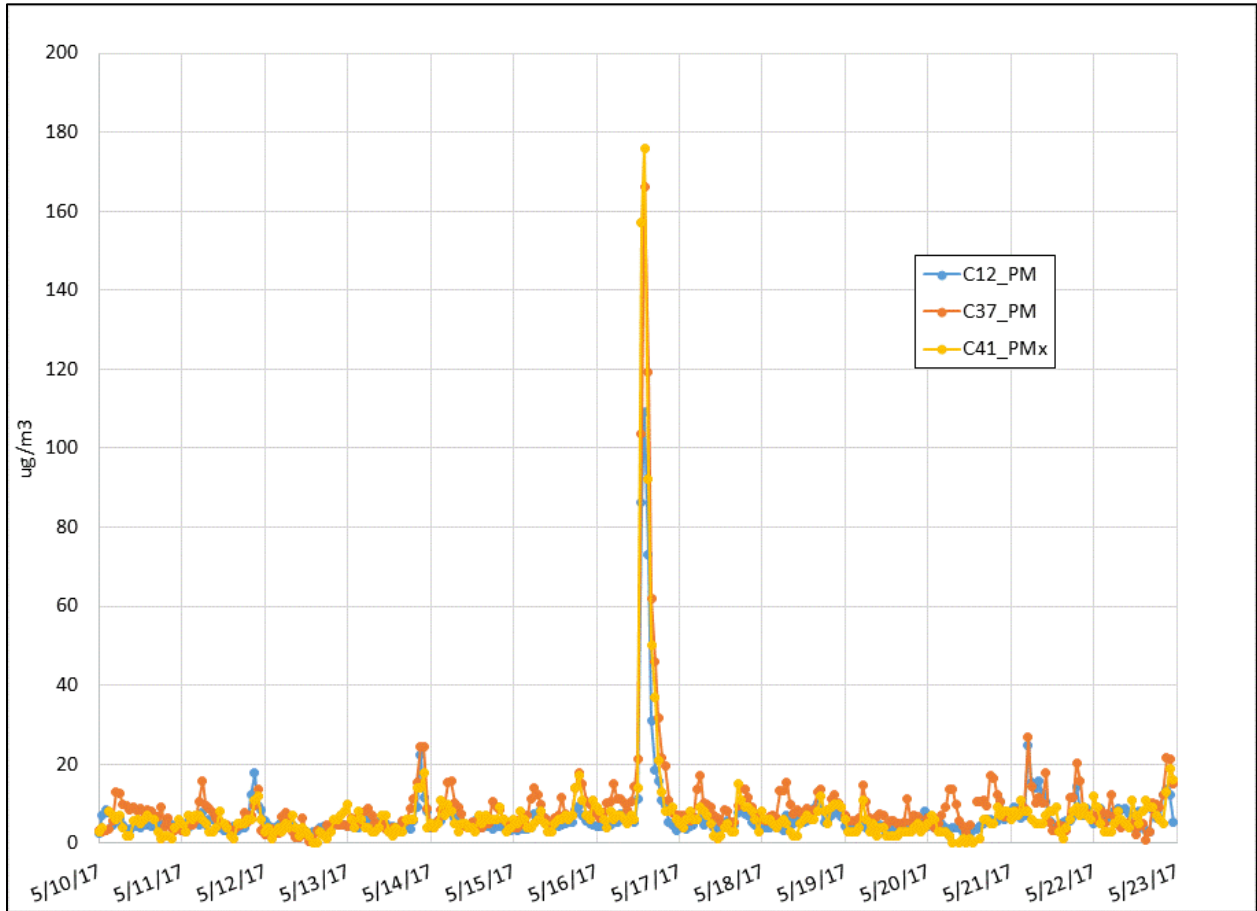
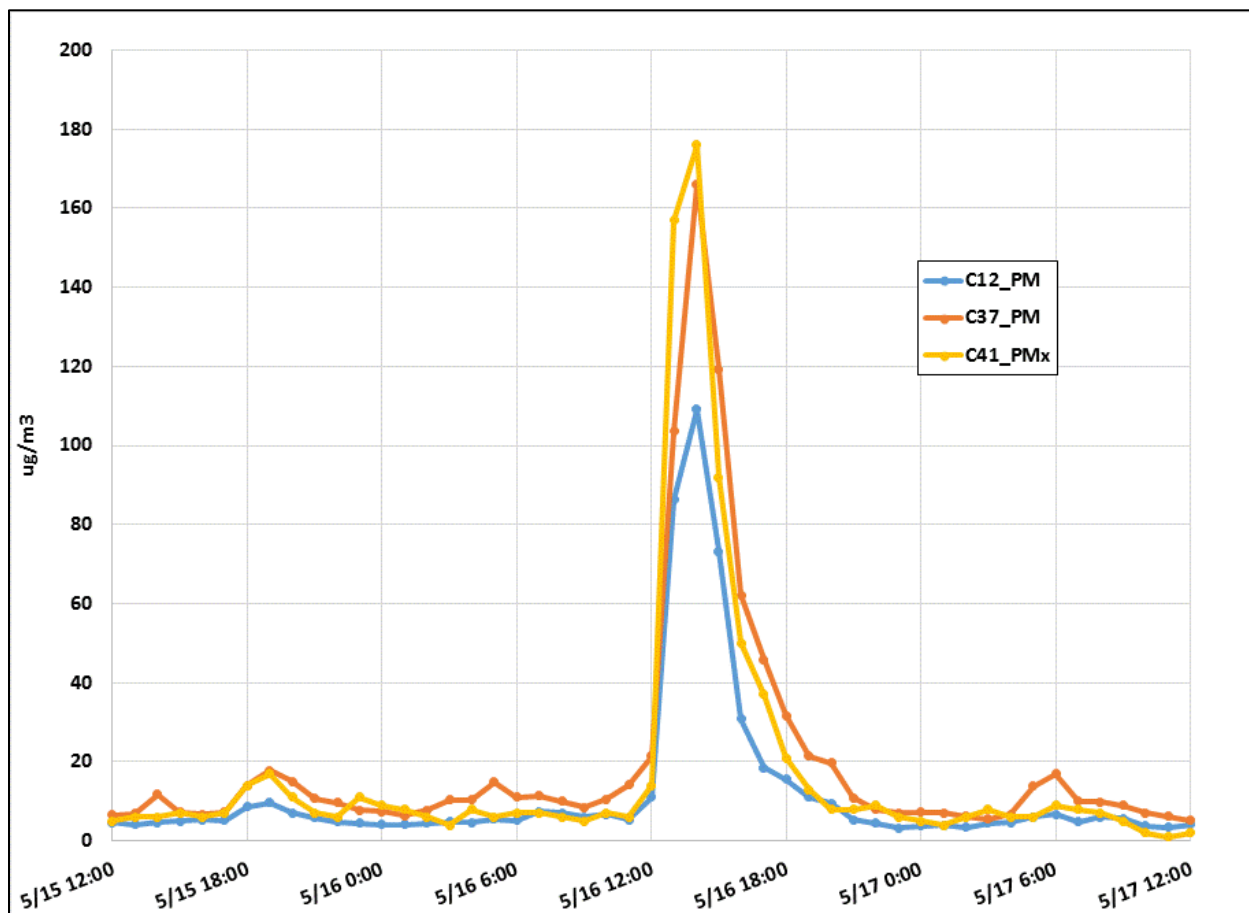


Figure 81. El Paso County PM_{2.5} monitor (TEOM & Beta-gauge) concentrations May 15 – 17, 2017



The El Paso radar wind profiler (RWP) operated by UT at the Socorro Hueco CAMS 49 site provides upper air winds that are used in models and tools such as HYSPLIT. The RWP, in Figure 82, shows on May 14, 2017, the area was experiencing light and variable winds, and Figure 83 for a HYSPLIT 24-hour ensemble back trajectory started at noon May 14 over the Chamizal site shows a fetch from the north and west. Figure 84, shows on May 15, 2017, the area was experiencing light and variable winds, and Figure 85 for a HYSPLIT 24-hour ensemble back trajectory started at noon May 15 over the Chamizal site shows a very short fetch indicating light and variable winds.

On May 16, shown in Figure 86, wind speed picked up under westerly flow over a deep range of the atmosphere. Surface winds had peak gusts around 50 miles per hour in mid-afternoon, although the RWP suggests the highest wind near the surface would have been just after noon MST. Figure 87 shows a HYSPLIT 24-hour ensemble back trajectory started at noon May 16 over the Chamizal site with a narrow starting fetch. Strong winds were still present in the early morning on the following day May 17, shown in Figure 88, which may have caused to the elevated PM_{2.5} at 6 a.m. MST in Figure 6 (above). Figure 89 shows a HYSPLIT 24-hour ensemble back trajectory started at noon May 17 over the Chamizal site.

Figure 90 shows a relatively short 6-hour ensemble back trajectory from Chamizal at noon on May 16, and Figure 91 shows a Google map image with the ensemble back-trajectory points from one and two hours back from noon. The air was fast moving coming over a dusty area and

this may explain the high concentrations that persisted over just a few hours on May 16 in the afternoon.

Figure 82. RWP data for El Paso on May 14, 2016

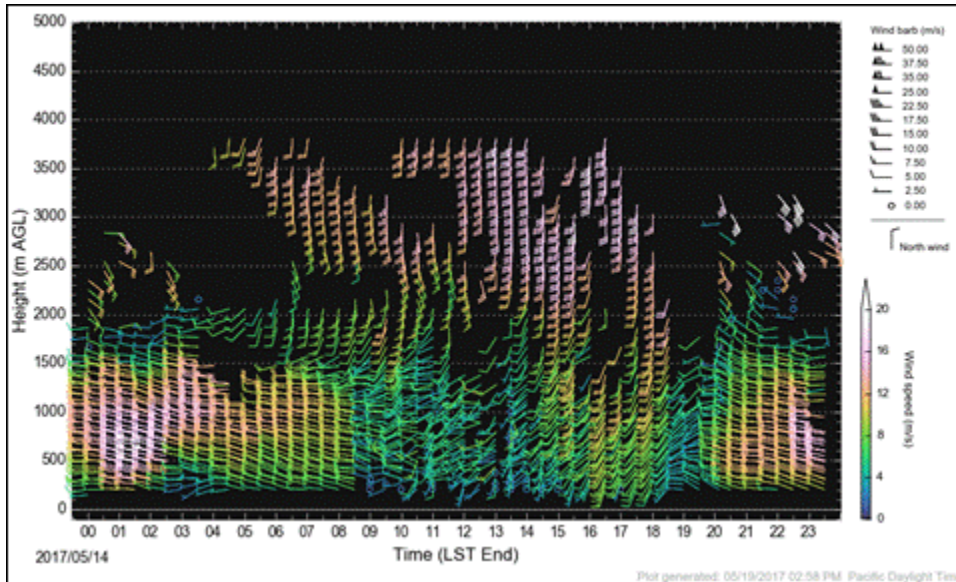


Figure 83. HYSPLIT ensemble 24-hour back trajectory from noon MST on May 14, 2017 from El Paso, TX

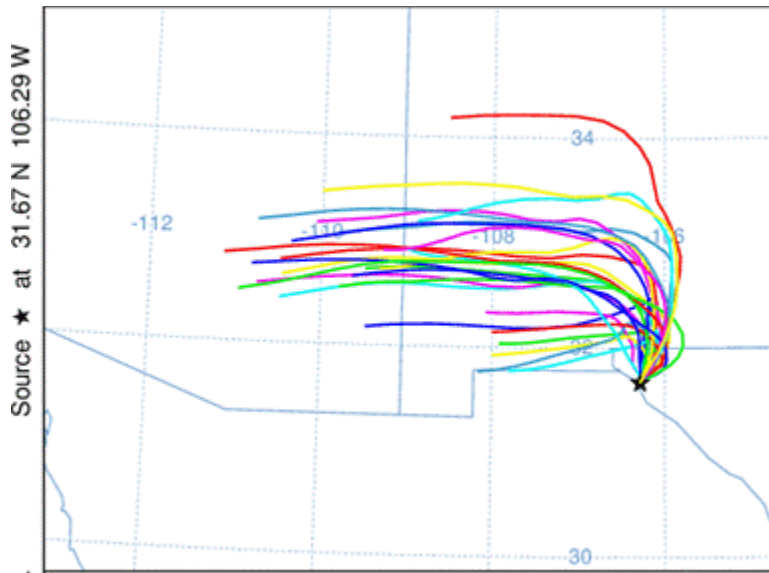


Figure 84. El Paso radar wind profiler on May 15, 2017, data before a high particulate matter day, light and variable mid-day winds picking up at night to strong westerly

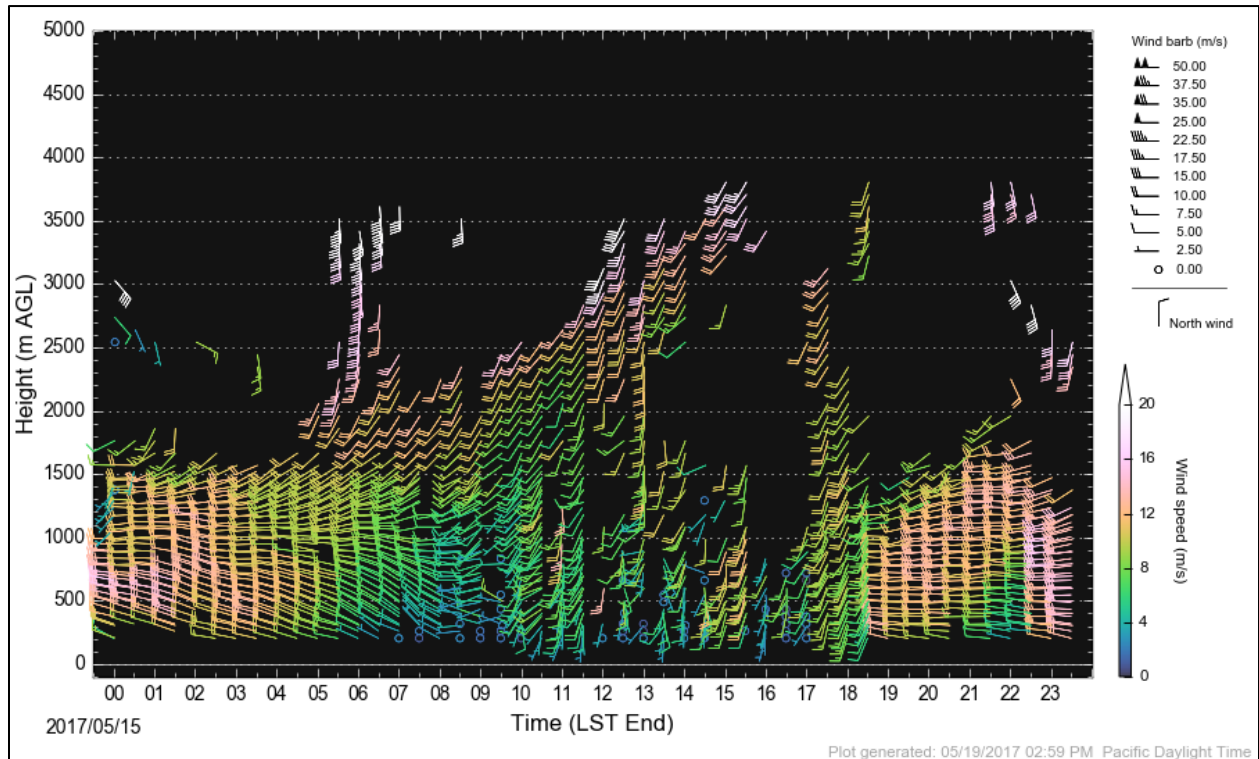


Figure 85. HYSPLIT ensemble 24-hour back trajectory from noon MST on May 15, 2017 from El Paso, TX

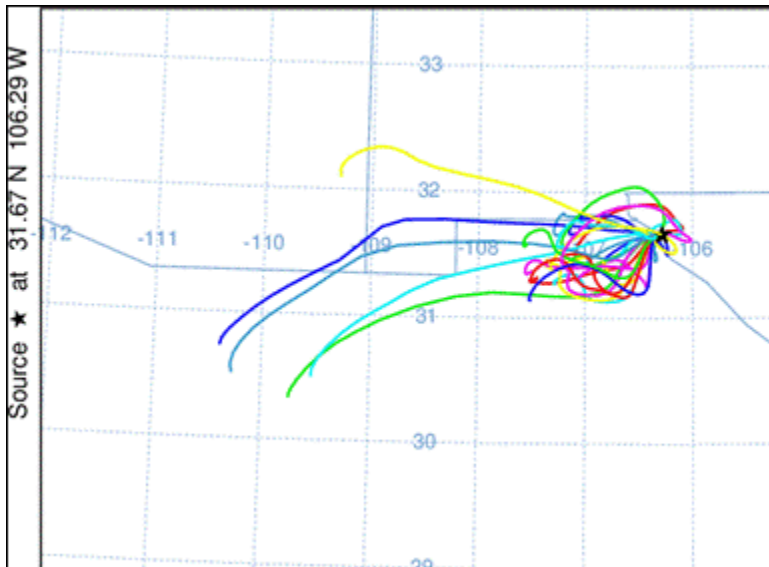


Figure 86. El Paso radar wind profiler on May 16, 2017, high particulate matter day, winds picking up and strong westerly flow

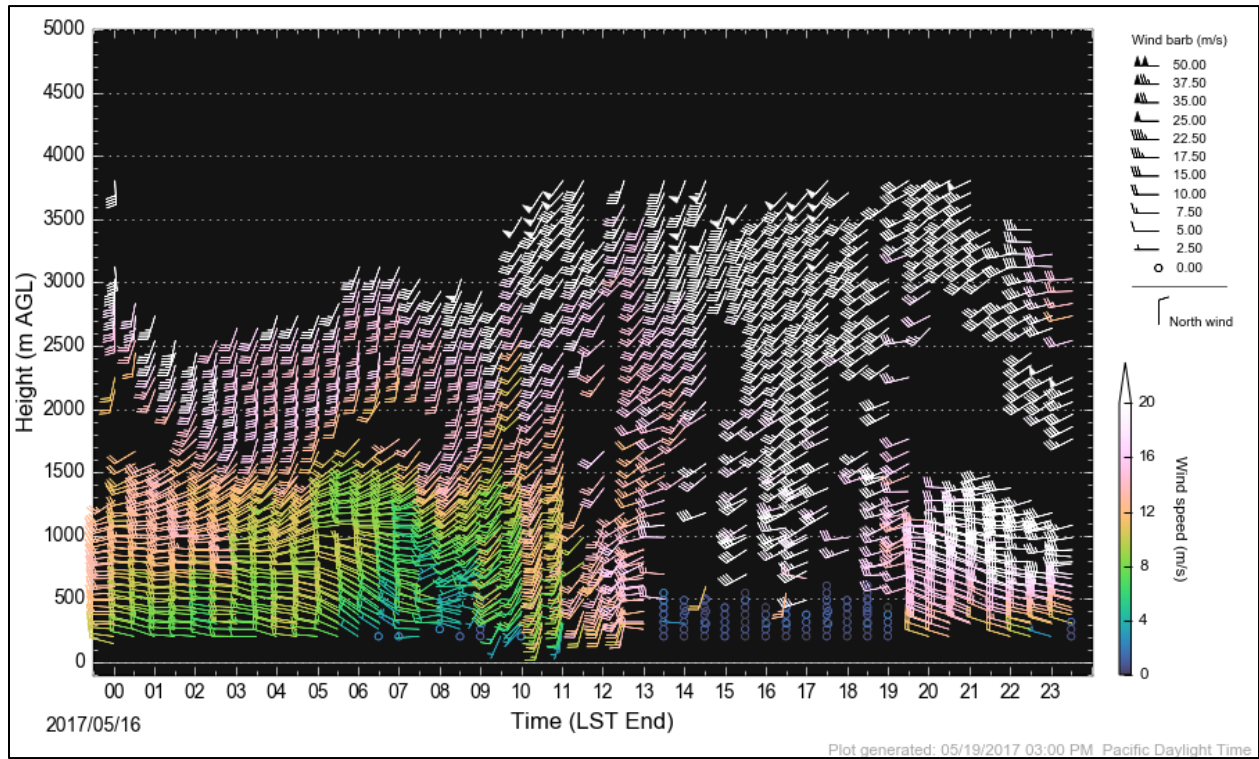


Figure 87. HYSPLIT ensemble 24-hour back trajectory from noon MST on May 16, 2017 from El Paso, TX

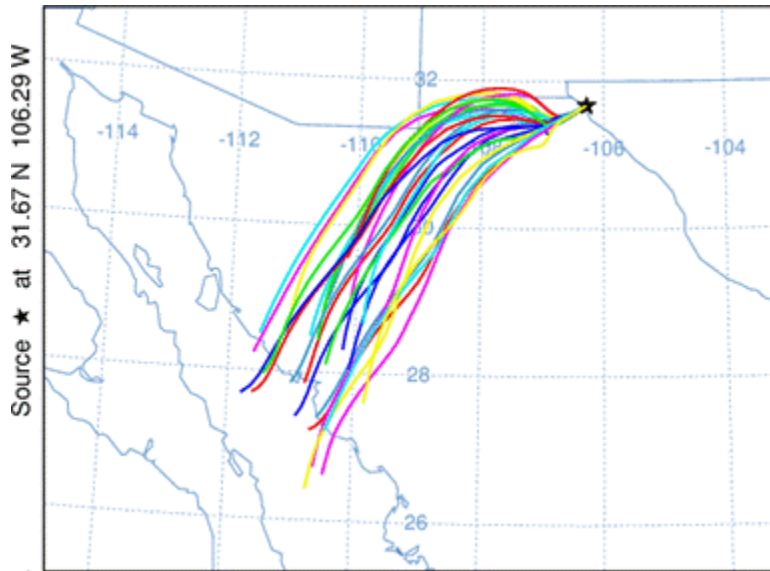


Figure 88. El Paso radar wind profiler on May 17, 2017, day after a high particulate matter day, more daytime light and variable winds

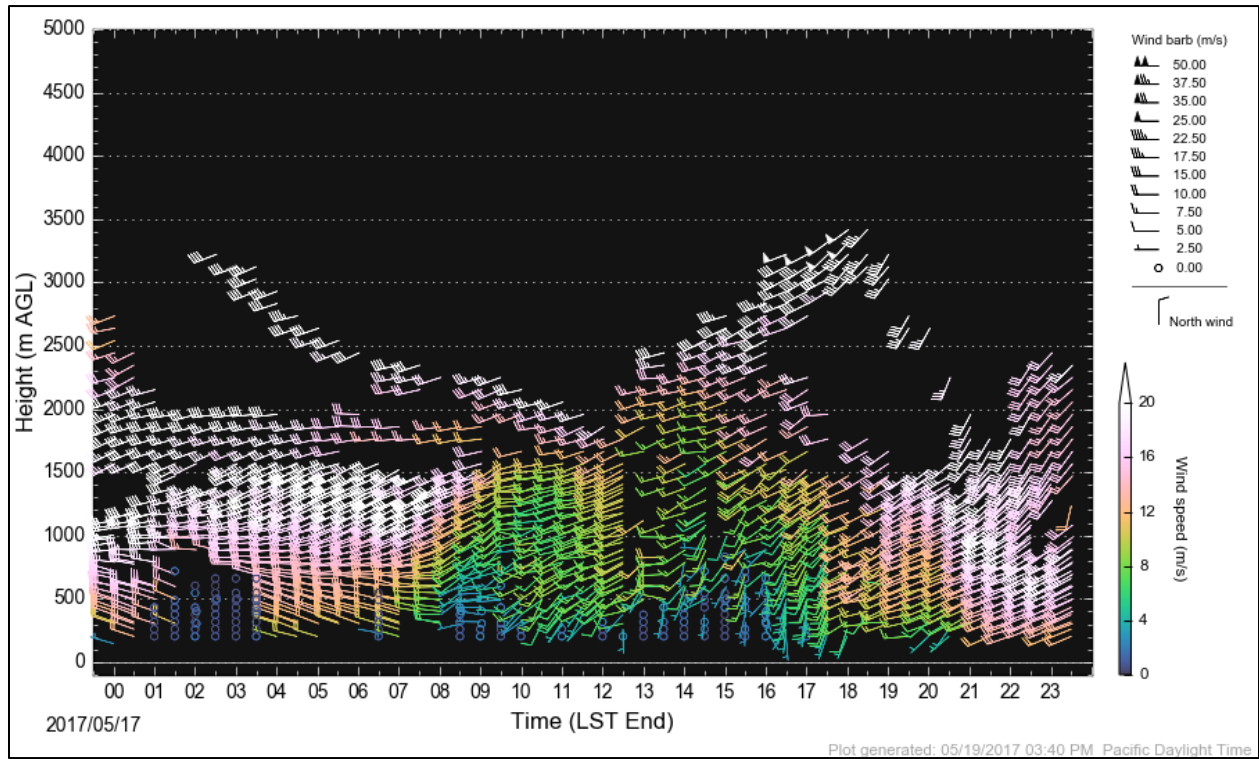


Figure 89. HYSPLIT ensemble 24-hour back trajectory from noon MST on May 17, 2017 from El Paso, TX

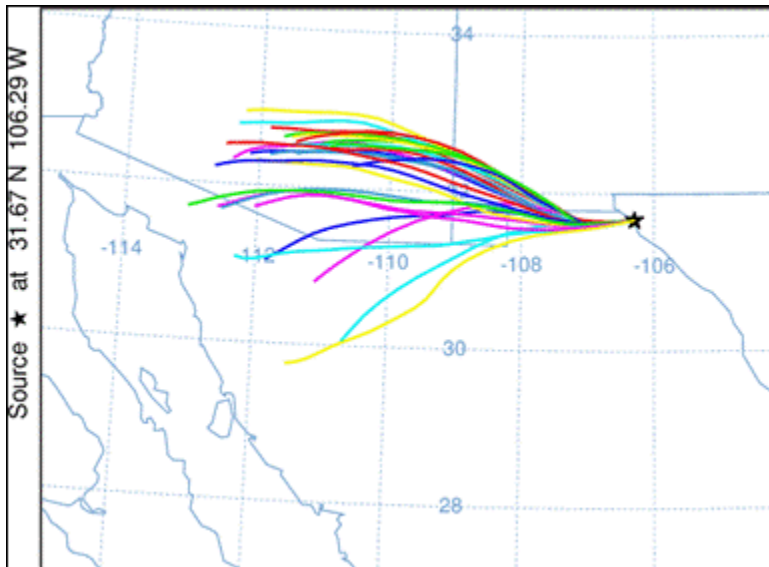


Figure 90. HYSPLIT ensemble 6-hour back trajectory from noon MST on May 16, 2017 from El Paso, TX

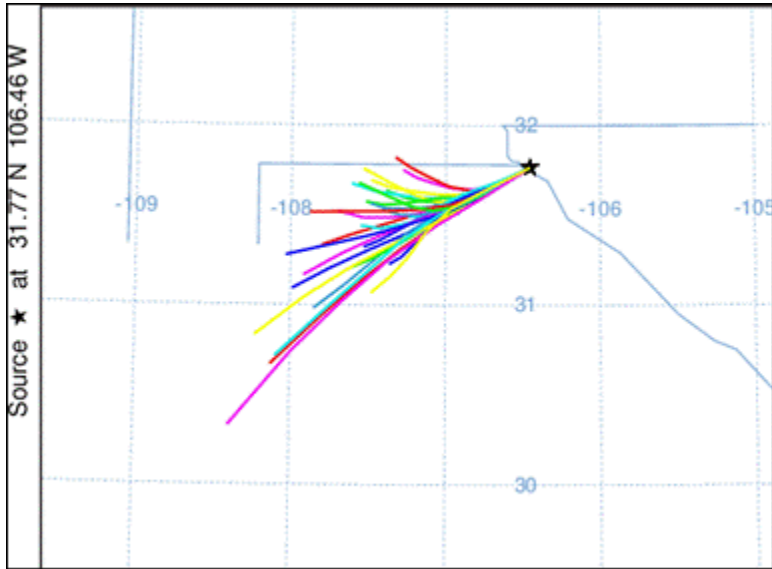
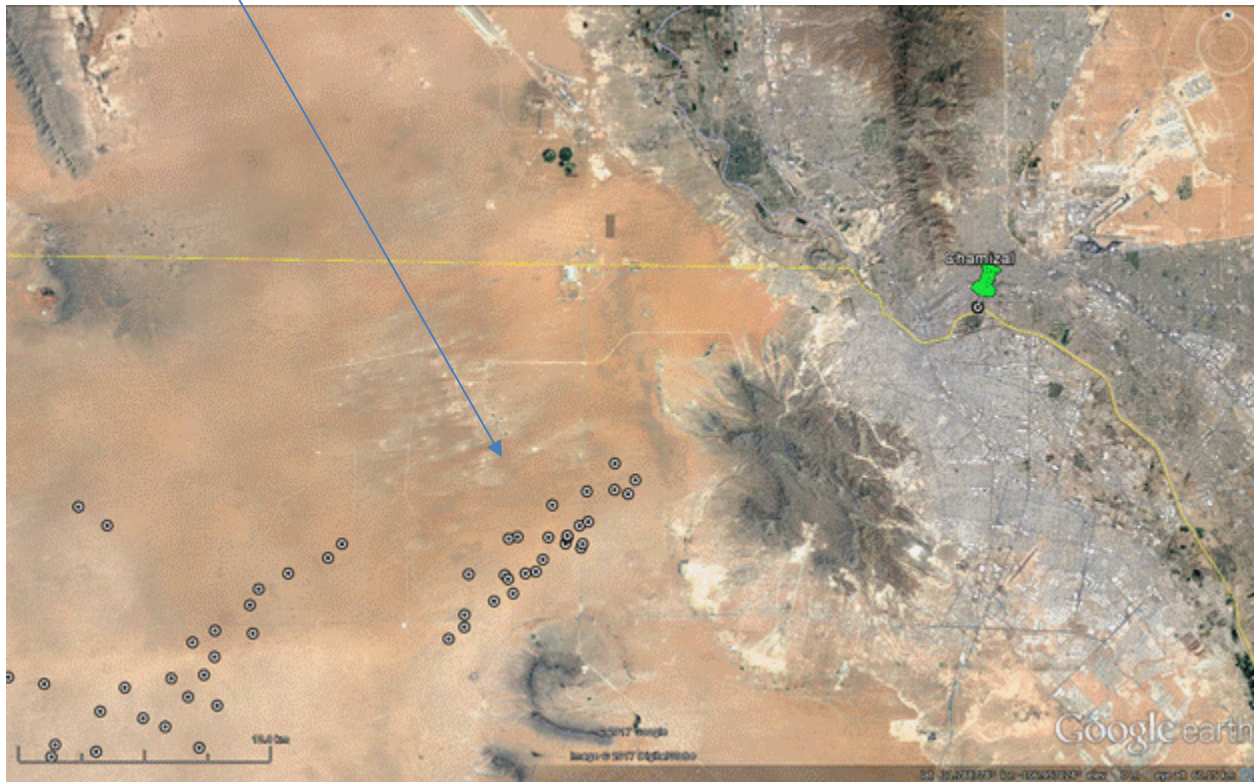


Figure 91. One hour back-trajectory end points from noon MST at Chamizal on May 16, 2017



3.4 West Texas PM_{2.5}

The Guadalupe Mountains GUMO1 site is 96 miles (155 kilometers) east of El Paso site (latitude 31.833, longitude -104.8094). Big Bend is 200 miles (321 km) south-southeast of GUMO1 and 260 miles (418 km) southeast of El Paso. Figure 92 shows a map of the West Texas sites in relation to much of central U.S. and northern Mexico.

3.4.1 Guadalupe Mountains National Park PM_{2.5} Data

This section is dedicated to use of the data collected at the Guadalupe Mountains GUMO1 particulate matter sampling site. Multivariate analysis has been conducted using the PMF 5.0. The most recent data download included data through April 2017. The modeling used the temperature fractions of elemental (EC1, EC2) and organic carbon (OC2, OC3, OC4), as these species had better error estimates compared to total EC and OC.

UT has examined the GUMO1 speciated PM_{2.5} data downloaded from the Interagency Monitoring of Protected Visual Environments aerosol data from the Federal Land Manager Environmental Database at <http://views.cira.colostate.edu/fed/DataWizard/Default.aspx> (accessed March 2018). In this analysis, UT used speciated PM_{2.5} data from January 1, 2011 to April 30, 2017 for the multivariate PMF analysis. The character of the relationship between measurements and the associated measurement uncertainties for several species changed starting in 2011. This is reflected in Figure 93, Figure 94, Figure 95, and Figure 96 for elemental selenium and potassium, to provide examples of the change in data behavior.

Figure 92. Three West Texas PM_{2.5} sampling sites.

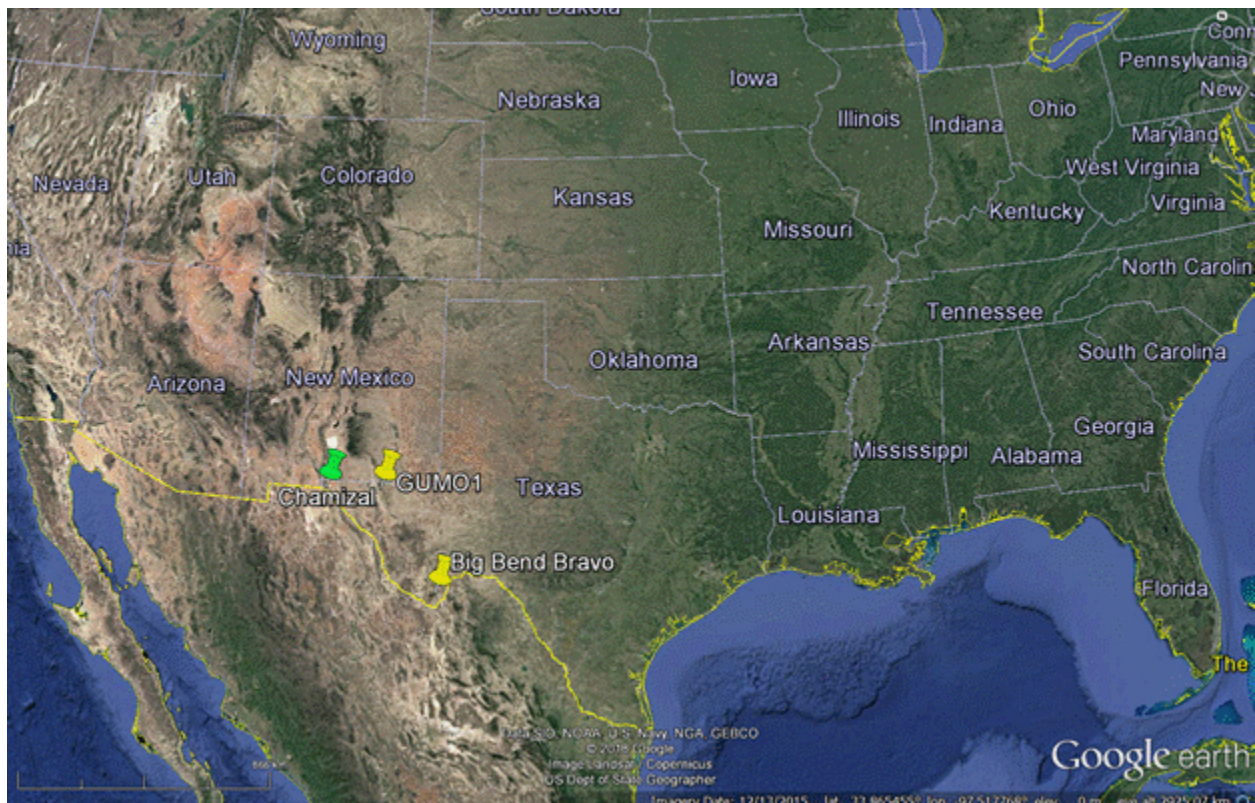


Figure 93. Elemental selenium (Se) uncertainty by mass at Guadalupe Mtn. site, 2008 - 2017

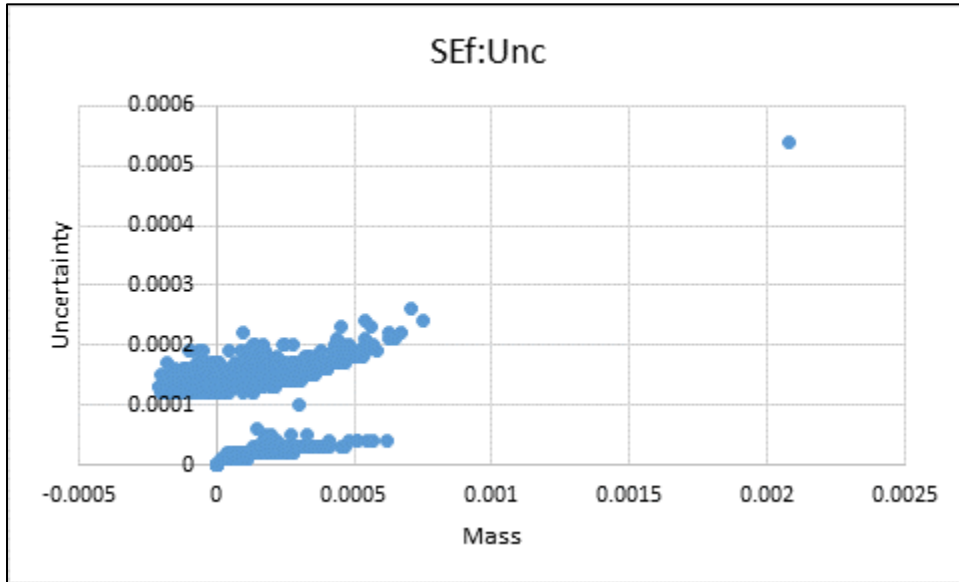


Figure 94. Ratio of uncertainty to mass for Se at Guadalupe Mtn. site, 2008 - 2017

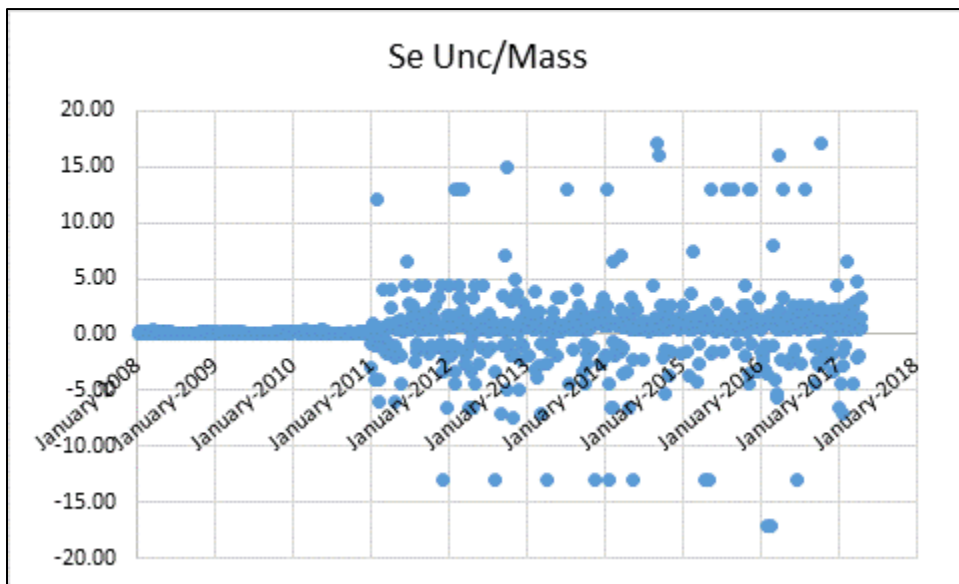


Figure 95. Elemental potassium (K) uncertainty by mass at Guadalupe Mtn. site, 2008 - 2017

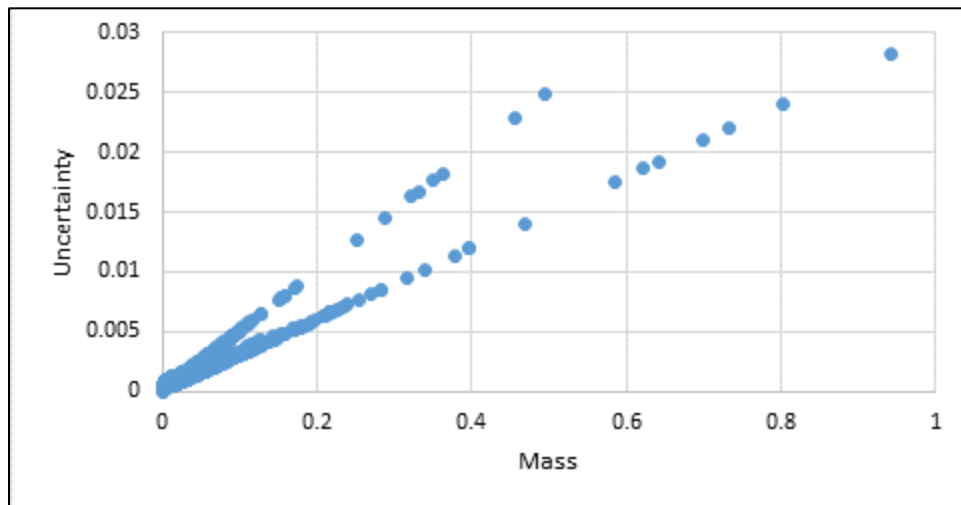
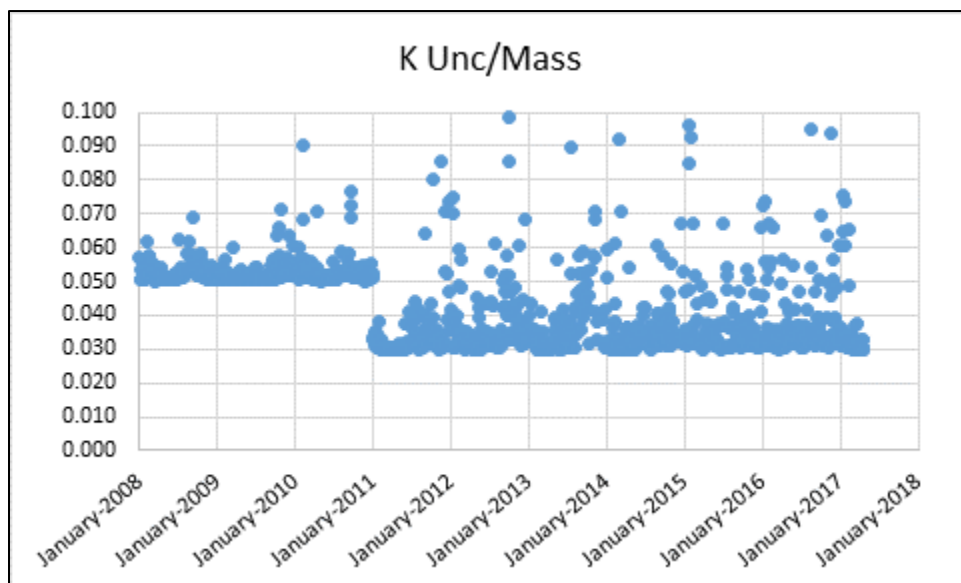


Figure 96. Ratio of uncertainty to mass for K at Guadalupe Mtn. site, 2008 - 2017



3.4.2 Wind Speed and Direction at Guadalupe Mountains National Park

UT also downloaded meteorological data from the TCEQ LEADS from the Guadalupe Mountains NP National Weather Service (NWS) KGDP station continuous ambient monitoring station (CAMS) 5018. Photos taken from the NWS KGDP / CAMS 5018 site were pulled from the TCEQ Website and are shown in Figure 97, Figure 98, Figure 99, and Figure 100. Figure 101 is an aerial image of the site and surrounding terrain, and Figure 102 is a similar view from a higher altitude. Figure 103 shows a topographic map, which is important in interpreting the wind data collected at the site.

Figure 97. West view from NWS KGDP / CAMS 5018 site



Figure 98. South view from NWS KGDP / CAMS 5018 site



Figure 99. East view from NWS KGDP / CAMS 5018 site



Figure 100. North view from NWS KGDP / CAMS 5018 site



Figure 101. Aerial view of NWS KGDP / CAMS 5018 site



Figure 102. Aerial view of NWS KGDP / CAMS 5018 site

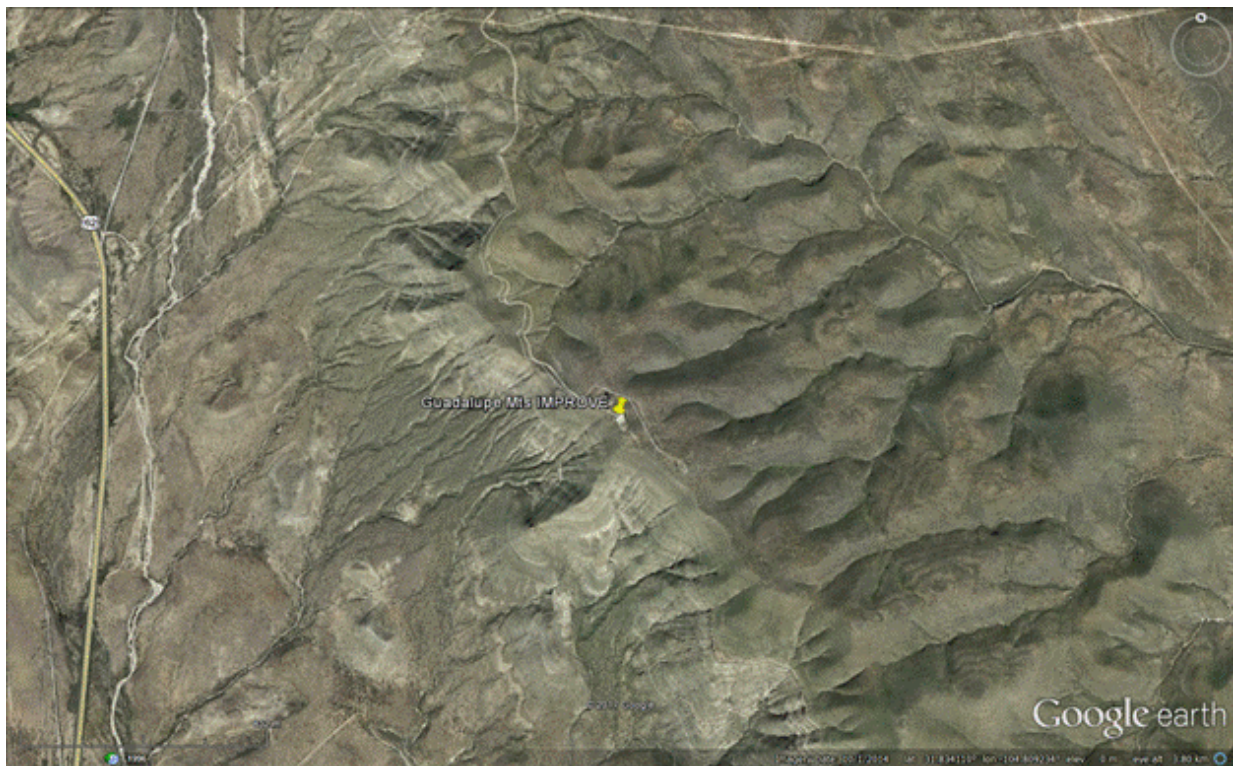
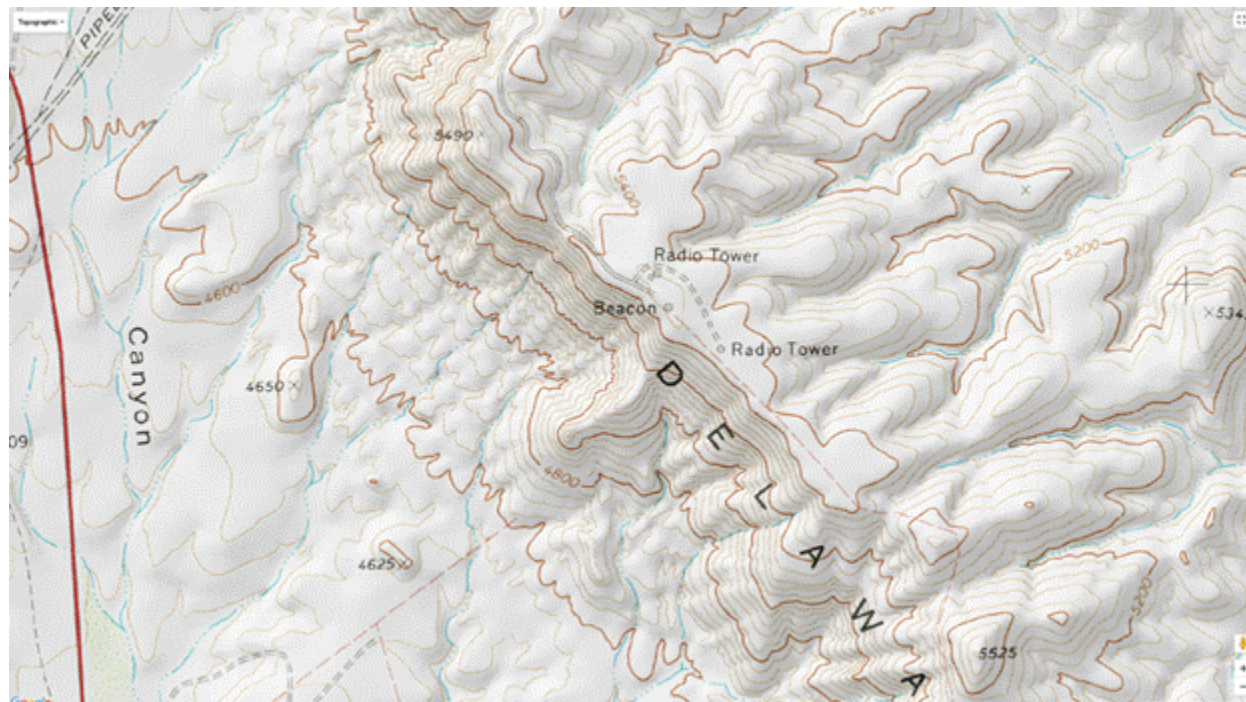
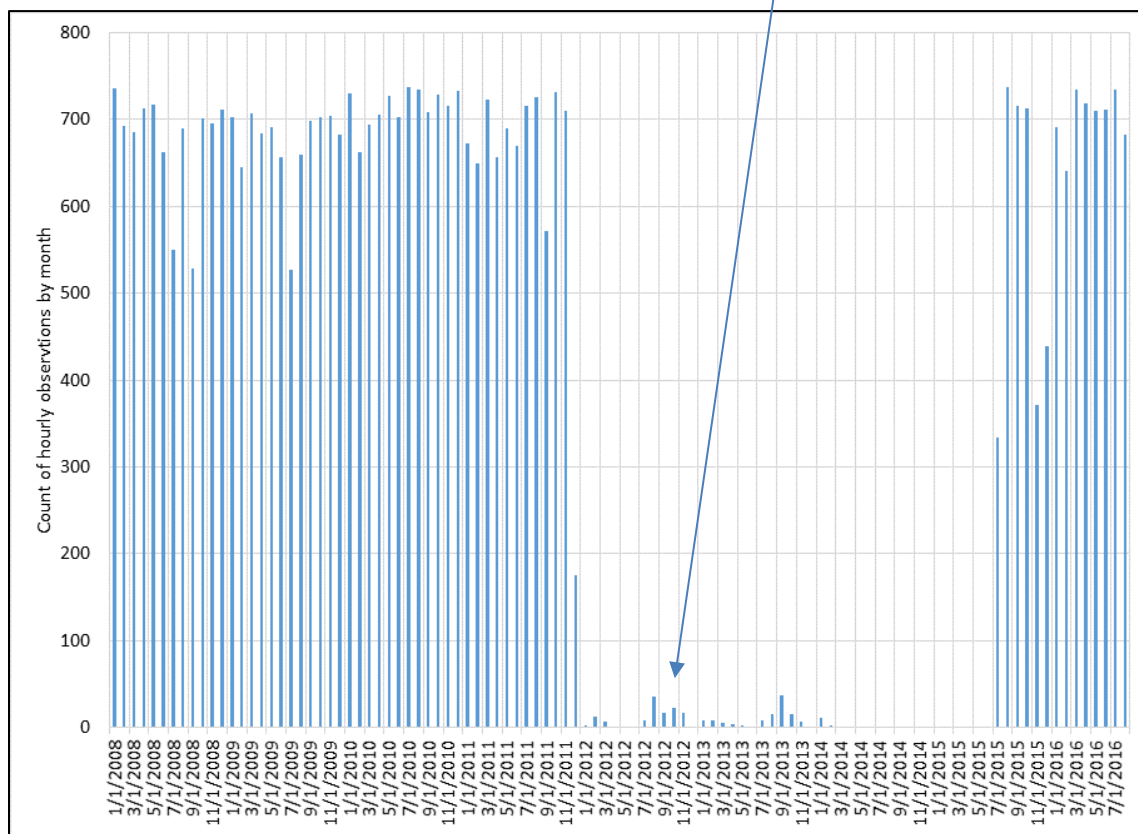


Figure 103. Topological view of NWS KGDP / CAMS 5018 site



A review of the CAMS 5018 data shows a significant gap in wind speed and direction data from December 15, 2011 to July 15, 2015. The periods with available wind speed and direction data are shown in Figure 104. This data gap severely hampers the assessment of particulate matter species or factors as a function of wind direction or speed during this period. On another monitoring project in 2018, UT found that near-surface wind speeds and directions could be “backed-out” of modeling data compiled for larger scale meteorological modeling, in particular with the HYSPLIT data produced by the National Oceanographic and Atmospheric Administration (NOAA) Air Resources Laboratory. Winds at TCEQ monitoring sites are typically measured at 10 meters (m) above ground level (AGL). For this application, a height of 40 m AGL was selected to better represent transport winds, and HYSPLIT 4 desktop application was used with EDAS 40-km gridded data files to generate hourly one-hour back trajectories from the Guadalupe Mountains GUMO1 sampling site from 2008 through 2017.

Figure 104. Counts of the hourly observations by month of wind speed and direction at Guadalupe Mts CAMS 5018, 2008 – mid 2016; few observations 2012 – mid 2015 appear to be invalid



When the wind directions measured at the site were examined, it turned out that the large majority of hourly observations fell into two general wind directions, and this is most likely related to the channelization of air flow by nearby topography. Figure 105 and Figure 106 show graphs of the histograms of 10-m CAMS 5018 observations of composite daily winds (24-hour average of Cartesian wind components converted to polar components) with 5 degree bins for direction and 2.5 mile per hour (mph) bins for wind speed. The peak directions for winds in Figure 105 are 55-59 degrees (northeast) and 240-244 degrees (west-southwest). In Figure 106, the mean and median wind speeds are 15.4 mph and 14.6 mph, respectively.

Figure 107 and Figure 108 show graphs of the histograms of HYSPLIT-derived 40-m composite daily winds with 5 degree bins for direction and 2.5 mph bins for wind speed. The peak directions for winds in Figure 107 are, broadly, 90-120 degrees (east-southeast) and 255-260 degrees (west-southwest). In Figure 108, the mean and median wind speeds are 8.2 mph and 7.4 mph, respectively. Note that the westerly winds are more in agreement on direction, and overall wind speeds are significantly lower with the 40-m HYSPLIT derived winds.

Figure 109 shows a scatter plot comparison of the wind direction 24-hour composites, which is very statically significant with a slope close to 1.0, but certainly not qualitatively satisfying in term of agreement. Figure 110 for the winds is more linear but shows the HYSPLIT modeled wind speeds significantly lower than the observed wind speeds.

Figure 105. Distribution of daily composite 10 m wind directions at the Guadalupe Mountains PM_{2.5} monitoring site

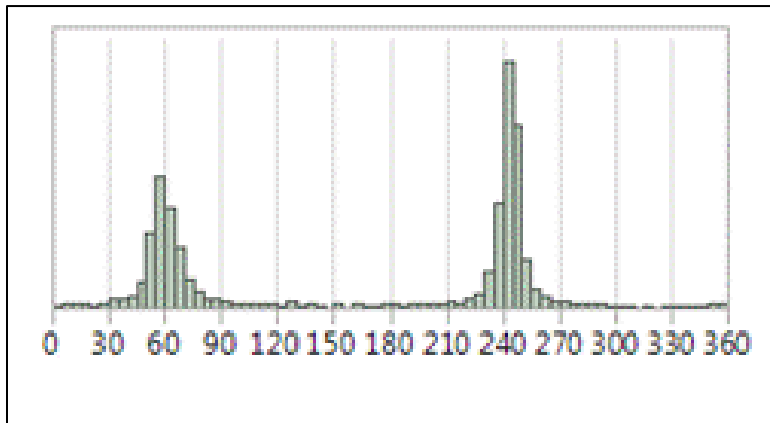


Figure 106. Distribution of daily composite 10 m wind speeds (mph) at the Guadalupe Mountains PM_{2.5} monitoring site

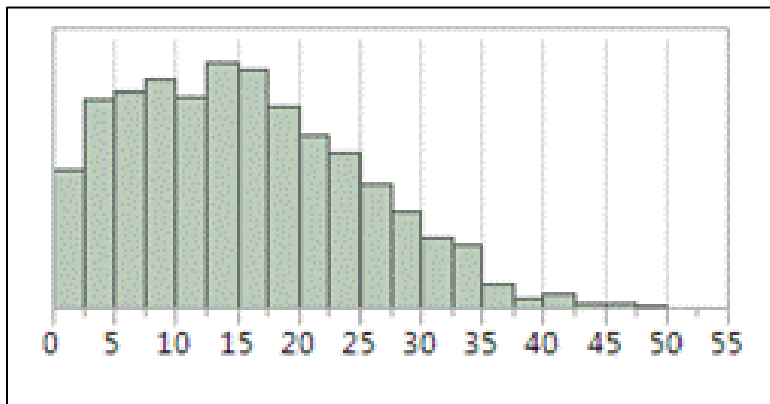


Figure 107. Distribution of daily composite HYSPLIT-derived 40 m wind directions at the Guadalupe Mountains PM_{2.5} monitoring site

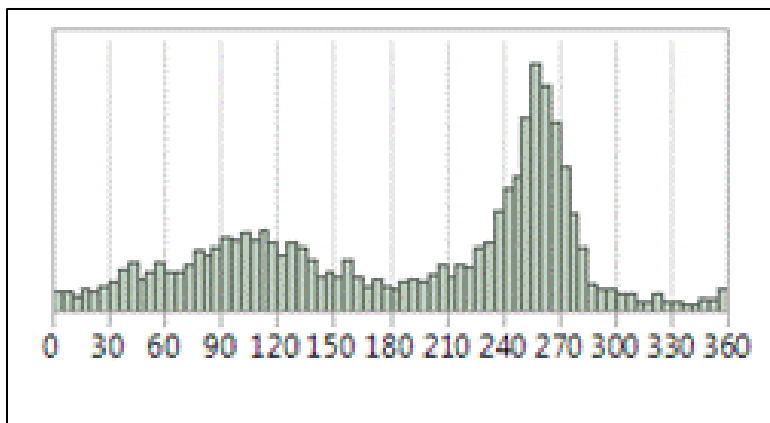


Figure 108. Distribution of daily composite HYSPLIT-derived 40 m wind speeds at the Guadalupe Mountains PM_{2.5} monitoring site

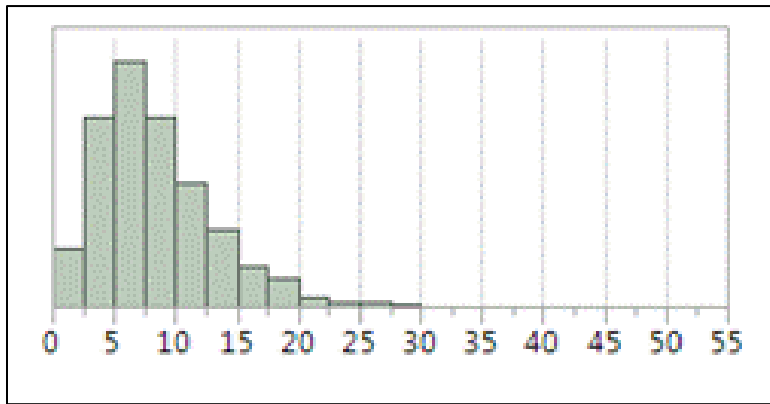


Figure 109. CAMS 5018 composite daily wind direction (10m AGL) vs derived HYSPLIT composite daily wind direction (40 m AGL)

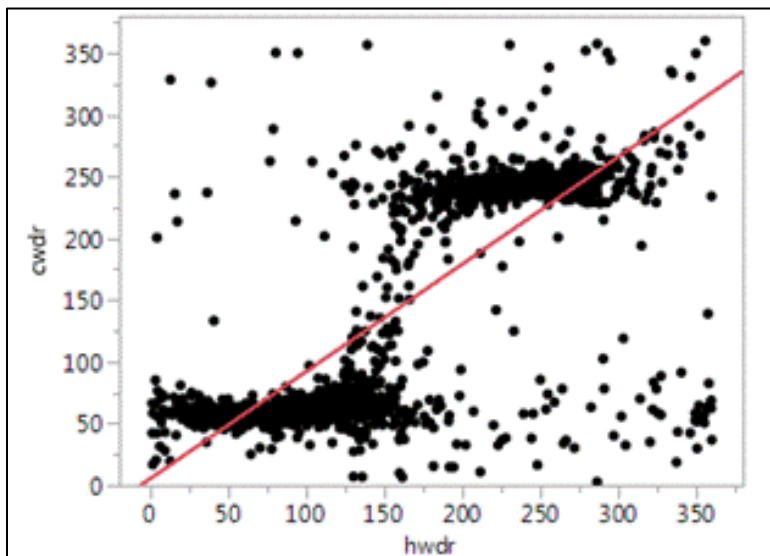
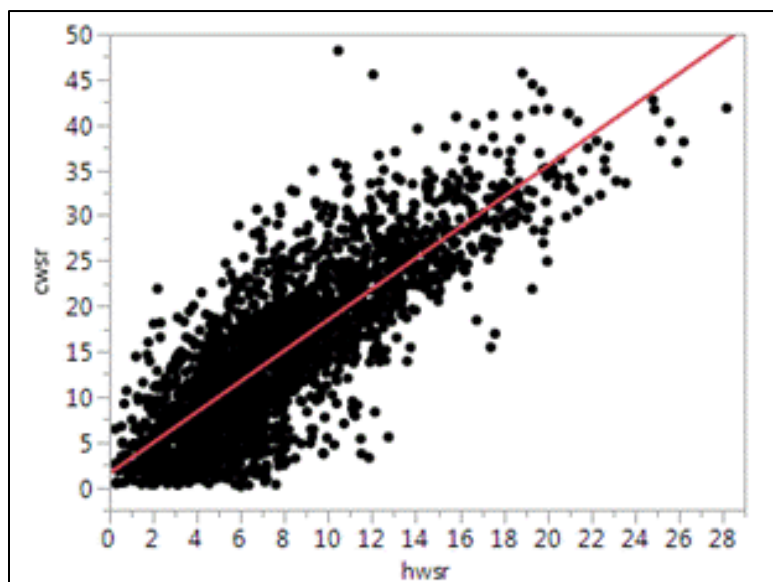


Figure 110. CAMS 5018 composite daily wind speed (10m AGL) vs derived HYSPLIT composite daily wind speed (40 m AGL)



In examining all the 2017 wind speed data at 31 West Texas CAMS sites (TCEQ Regions Amarillo, Lubbock, Abilene, San Angelo, Midland, El Paso, Laredo), the Guadalupe CAMS 5018 averaged 19.1 mph, and the next highest values were 13.0 mph at both PANTEX CAMS 105 and Amarillo CAMS 1077. The 2017 average across all 30 West Texas sites excluding CAMS 5018 is 8.0 mph. Thus, the *reported* winds at Guadalupe National Park are very high compared to every other TCEQ site.

3.4.3 PMF Analysis for Guadalupe National Park

The PMF analyses for GUMO1 data used temperature fractions of EC and OC with relatively high signal to noise ratios, and total EC and OC were not used. Seven robust factors were found. The FPEAK rotation was applied and a boot-strapping run produced nearly 100 percent matching for all seven factors over 200 runs and a 0.6 correlation test. The factor with higher EC and OC temperature fractions was assigned the “Fire & Smoke” label, and the other with higher elemental Zinc (Zn) and Lead (Pb) as assigned the “Combustion” label. The charts showing the bootstrapping results on the FPEAK rotation were exported from PMF 5.0 and are shown in Figure 111, with each graph labeled with a source name.

One factor is labeled “Sodium Chloride”, which also composes sea salt, despite the far inland location of the sampling site. The source is hypothesized to be the Salt Flats to the southwest of the site, According Nations Park Service

“The Salt Flats are playas that for years had shallow groundwater (1-3 m below surface). The high evaporation rates concentrated salts from the briny Bone Spring-Victorio Peak (BS-VP) aquifer in the subsurface. The brines in the BS-VP are probably sourced from evaporitic deposits in the San Andres-Victorio Peak and Bone Spring Formations. The playas themselves are Pleistocene features, the brines from which the salts derive are

probably late Pleistocene/Holocene meteoric water that has dissolved Permian evaporates as the water moved through the subsurface.”⁵

A day of the week analysis is often useful in urban areas to assess motor vehicle factor presence, as significantly higher concentrations are expected Monday through Friday compared to weekends for light duty vehicles, with a smaller weekday/weekend contrast for heavy duty vehicles. However, at a rural National Park location, such a contrast may not be detectable, or may be the inverse if there is more weekend recreational traffic than weekday commuter traffic. Figure 112 shows the mean of the “Combustion” factor by day of the week, and no systematic pattern appears to be present. T-tests performed on each of the seven factors for mean weekday vs mean weekend and no t-test showed even a marginally significant difference.

Using the HYSPLIT derived 24-hour composite winds described earlier, a combined data set of the daily seven factor loadings (which are normalized to average 1.0 within each factor) and corresponding wind speed and direction was created. Using SAS, JMP, and MS Excel software tool, the factors loadings were averaged by 30 degree wind direction bins and plotted. Wind speed has not been included in this analysis. Wind speed intensity, direction, and comparisons of coincident PM_{2.5} and PM₁₀ may be useful in further determining the upwind sources of the crustal and mineral factors.

Figure 113 shows a radar plot for the frequency of HYSPLIT-derived composite 24-hour wind directions by 30-degree wind direction bin on the days for which factor data exist. As was the case in the earlier Figure 107 the westerly winds are most common, followed by southeast winds.

The results of merging factor loadings (not mass) with HYSPLIT-derived wind data and averaging within 30-degree wind bins and accompanying time series graphs of the normalized factor strengths appear in Figure 124 through Figure 127.

For the “Sulfate” factor, the pattern fits having transport from Texas and beyond but mainly from the Carbon power plants in Northern Mexico and from the Gulf of Mexico with spring agricultural burning smoke. There is some sulfate mass assigned to the Calcium/Magnesium factor; however, it is a tiny fraction of the total sulfate measured at the site.

For the “Nitrate” factor, the concentrations peak during the winters. Several other factors have their highest factor strengths in the mid-year periods.

⁵ Dr. Jonena Hearst, PhD, Geologist, Guadalupe Mtns NP, 400 Pine Canyon Dr., Salt Flat TX 79847, personal communication, May 2018

Figure 111. FPEAK rotation (0.5) resulting Guadalupe National Park PMF factors

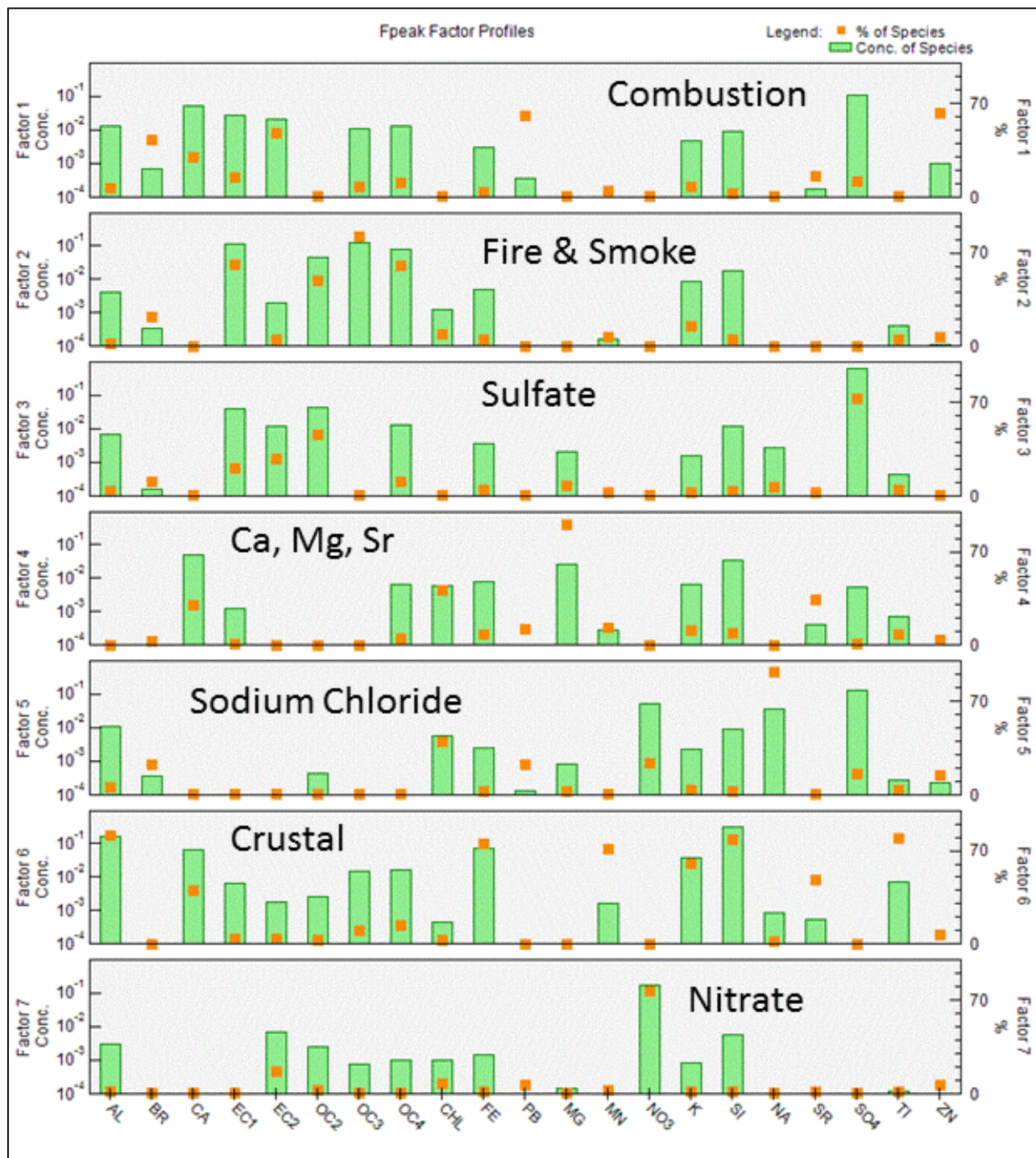


Figure 112. Means of Guadalupe National Park factor loadings by day of week for the “Combustion” factor

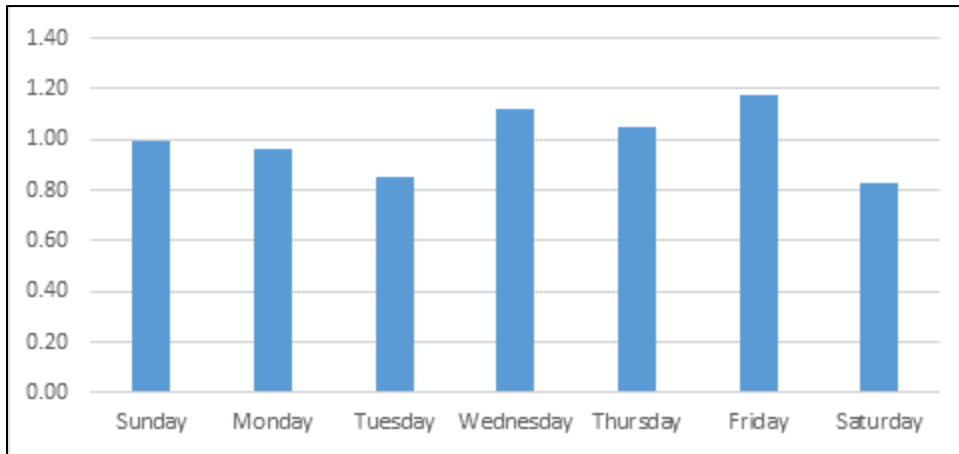


Figure 113. Frequency of HYSPLIT-derived wind directions by 30-degree wind bin on days 2011 – 2017 for which factors were calculated; westerly winds dominate

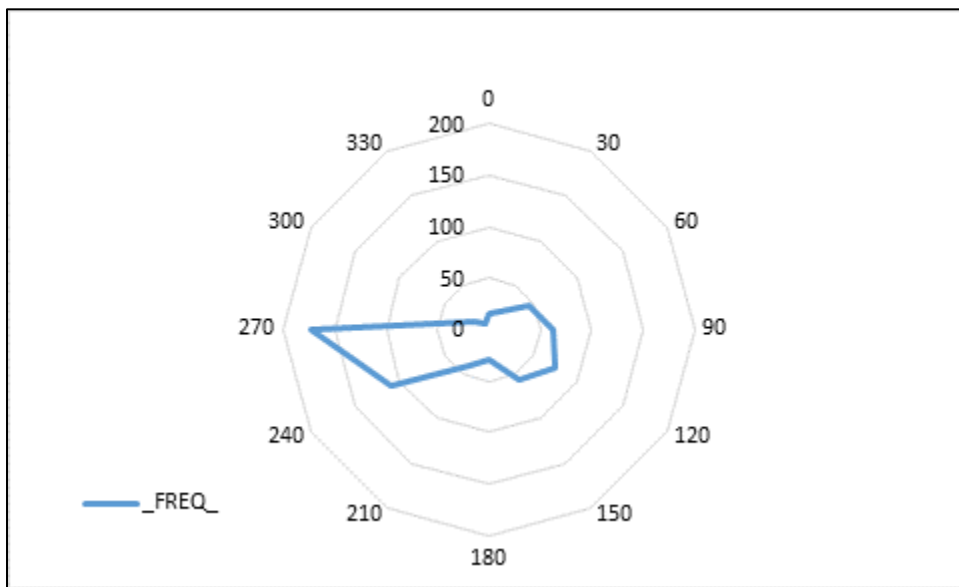


Figure 114. Mean *hypothesized Combustion* factor loading by 30-degree wind bin; highest loading from southwest through northwest

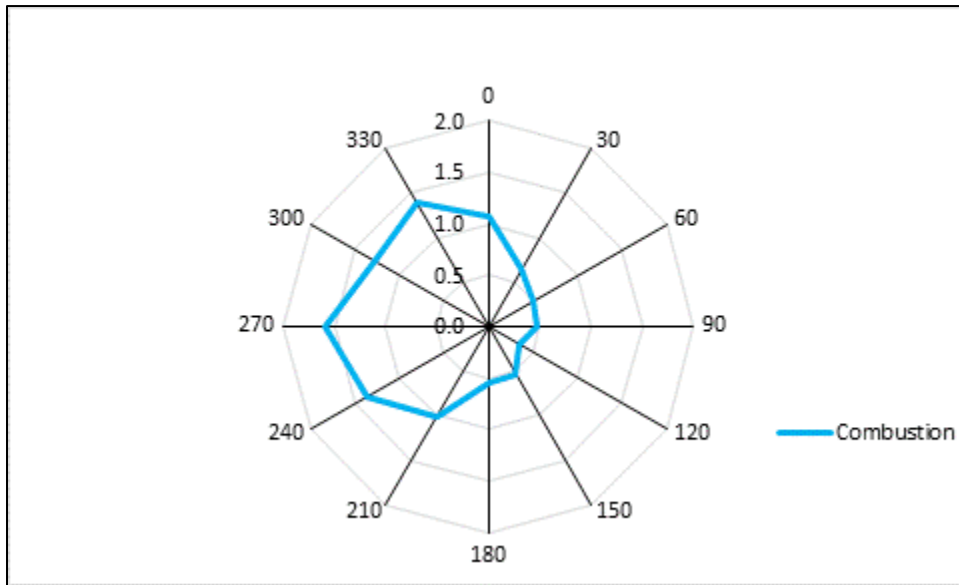


Figure 115 Guadalupe NP time series *Combustion* factor normalized factor strength

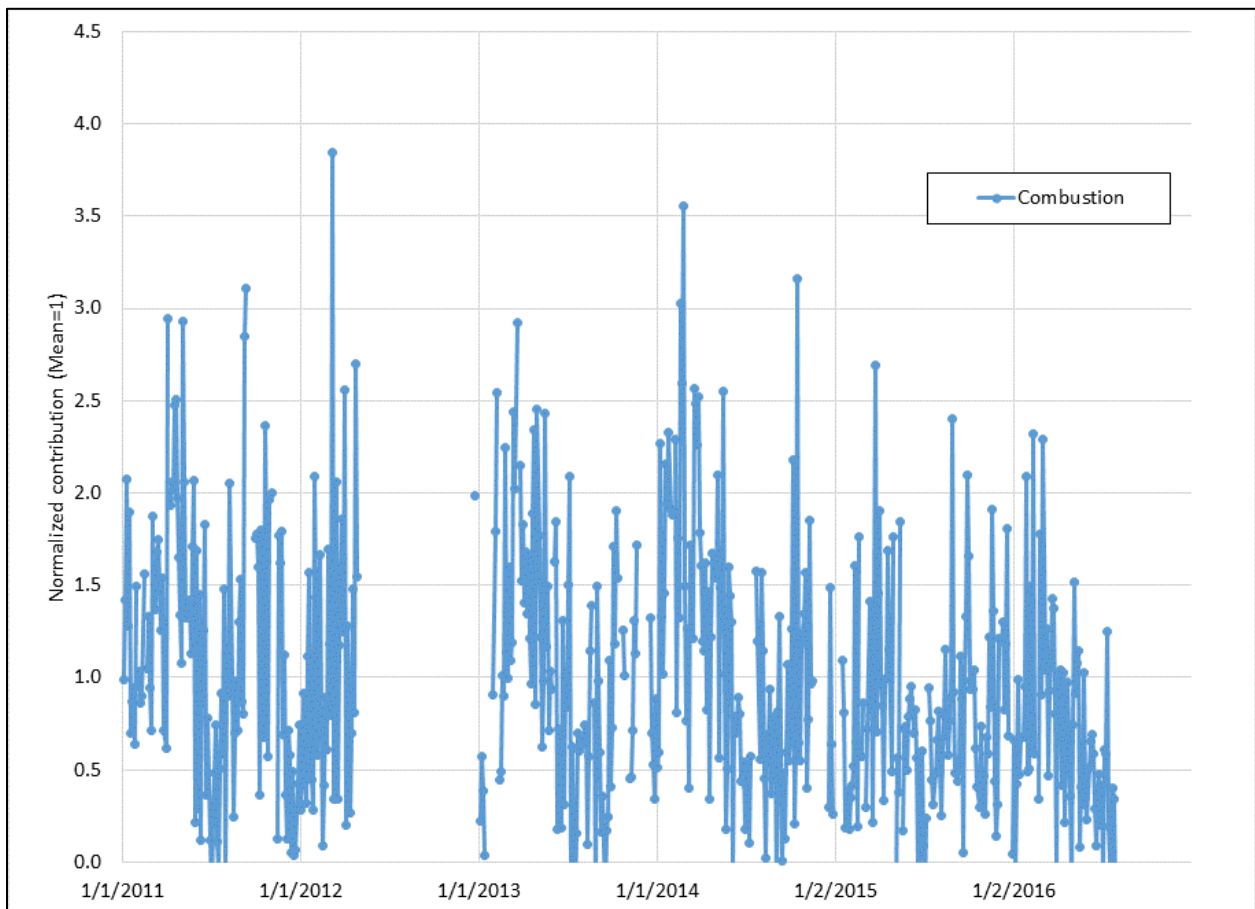


Figure 116. Mean *hypothesized Fire&Smoke* factor loading by 30-degree wind bin; highest loading from southeast

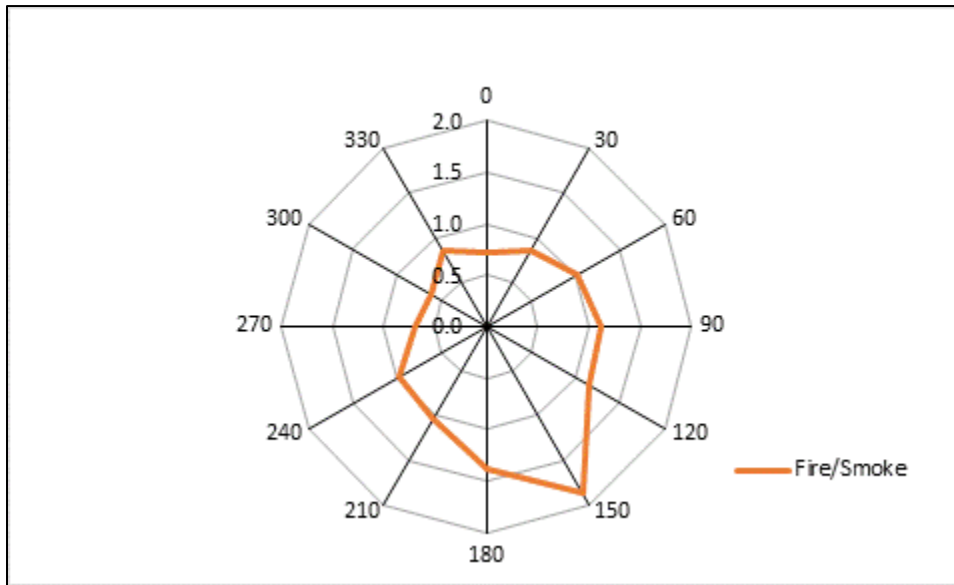


Figure 117 Guadalupe NP time series *Fire&Smoke* factor normalized factor strength

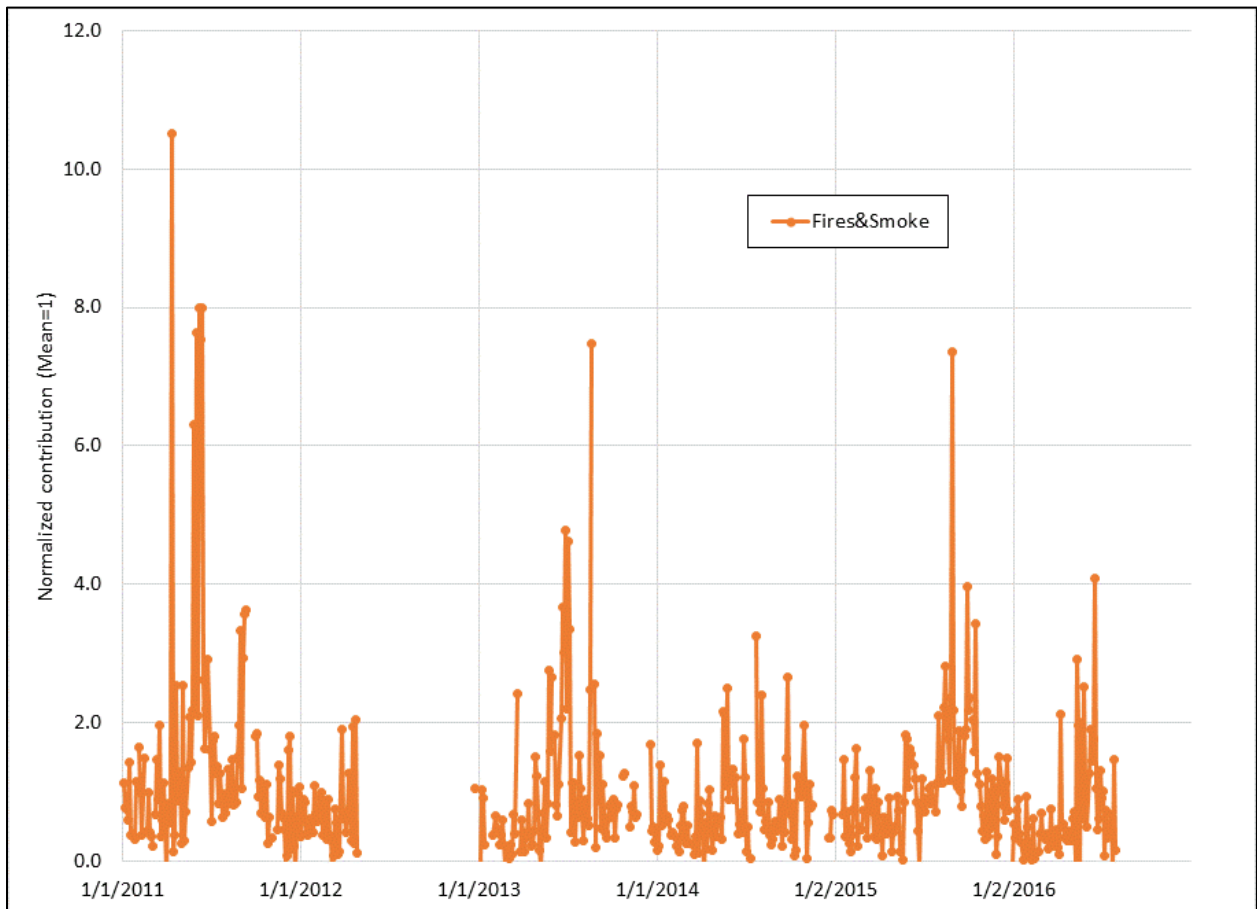


Figure 118. Mean *transported Sulfate* factor loading by 30-degree wind bin; high loading from 60 through 210 deg.

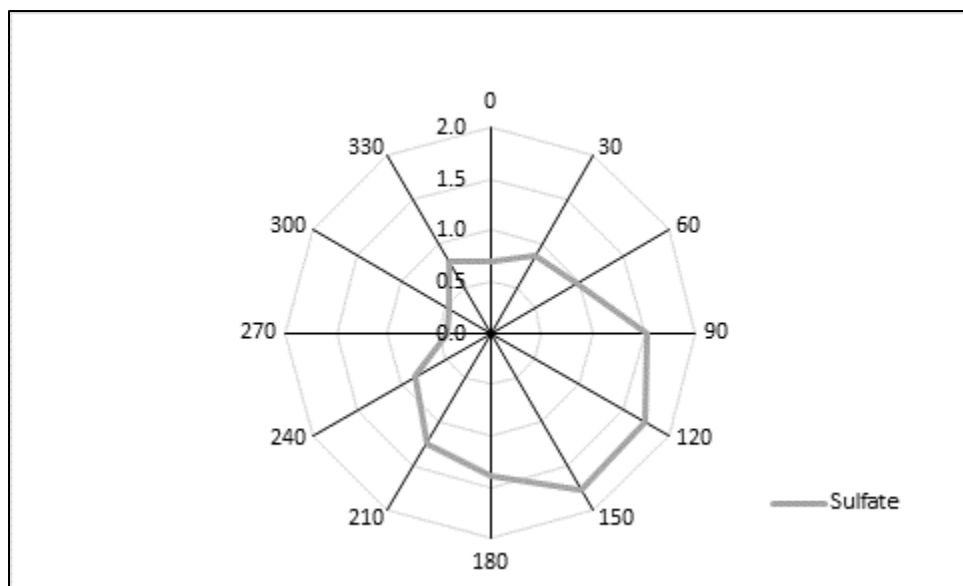


Figure 119 Guadalupe NP time series *Sulfate* factor normalized factor strength

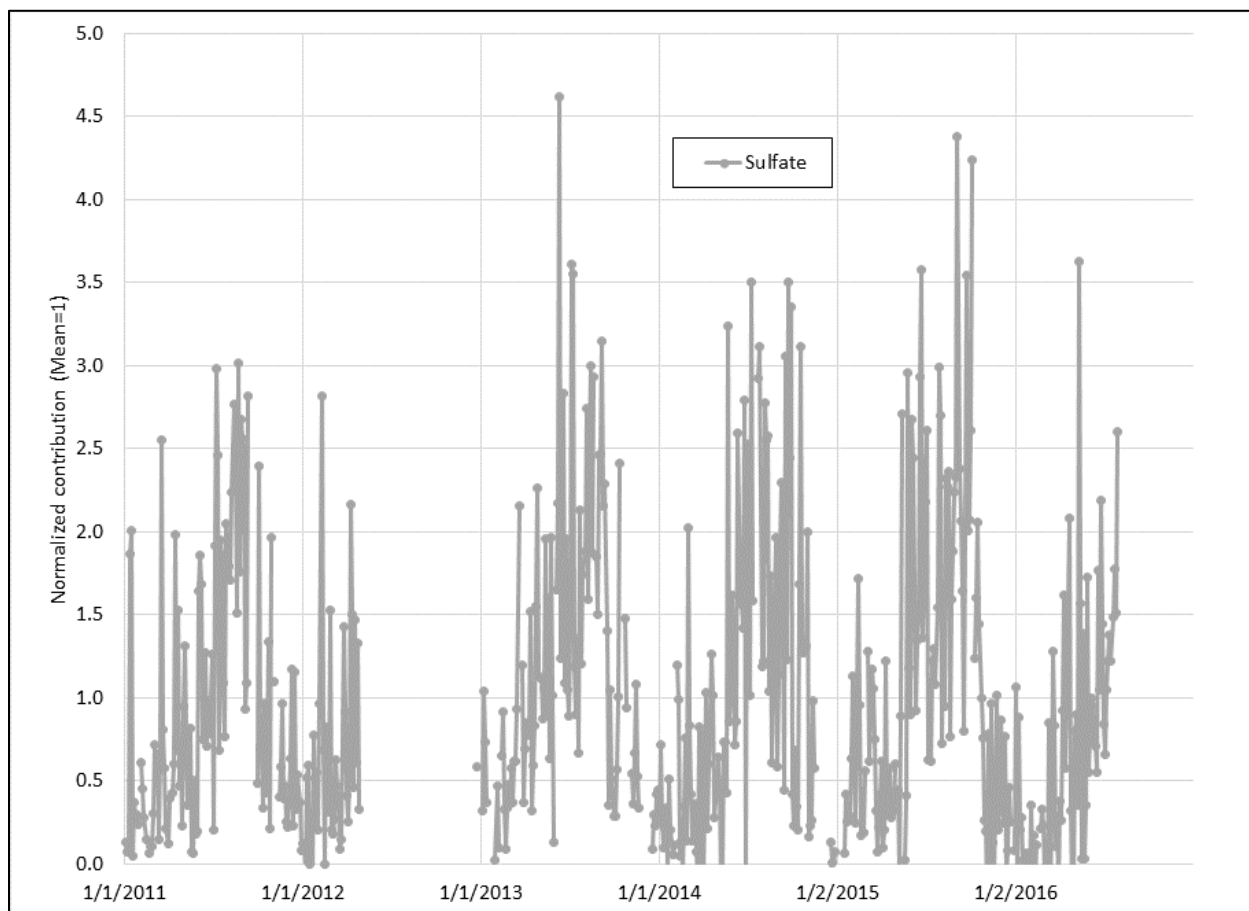


Figure 120. Mean *Calcium/Magnesium* factor loading by 30-degree wind bin; highest loading from southwest

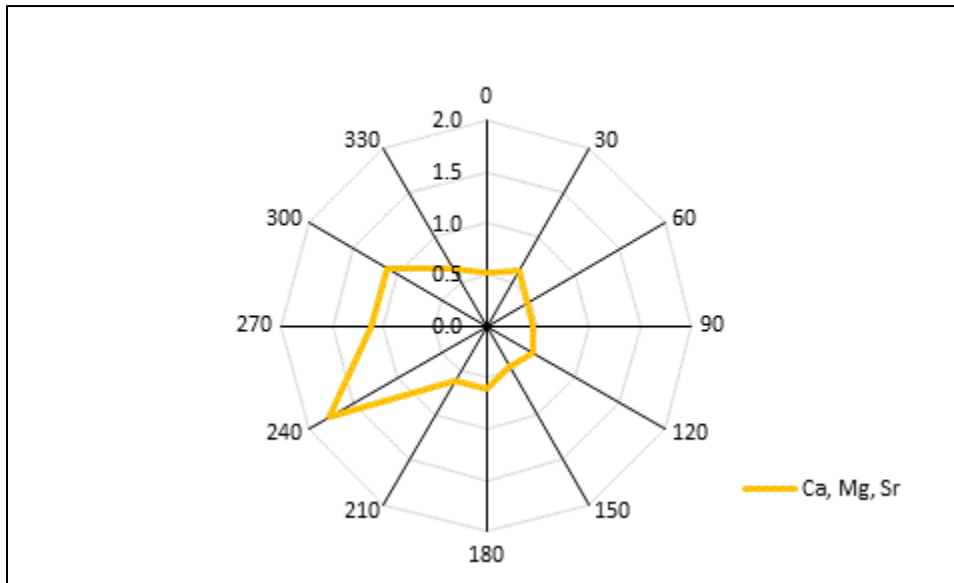


Figure 121 Guadalupe NP time series *Ca, Mg, Sr* factor normalized factor strength

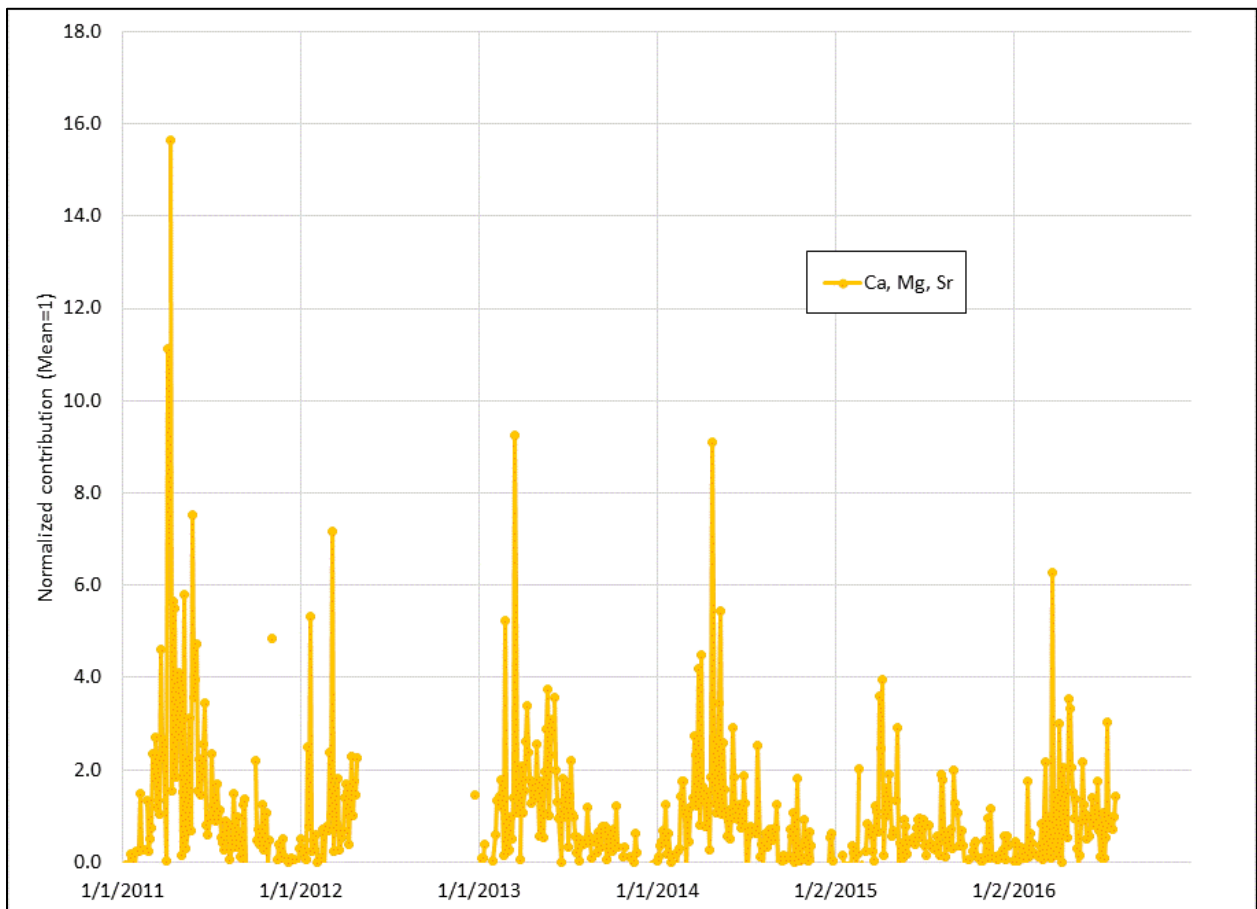


Figure 122. Mean *Sodium Chloride* factor loading by 30-degree wind bin; highest loading from southeast and southwest

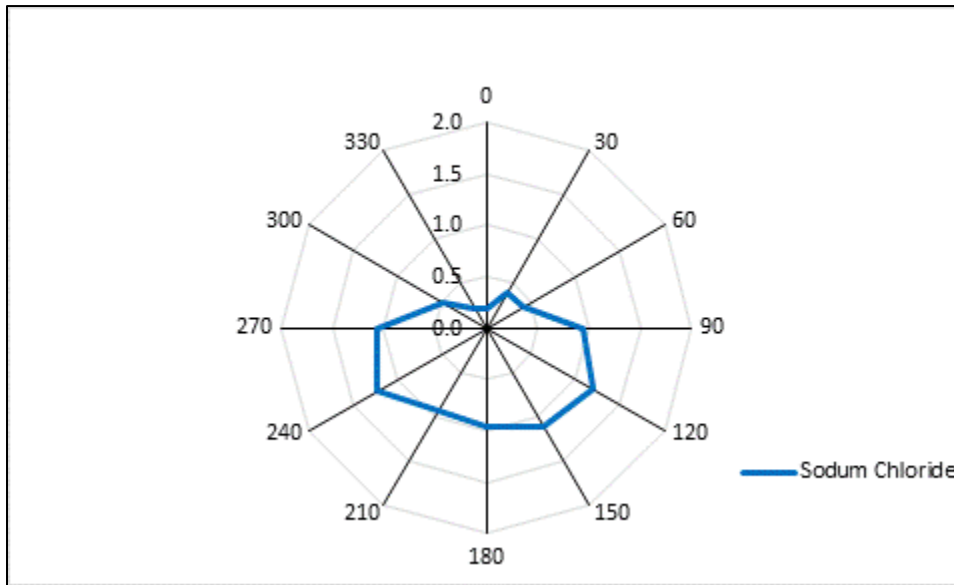


Figure 123 Guadalupe NP time series *Sodium Chloride* factor normalized factor strength

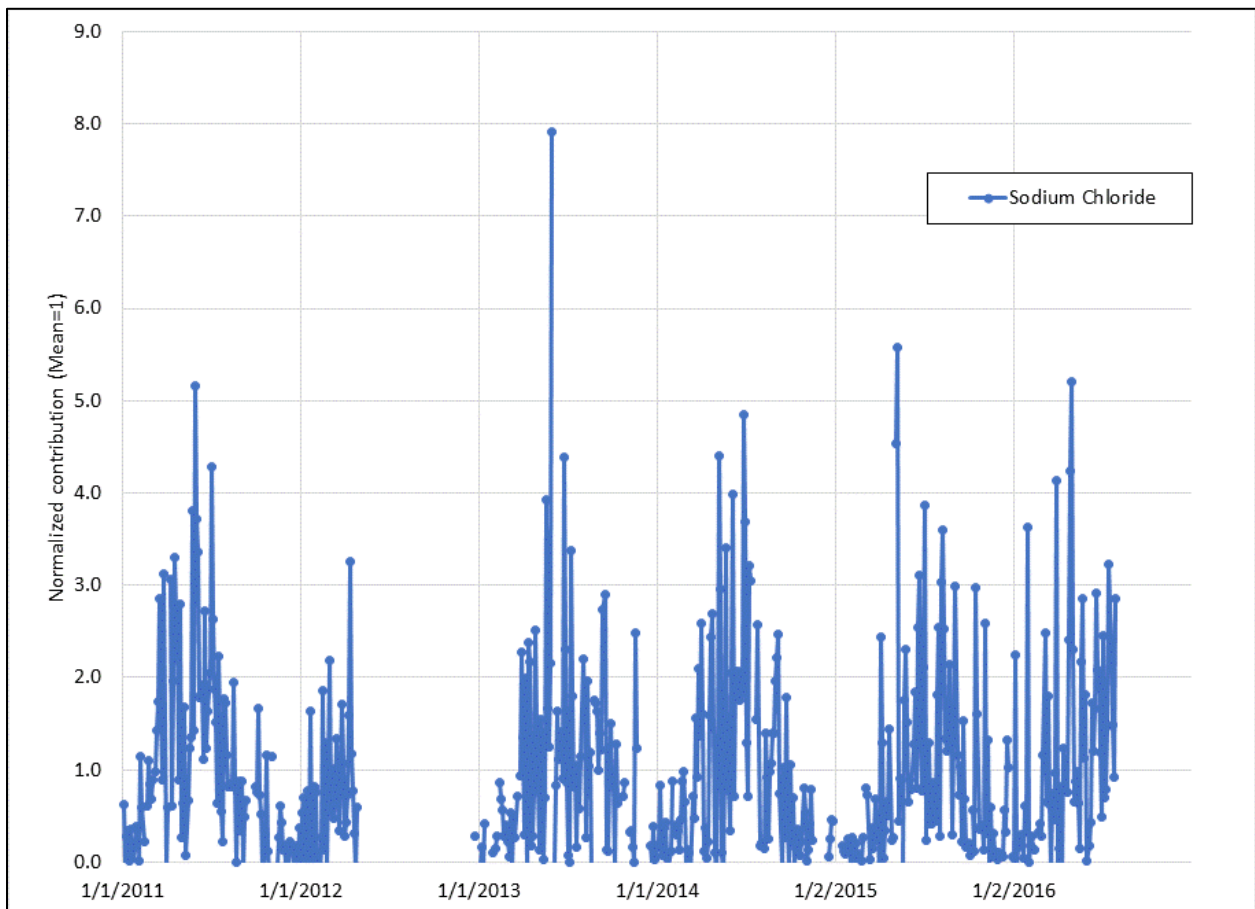


Figure 124. Mean *Crustal* factor loading by 30-degree wind bin; highest loading from southwest

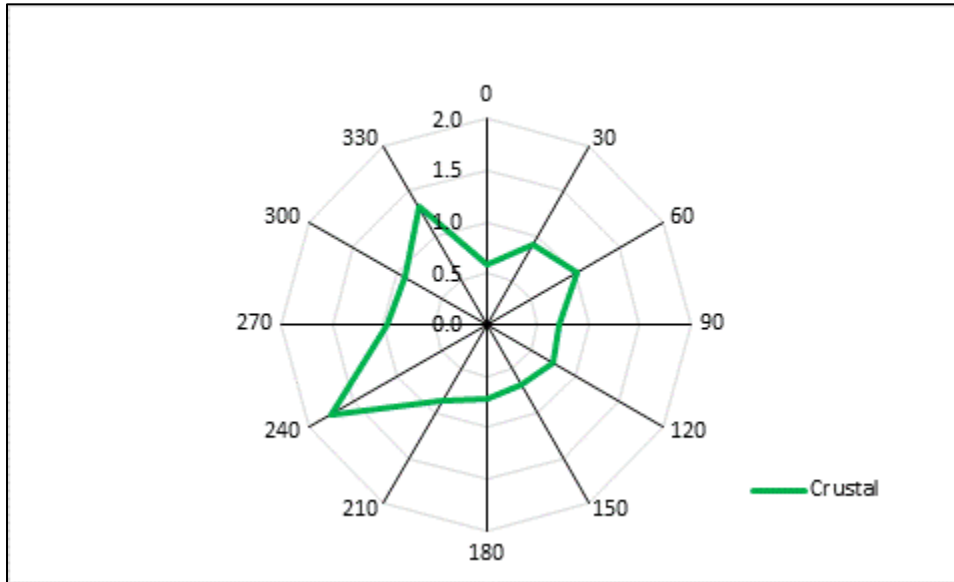


Figure 125 Guadalupe NP time series *Crustal* factor normalized factor strength

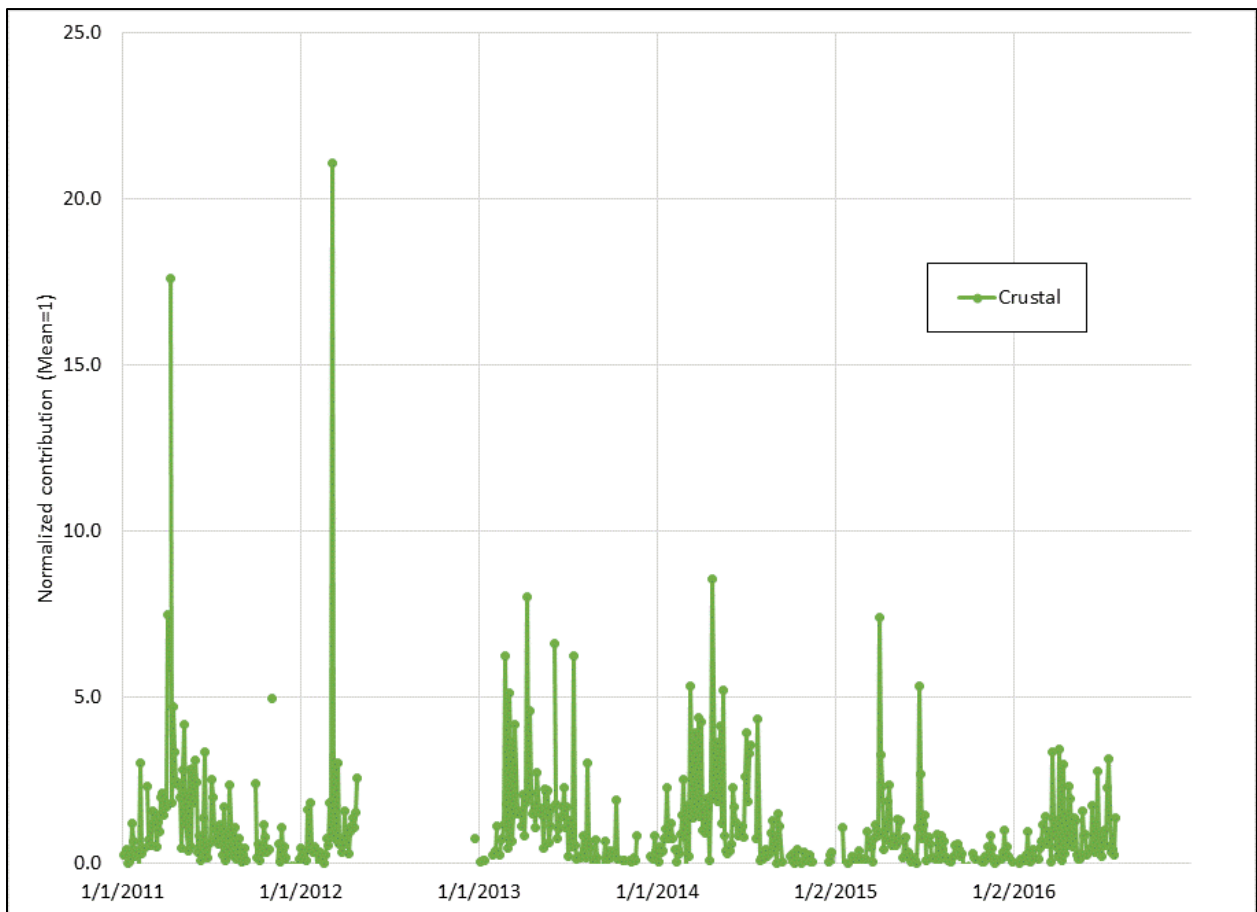


Figure 126. Mean *transported Nitrate* factor loading by 30-degree wind bin; highest loading from north through east

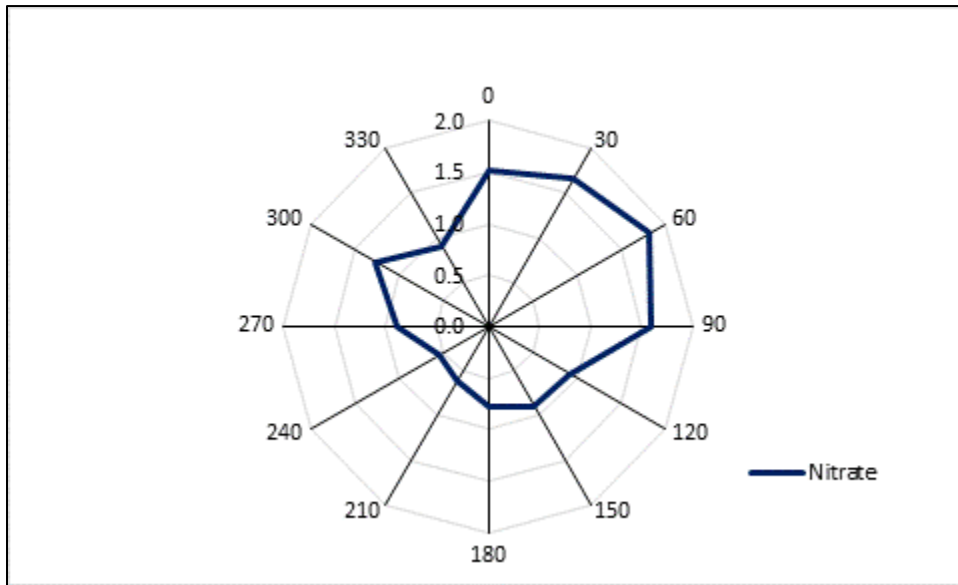
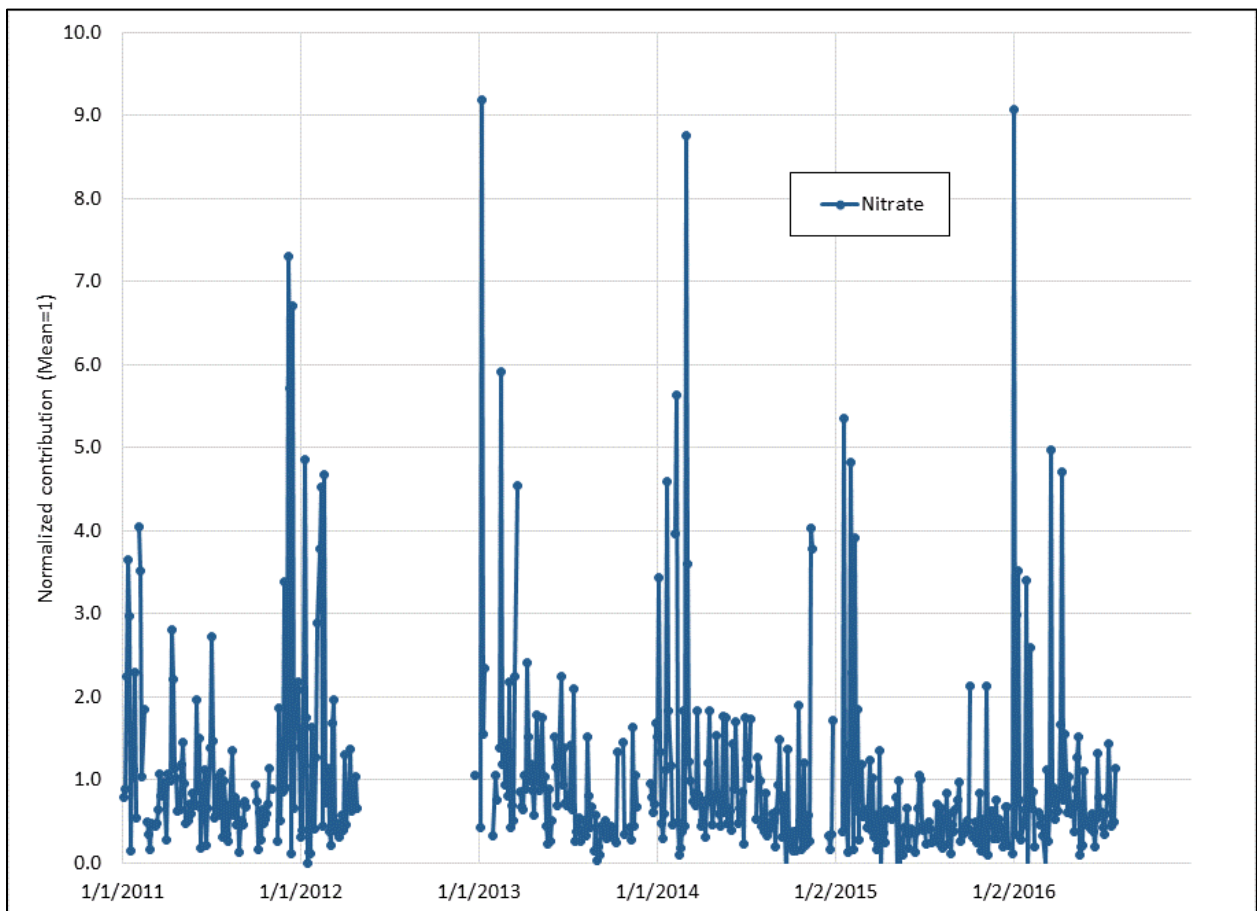


Figure 127 Guadalupe NP time series *Nitrate* factor normalized factor strength



4. Conclusion and Recommendations

As was stated at the beginning of this report, there were five purposes of this project:

- 1) One purpose was to produce PM_{2.5} chemical speciation data from the TCEQ Galveston monitoring site. This was successfully completed.
- 2) A second purpose was to carry out advanced analysis of the data from all PM_{2.5} monitoring sites in the Houston region to determine quantitatively the contribution of African dust and smoke from southern Mexico and Central America to PM_{2.5} concentrations measured on individual days impacted by either or both of these sources at Clinton Dr. This was accomplished through positive matrix factorization analysis at UT and through cooperation the Texas A & M University researchers.
- 3) A third purpose was to help determine the contribution of incoming regional PM_{2.5} concentrations from the continental U.S. to PM_{2.5} concentrations measured at Clinton Dr. Similarly, this was accomplished through PMF analysis at UT and through cooperation the TAMU researchers.
- 4) A fourth purpose is to determine the source types and directions contributing to local and regional contributions to the PM_{2.5} concentrations measured at Clinton Dr. Similarly, this was accomplished through PMF analysis at UT coupled with meteorological assessments of wind directionality and HYSPLIT back-trajectory analyses.
- 5) A fifth purpose is to identify the impacts of regional dust storms on PM_{2.5} concentrations at the Chamizal monitoring site in El Paso. This was accomplished with PMF analyses with data from Chamizal and also data from the Guadalupe Mountains National park.

Additional analyses may be requested at any point.